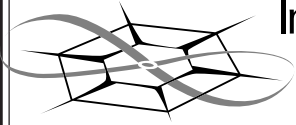


**The University of Kansas**



**Information and  
Telecommunication  
Technology Center**

Technical Report

**Characterization of Polarization-Mode  
Dispersion on Buried Standard  
Single-Mode Fibers**

Pradeep Kumar Kondamuri  
and Chris Allen

ITTC-FY2003-TR-18834-01

November 2002

Project Sponsor:  
Sprint

Copyright © 2002:  
The University of Kansas Center for Research, Inc.,  
2335 Irving Hill Road, Lawrence, KS 66044-7612.  
All rights reserved.

<b>CHAPTER 1</b>	<b>3</b>
<b>CHAPTER 2</b>	<b>4</b>
<b>Terminologies</b>	<b>4</b>
2.1 Performance metrics	4
<b>CHAPTER 3</b>	<b>6</b>
<b>Scalability test</b>	<b>6</b>
3.1 Introduction	6
3.2 Test topology	6
3.3 Performance Metrics	10
3.4 Results and Analysis	10
3.5 Problems faced	16
3.6 Conclusion	17
<b>CHAPTER 4</b>	<b>18</b>
<b>Load test</b>	<b>18</b>
4.1 Introduction	18
4.2 Test topology	18
4.3 Performance Metrics	18
4.4 Results and Analysis	19
4.5 Problems faced	24
4.6 Conclusion	25
<b>CHAPTER 5</b>	<b>26</b>
<b>Effect of Peergrouping test</b>	<b>26</b>
5.1 Introduction	26
5.2 Test topology	26
5.3 Performance Metrics	34
5.4 Results and Analysis	34
5.6 Conclusion	43
<b>CHAPTER 6</b>	<b>44</b>
<b>Effect of Hierarchy</b>	<b>44</b>
6.1 Introduction	44
6.2 Test topology	44
6.3 Performance metrics	50
6.4 Results and Analysis	50

6.6 Conclusion	58
<b>CHAPTER 7</b>	<b>59</b>
<b>Effect of Crankback</b>	<b>59</b>
7.1 Introduction	59
7.2 Test topology	59
7.3 Performance metrics	59
7.4 Results and Analysis	59
7.5 Conclusion	63
<b>CHAPTER 8</b>	<b>64</b>
<b>Simulator Performance</b>	<b>64</b>
8.1 Introduction	64
8.2 Test topology	64
8.3 Parameter of interest	64
8.4 Results and Analysis	64
8.4 Conclusion	66
<b>CHAPTER 9</b>	<b>67</b>
<b>Summary</b>	<b>67</b>
9.1 Summary of Conclusions	67
<b>APPENDIX - I</b>	<b>69</b>
<b>Simulation Parameters</b>	<b>69</b>
<b>REFERENCES</b>	<b>71</b>

# Chapter 1

## Introduction

This technical report is a compilation of the results of various simulations conducted using the **KU-PNNI** simulator during the academic year 2001 – 2002. Analyses of the results are primarily based on evidence collected during the course of the simulation, in the absence of which the analysis is based on a plausible hypothesis drawn after extensive discussion. Pictorial representations of the test topologies and plots of results are provided wherever deemed necessary. For more information on the KU-PNNI simulator, refer to the KU-PNNI user's manual [1].

Chapter 2 provides a brief explanation of the meaning of each performance metric that is monitored during the simulations. Chapter 3 deals with the results and analysis of simulations conducted by scaling the topology in size. Chapter 4 deals with the analysis of the results of simulations conducted by varying load, while chapter 5 deals with analysis of the effect of peergrouping. Chapter 6 deals with the effects of changing the number of hierarchical levels, while chapter 7 deals with the effects of varying the crankback counts. Chapter 8 deals with the simulator performance (time taken to complete the simulation) measured as a function of load and size of the topology.

All tests were conducted on a Linux box running RedHat Linux 6.1, with 2GB RAM and an Intel P-III 533 MHz processor.

# Chapter 2

## Terminologies

### 2.1 Performance metrics

The performance of the network under consideration is assessed through various metrics as deemed appropriate. The following are all the performance metrics that are monitored during the entire set of simulations, and a brief explanation to each one of them:

#### *Mean Call setup time*

A non-zero time is required to setup a call between the caller and callee. The time elapsed from the moment the caller placed a request for the setup of a virtual circuit between the caller and the callee, to the moment the caller receives confirmation from the callee that a path was successfully setup, is called *Call setup time*. The average of call setup times of all the calls is called the “mean call setup time”.

#### *Call Success percentage*

A call is considered successfully setup if and only if a virtual path is successfully established between them, meeting all QoS requirements of the call. Hence, the call success percentage is the ratio of successful calls of all the nodes to the sum total of calls placed by all the nodes.

#### *Convergence time*

Convergence time is defined as the time taken for all the nodes in the network to exchange topological information, and eventually share the same view of the network. *Convergence time – low* refers to the least value of convergence time among all nodes, while *Convergence time – high* refers to the maximum value of convergence time among all the nodes

#### *Average Database size*

Each node maintains a database of topological information of all the nodes in the network. The average database size is the average of database sizes of all the nodes.

### ***Average number of hops***

The number of hops for a call can be defined as the number of links the call has to traverse before it reaches the destination. Hence the average number of hops is the ratio of the total number of hops over all successful calls, to the total number of successful calls.

### ***Average Utilization percentage***

Utilization percentage is the ratio of consumed bandwidth at a link to the total available bandwidth in the link at any instant, expressed as a percentage. Average utilization percentage is the ratio of the sum of all samples of utilization percentage collected over a period of time to the total number of such samples.

### ***Total floods***

The nodes in the network exchange PNNI control information through the mechanism of reliable flooding. The total floods metric is the count of the total number of floods initiated during the entire duration of the simulation.

### ***PNNI data / Flood***

PNNI data per flood is the total PNNI data exchanged via flooding (in bits) normalized over the total number of floods, or PNNI data normalized over the number of nodes and floods (per node). This is done to remove dependency of PNNI data over the number of nodes or the length of simulation (or number of floods). *PNNI data – high* refers to the maximum value of PNNI data flooded by any node, among all the nodes, while *PNNI data –low* refers to the least value of PNNI data flooded by any node, among all the nodes.

### ***Percentage Wasted Floods***

A flood is considered “wasted” if it conveys no new information to the node concerned. Hence percentage total wasted floods is the total number of wasted floods, normalized over the total number of floods and expressed as a percentage.

# Chapter 3

## Scalability test

### 3.1 Introduction

The aim of this test is to study the effect of scaling the topology (in size) on the various identified metrics. This is an important test for any topology, because it gives a rough idea on how much the topology can be expanded within acceptable limits of values of the performance metrics. For all topologies, calls were generated with exponential *mean call inter-arrival times* of 20 sec, 15 sec, 10 sec, 5sec, and 2 sec.

### 3.2 Test topology

#### 3.2.1 Edge-core with 20 nodes

This topology (see fig 3.1) has 16 edge nodes and 4 core nodes. The edge nodes are grouped in 4 peergroups of 4 nodes each, and core nodes are grouped in one peergroup. Each node has one host connected to it with 120 calls generated per host.

The hosts are connected to the nodes via 10Mbps links; the border edge node in each peergroup connects to the three other edge nodes in the peergroup via DS3 (approximately 45Mbps) links, while the border edge nodes connect to the core nodes via OC3 (approximately 155.6 Mbps) links. Finally, the core nodes interconnect among themselves via OC12 (approximately 622 Mbps) links. One point to be noted is that the core nodes do not have any hosts attached to them.

A two-level hierarchical structure is followed while designing the topology. The border edge nodes are numbered as '1' in each peergroup; the core nodes are contained in the 'E' peergroup.

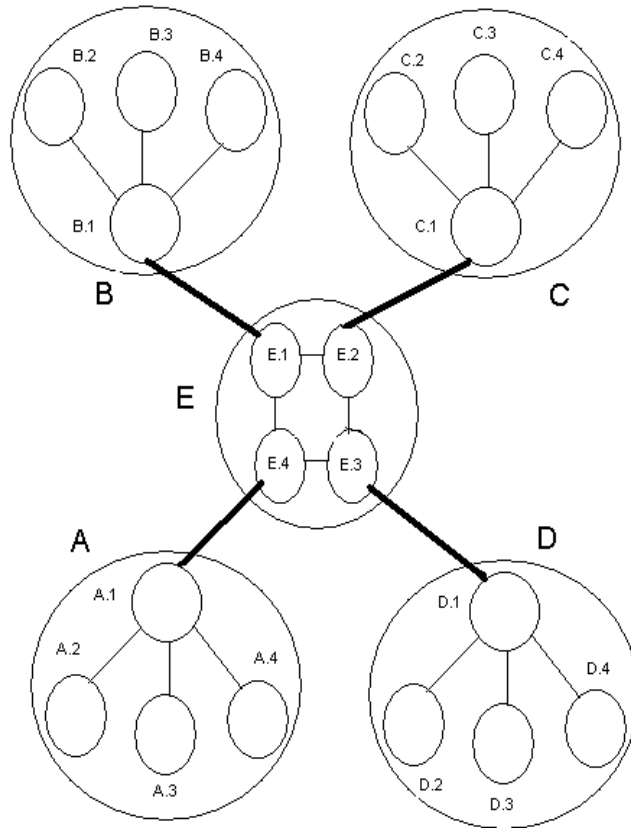


**Fig 3.1 Edge-Core 20 nodes**

### 3.2.2 Edge-core with 40 nodes

This topology (fig 3.2) is composed of 32 edge nodes and 8 core nodes. The edge nodes are grouped in 8 peergroups of 4 nodes each, and core nodes are grouped in one peer group 'Core'. Each node has one host connected to it and the number of calls generated is 60 calls per host.

The links used to interconnect the nodes to nodes, and nodes to hosts follow the same pattern as in the edge-core with 20 nodes topology. The core nodes, instead of simply being in connected in a ring-like fashion, have a couple of other inter-connections, allowing any core node to reach any other code node in one or two hops.



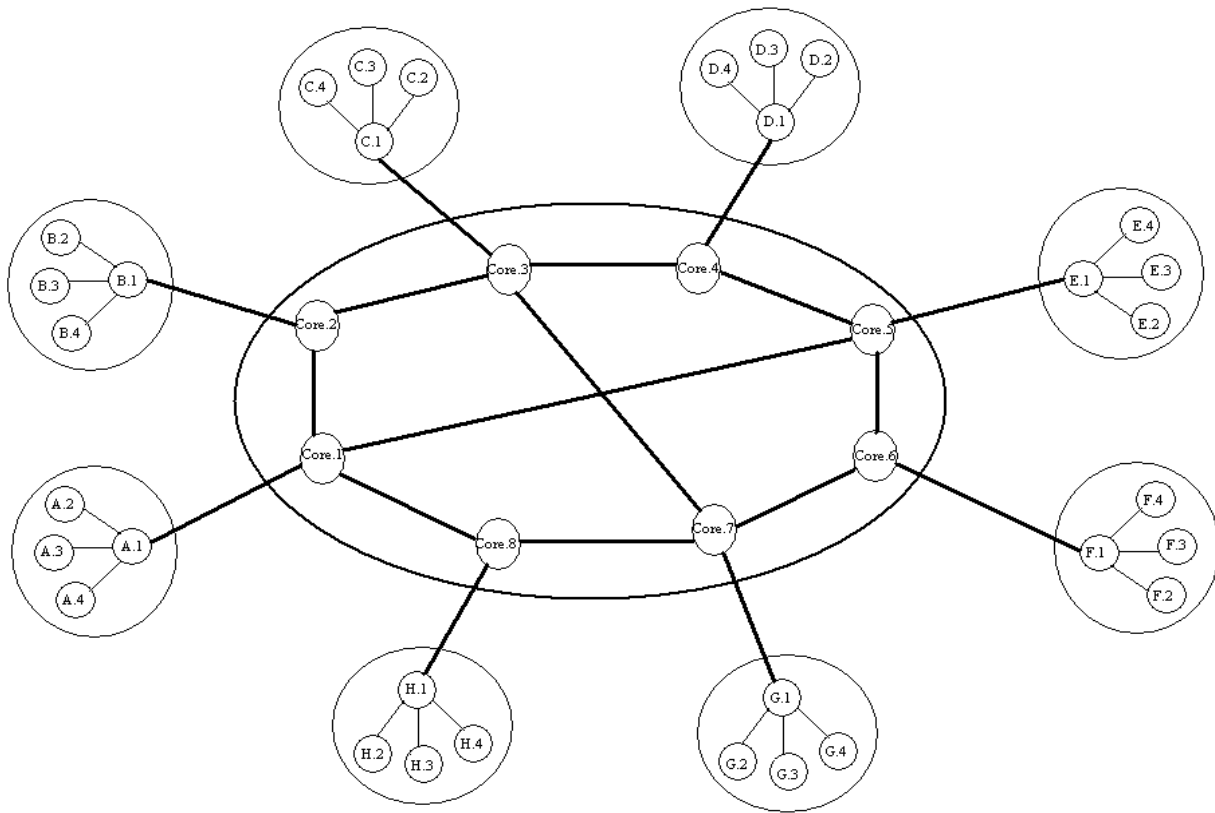


**Fig 3.2 Edge-Core 40 nodes**

### 3.2.2 Edge-core with 80 nodes

This topology (fig 3.3) is composed of 64 edge nodes and 16 core nodes with the edge nodes grouped in 16 peergroups of 4 nodes each, and core nodes in one peergroup. Each node has *one host* connected to it and the number of calls generated is *30 calls per host*. The interconnecting links follow the same pattern as in the Edge-core 40 node topology.

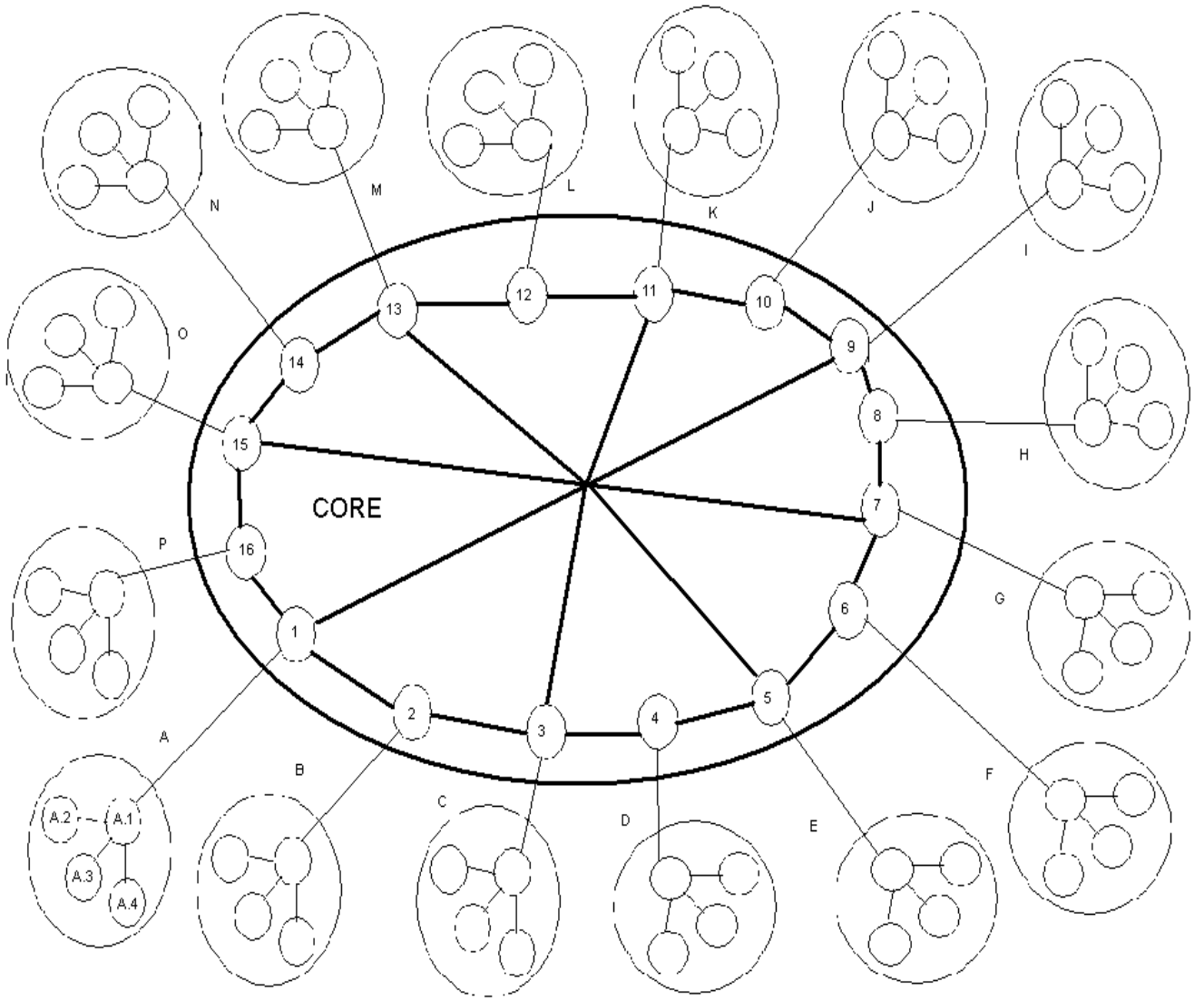


**Fig 3.3 Edge-Core 80 nodes**

### 3.3 Performance Metrics

The metrics of *primary* interest in this set of simulations are:

- Mean Call setup time
- Call success percentage
- Average Database size
- Convergence time

Along with these metrics, the other metrics such as Average number of hops, Average utilization percentage and PNNI data / flood are also monitored.

### 3.4 Results and Analysis

#### 3.4.1 Average Database size

Figure 3.4 gives the variation of average database size with increase in the number of nodes in the topology. The average Database size increases as the number of nodes is increased in the topology, as expected.

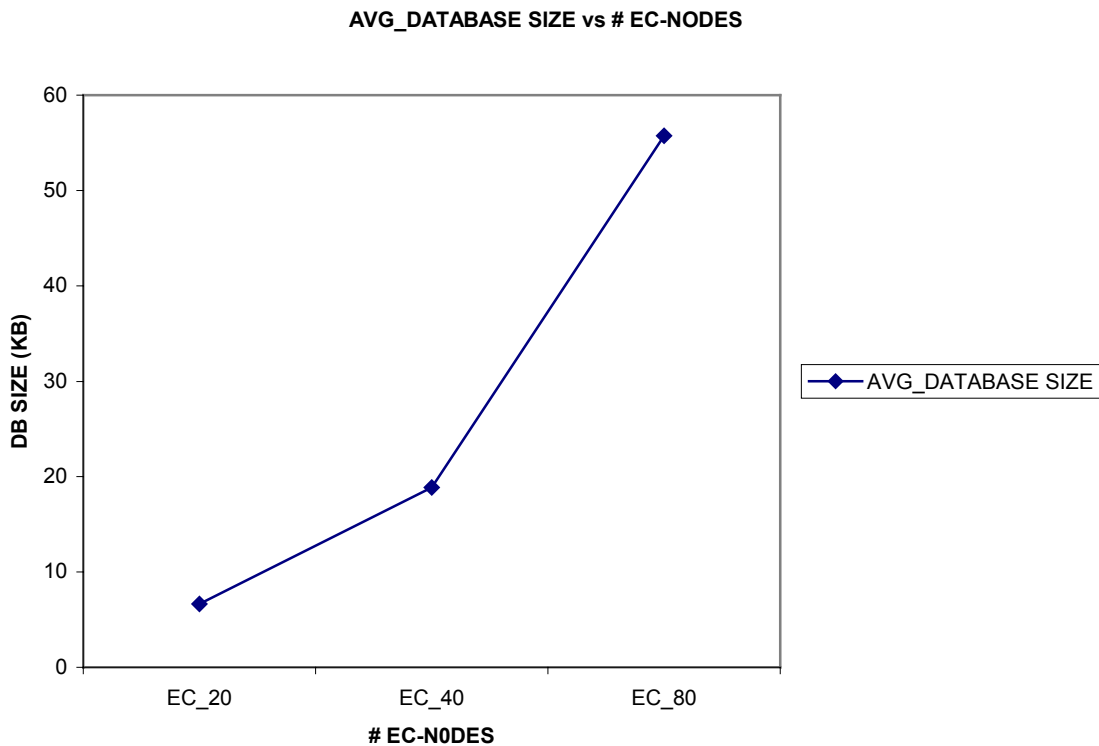


**Fig 3.4 Average database size vs. Topology size**

This is because each node has to record more connectivity information to other peergroups (more the number of nodes, more is the number of peergroups).

### 3.4.2 Call success percentage

Figure 3.5 gives the variation of call setup success rate as a function of the number of nodes in the edge-core topology. For any given load, the call success percentage tends to decrease with an increase in the size of the topology. The test topologies have been designed such that a call never fails due to lack of bandwidth; it fails only due to time outs (8 seconds) that occur when the link is down or when the peer node is very busy processing other calls.

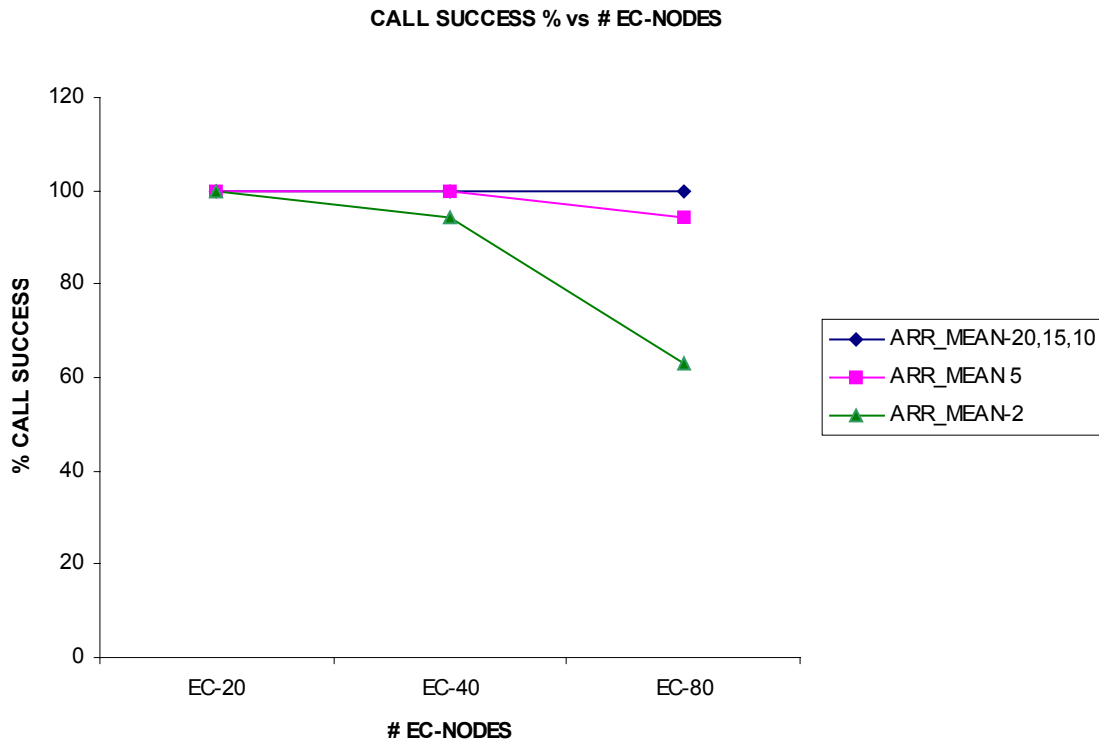


Fig 3.5 Call success rate vs. Topology size

The call success rate is fairly constant (nearly 100 percent) at light load for all topologies, but decreases as the load increases. The effect is more pronounced in a bigger topology. This is because the nodes receive calls at a higher rate than they can process the calls. For example, the core nodes serve as gateways for edge nodes, and hence for a larger topology the rate at which the core nodes receive calls is much higher than the rate at which core nodes in a smaller topology receives calls. Also, flood messages also increase call delay. This is because the flood messages are also queued and they consume processing resources. If the queue size were sufficiently large so that the waiting time of any call setup request exceeds 8 seconds, then the caller would be timed out because timer T303 would expire twice and the call would be cleared.

### 3.4.3 Mean Call setup time

Figure 3.6 gives the variation of mean call setup time as a function of the topology size. For any given load, the mean call setup time increases with an increase in the size of the topology. The term *light load* refers to call inter-arrival times of 20 secs, 15 secs and 10 secs, while *heavy load* refers to call inter-arrival times of 5 secs and 2 secs.

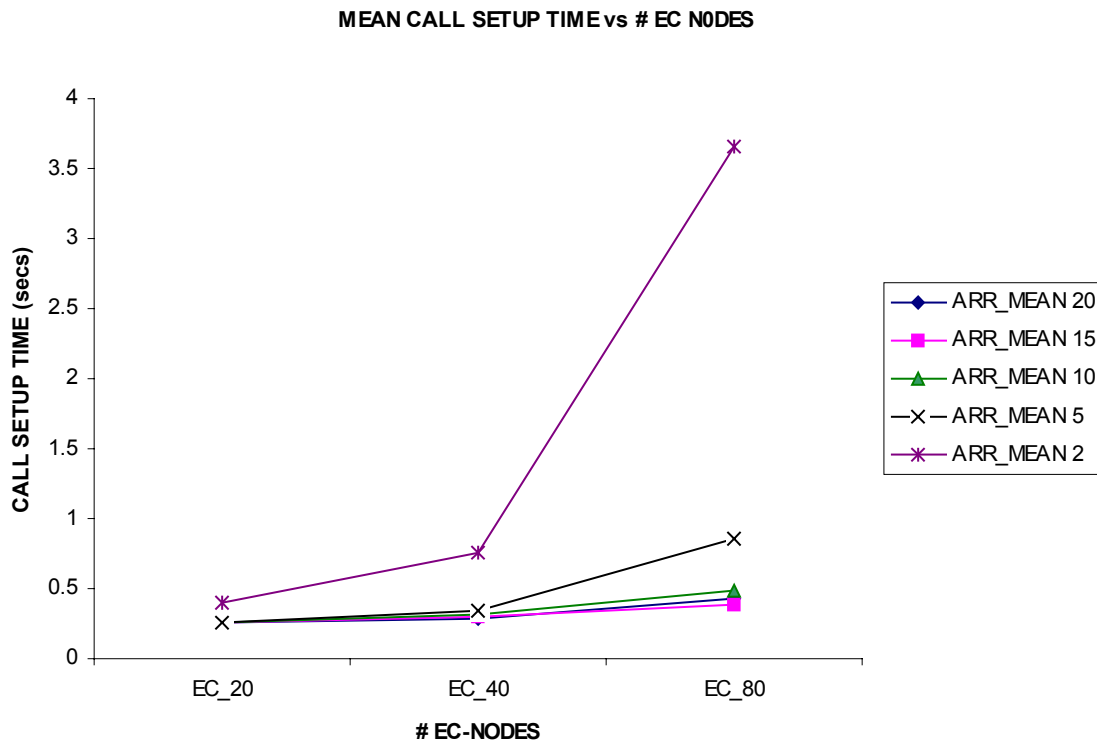
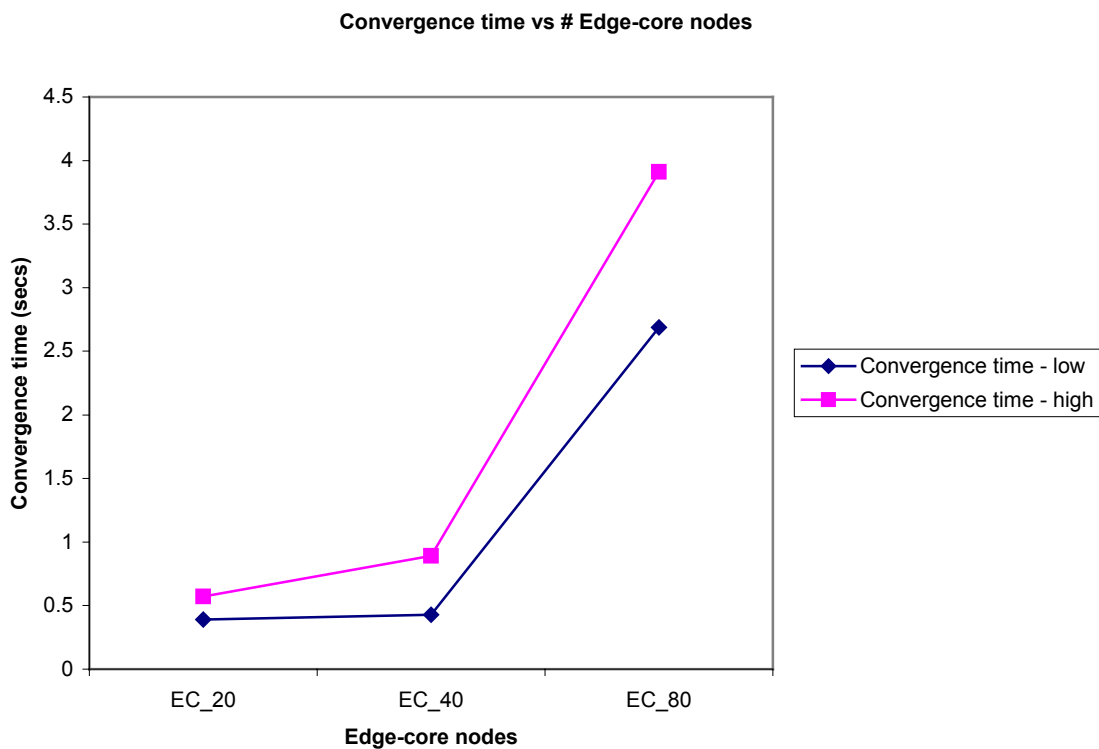


Fig 3.6 Mean Call setup time vs. Topology size

Under light load, the call setup time is mainly composed of the time taken to find a route; hence at light load, the call setup time is fairly a constant for all topologies. Under heavy load, the time a call has to wait in the queue before it gets processed becomes dominant. The time a call has to wait for service is much higher with a larger topology, because of the higher arrival rate to the core nodes (as seen above).

### 3.4.4 Convergence time

Figure 3.7 gives the variation of convergence time as a function of the number of nodes in the topology. Convergence time increases as the topology is increased in scale. This is because the number of nodes that has to converge is higher in a bigger topology.



**Fig 3.7 Convergence time vs. Topology size**

### 3.4.5 PNNI data

Figure 3.8 gives the variation of PNNI data / flood as a variation of topology size. As the number of nodes increases, so does the average database size; hence the average PNNI data/flood also increases.

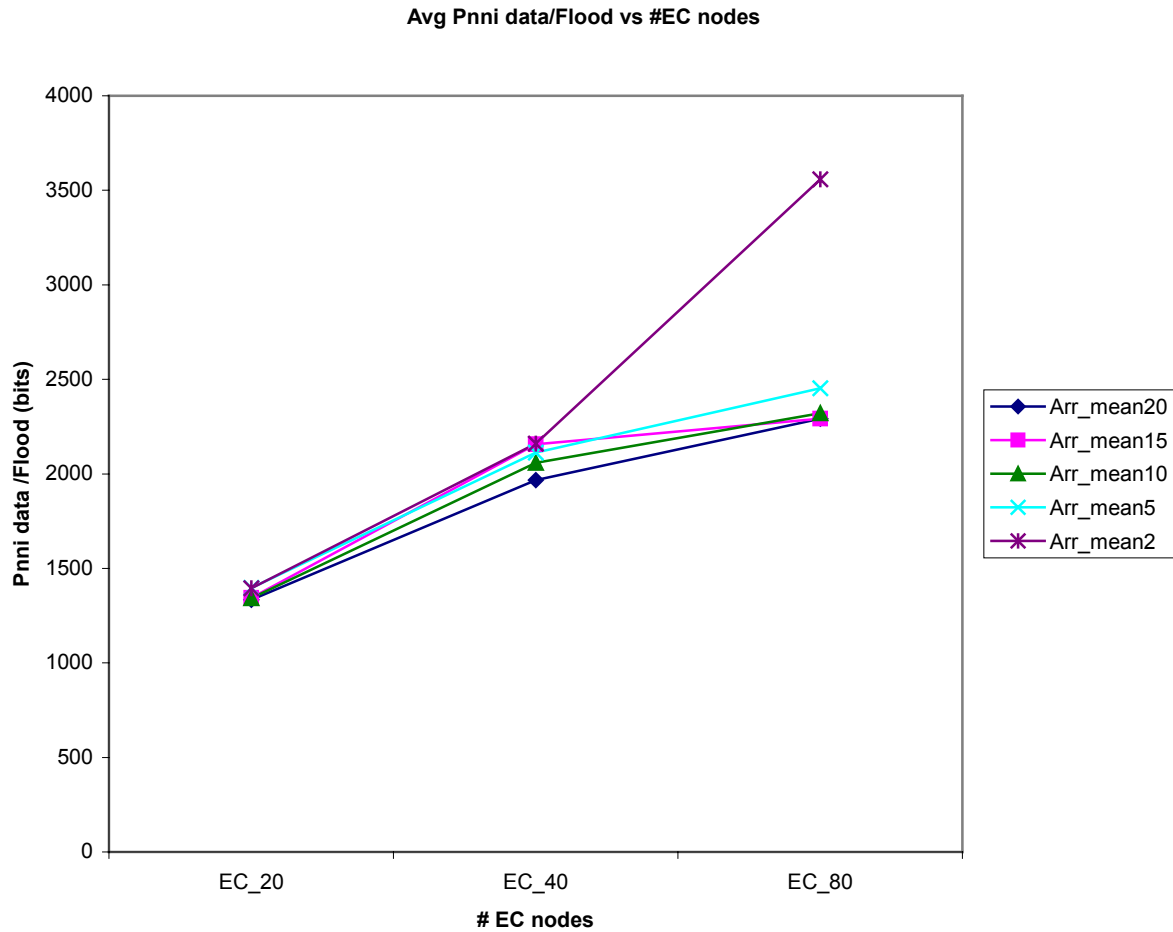


**Fig 3.8 PNNI data / flood vs. Topology size**

As load increases, *significant changes* occur at a faster rate, which results in the *PNNI Topology State Packets (PTSPs)* carrying more *PNNI Topology State Elements (PTSEs)*. Hence, the average value of PNNI data /flood increases with an increase in load.

### 3.4.6 Average Bandwidth Utilization percentage

Figure 3.9 shows average bandwidth utilization as function of both load and topology. For any given load, for similarly scaled topologies, the average utilization would be almost equal. The pattern as exhibited by the graph is due to the fact that the topologies exhibit significant differences.

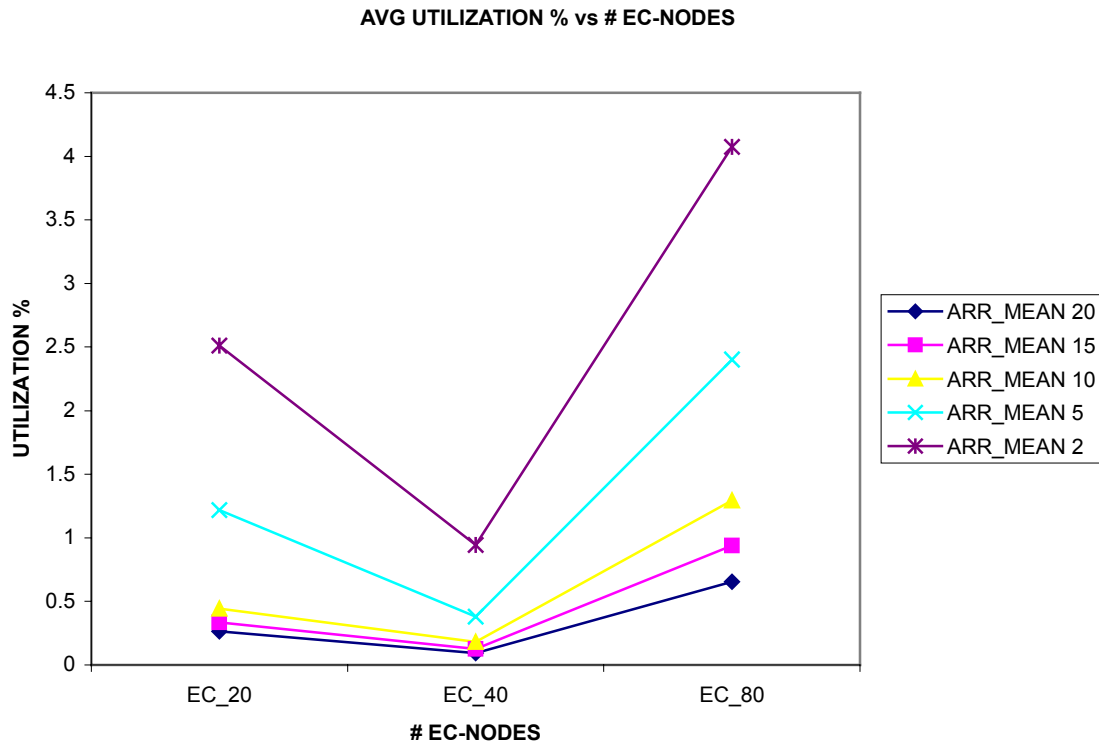


Fig 3.9 Average Utilization percent vs. Topology size

For example, EC-40 has a semi-full mesh core, all inter-connected through OC-12 links, which tends to decrease utilization percentage considerably. On the contrary, the EC-80 has a relatively less-densely interconnected core and hence the average utilization for EC-80 is higher when compared to that of EC-40.

### 3.4.7 Average number of hops

Figure 3.10 gives the variation of average number of calls with respect to topology size. In exactly similarly scaled topologies, the average number of hops per call would be the same. But, for practical purposes, exactly similar scaling of topologies is very difficult. Hence, the average number of hops can be expected to vary with the *maximum number of*



*hops* that any successful call has to take. In the test topologies, the possible values for hops are 2, 5 and 6 (for 20 nodes and 40 nodes), and 2, 5, 6 and 8 (for 80 nodes).

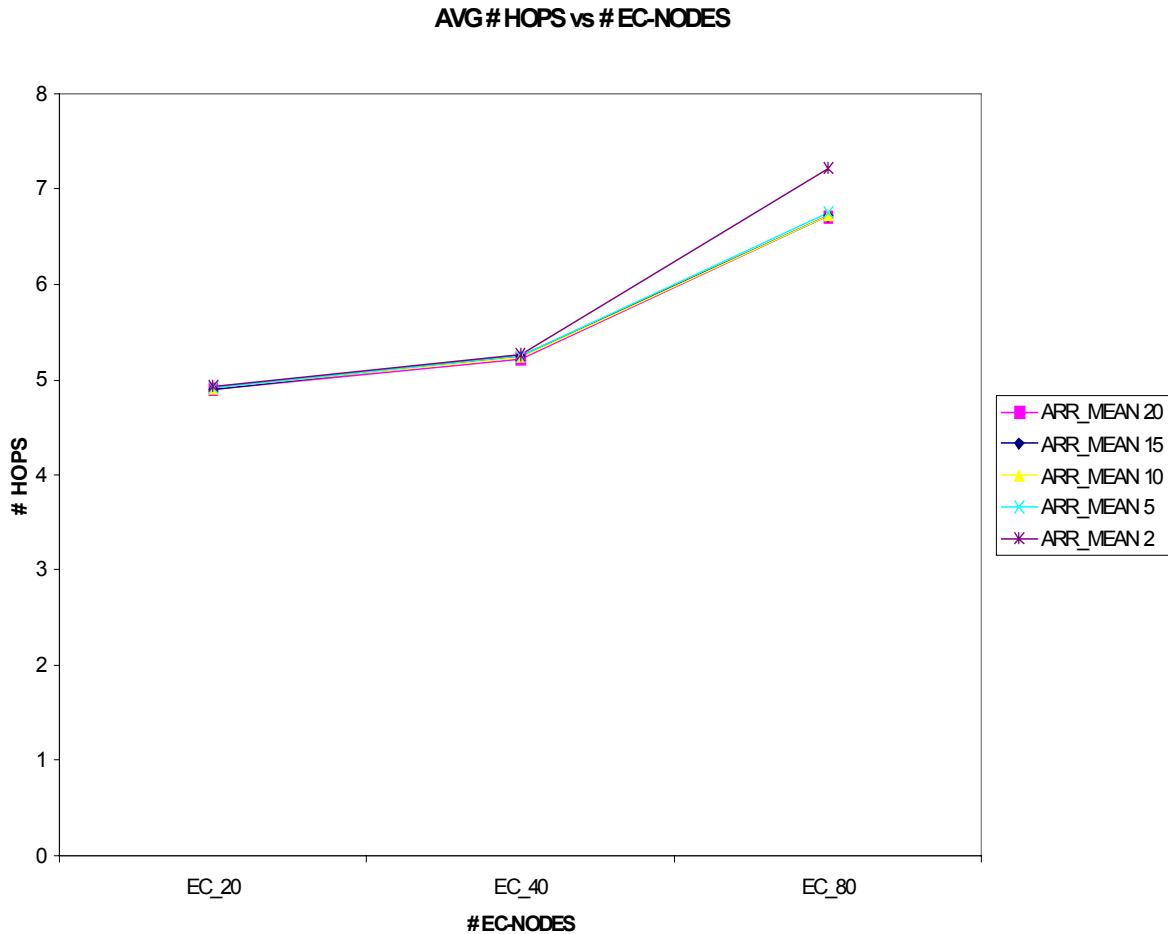


**Fig 3.10 Average hops vs. Topology size**

The variation in the number of hops for various loads is purely due to randomness in choosing the destination to setup a call.

### **3.5 Problems faced**

The following were the problems faced during the course of conducting the simulations listed above:

1. The topology could not be scaled beyond 80 nodes because the simulator core dumped even at light load beyond a topology size of 80 nodes. The simulations could have been run to completion at bigger topologies, but with a lesser number of calls/host. This would have given only a lesser (and insufficient) number of samples of the performance metrics for analysis to be conducted, the results of which would be biased due to the effect of variance in the sampled values. Hence, as a compromise, it was decided that the simulations would be based on roughly 2000 calls (64 hosts x 30 calls/host, 32 hosts x 60 calls/host, 16 hosts x 120 calls/host). Moreover, 30 calls/host was the maximum the simulator could be strained at high loads with 80 nodes.

### **3.6 Conclusion**

It can be thus concluded that as the topology is scaled in size for bandwidth-rich networks,

- Mean Call setup time increases
- Call success percentage decreases
- Average Database size increases
- Convergence time increases
- Average PNNI data / flood increases
- Average number of hops increases (in general, but depends on topology)

# Chapter 4

## Load test

### 4.1 Introduction

The aim of this test is to study the effect of varying the load (call arrival rate) on the various identified metrics. This is an important test for any topology, because it gives a rough idea on how much the network can be loaded before the values of performance metrics begin to degrade to unacceptable levels. The simulation results in this chapter are identical to those in chapter 3, but the results are presented to highlight the effects of load variations rather than network size.

### 4.2 Test topology

The simulations were run for mean call inter-arrival times of 20 seconds, 15 seconds, 10 seconds, 5 seconds and 2 seconds over Edge core topologies with:

- 20 nodes (same as in scalability test, fig 3.1)
- 40 nodes (same as in scalability test, fig 3.2)
- 80 nodes (same as in scalability test, fig 3.3)

### 4.3 Performance Metrics

The metrics of *primary* interest in this set of simulations are:

- Mean Call setup time
- Call success percentage
- Average Utilization percentage
- PNNI data / flood
- Average number of hops

Other metrics (like average data base size and convergence time) are load independent, and hence are not considered here

## 4.4 Results and Analysis

### 4.4.1 Mean Call setup time

Figure 4.1 gives the variation of mean call setup time with respect to variation in load.

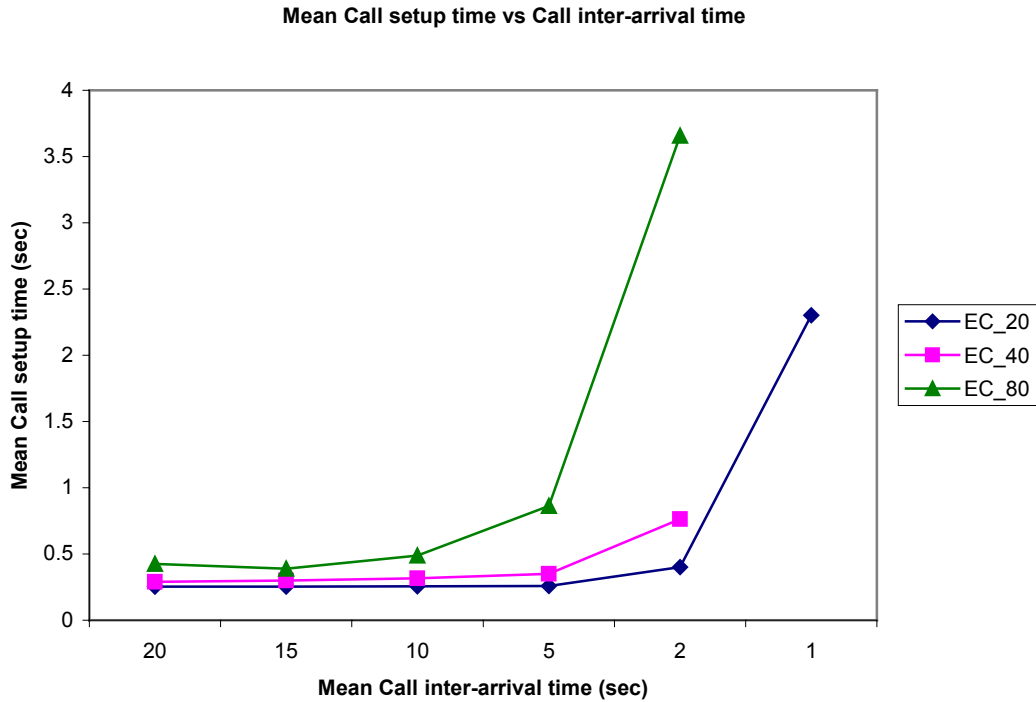


**Fig 4.1 Mean Call setup time vs. Load**

The mean call setup time increases with increase in load because the call arrival rate to each node keeps increasing, and hence the time each call has to wait (in the queue) for service also increases. This effect is more pronounced in topologies with a larger number of nodes. The mean call setup time is purely a function of call processing rate of the nodes.

### 4.4.2 Call success percentage

Figure 4.2 gives the variation of call success percentage as a function of load. The call success percentage decreases as load increases. This is because the rate of call arrival to any node is so high, that some calls have to wait for a very long time before they get timed out and the call fails.

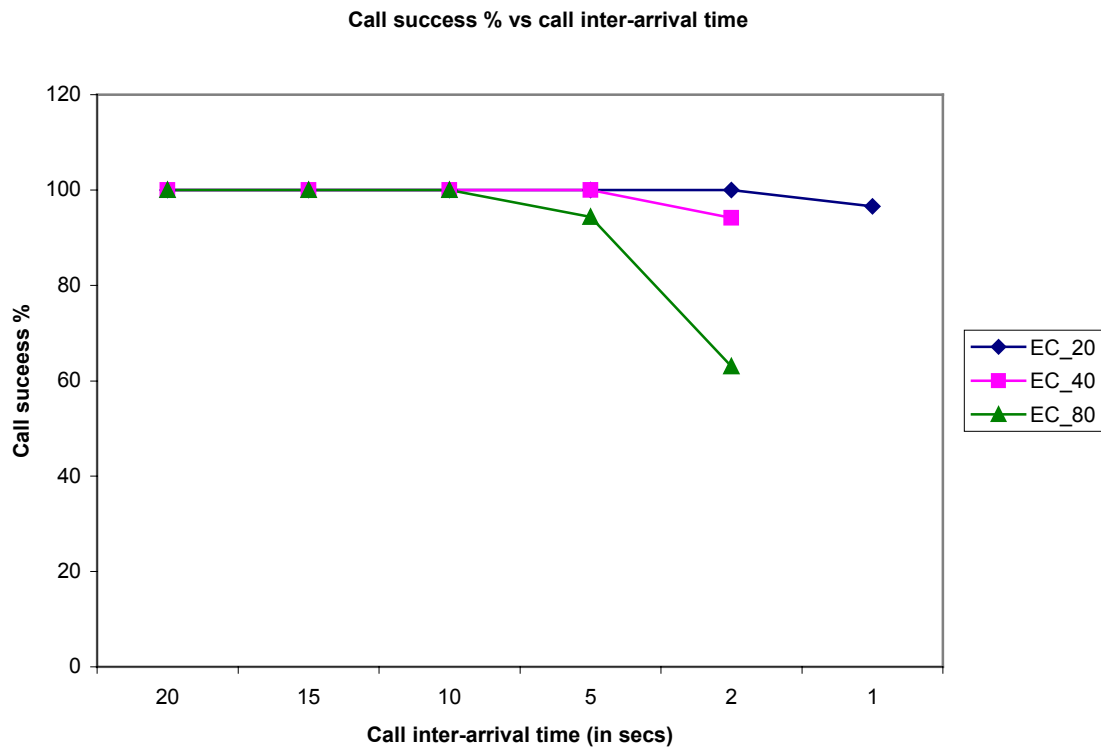


**Fig 4.2 Call success rate vs. Load**

The call success rate is again purely a function of the call-processing rate of the nodes; the link bandwidth is always sufficient to handle all the calls generated, and hence lack of link bandwidth never occurs to cause a call failure.

#### **4.4.3 Average bandwidth utilization percentage**

Figure 4.3 shows the variation of average bandwidth utilization percentage with change in load. The average utilization increases as the load increases, since more calls are active and consuming link bandwidth.

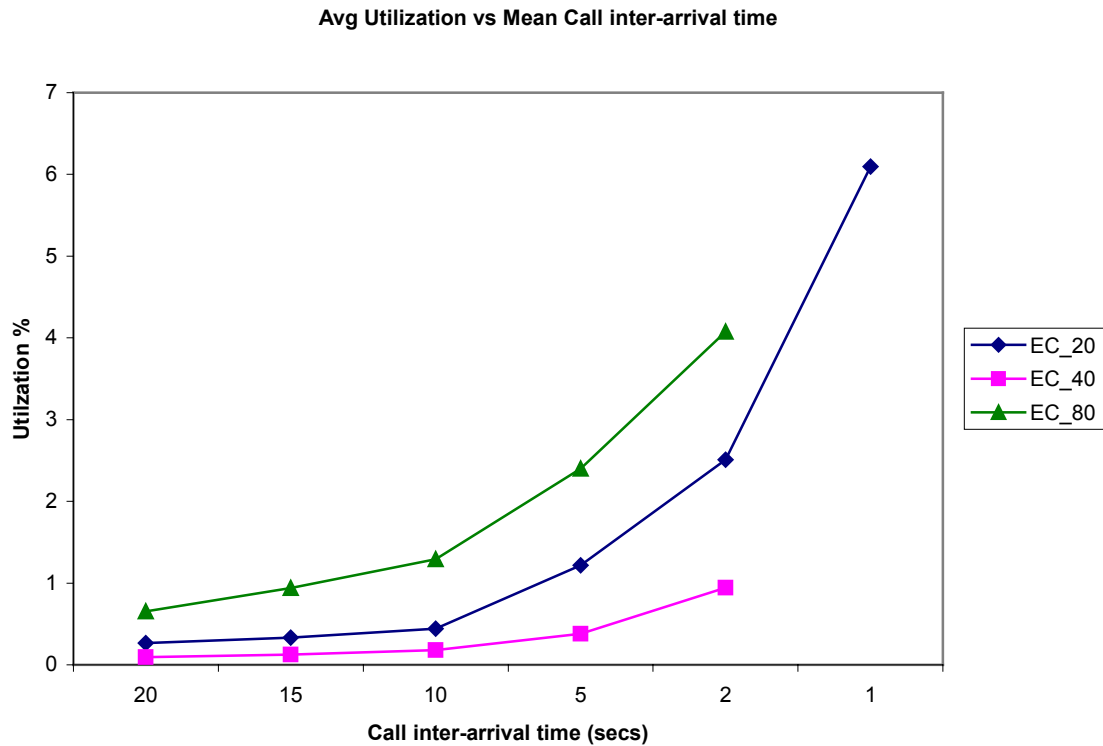


**Fig 4.3 Average Utilization percentage vs. Load**

It can be seen (and has already been shown – figure 3.9) that the variation of the utilization percentage with respect to topology size does not show a monotonic trend due to topological dissimilarities during scaling from one size to another.

#### **4.4.4 PNNI data/ Flood**

Figure 4.4 (a)-(c) give the variation of the average PNNI data / flood with respect to variation in load for the three test topologies – 20 nodes, 40 nodes and 80 nodes. The PNNI data (low, high and average) have been normalized to PNNI data /flood (bits /flood). This gives a better picture of how much PNNI data is flooded on an average.

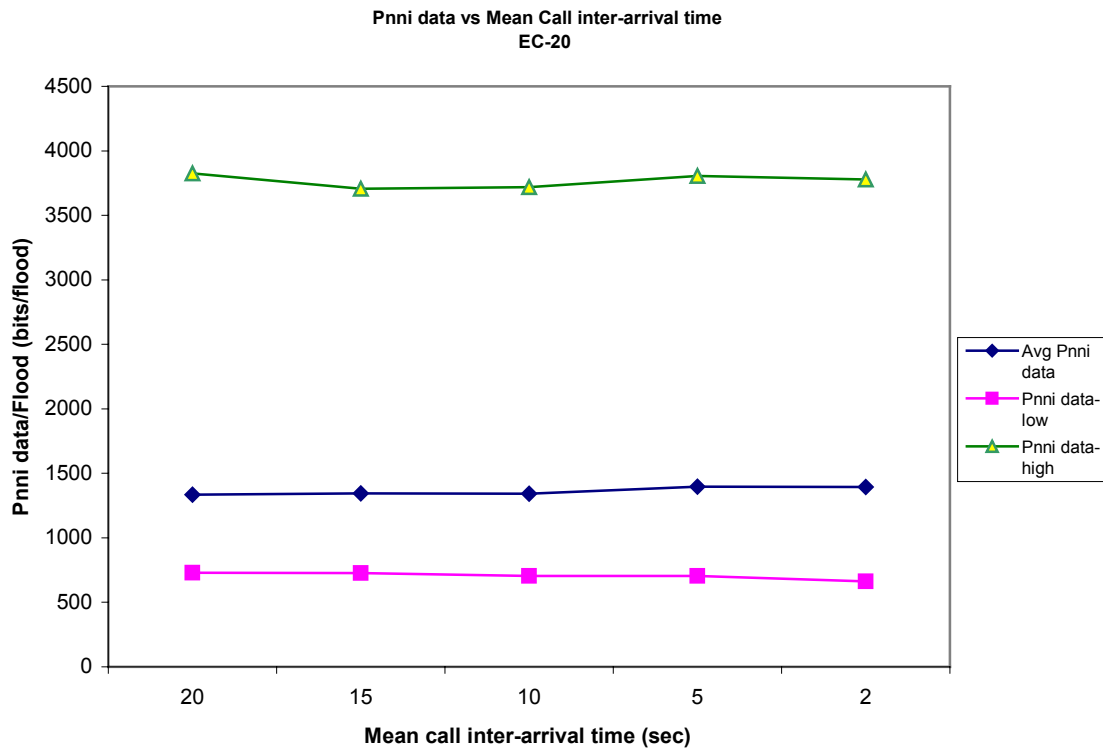


**Fig 4.4(a) PNNI data/Flood vs. Load**

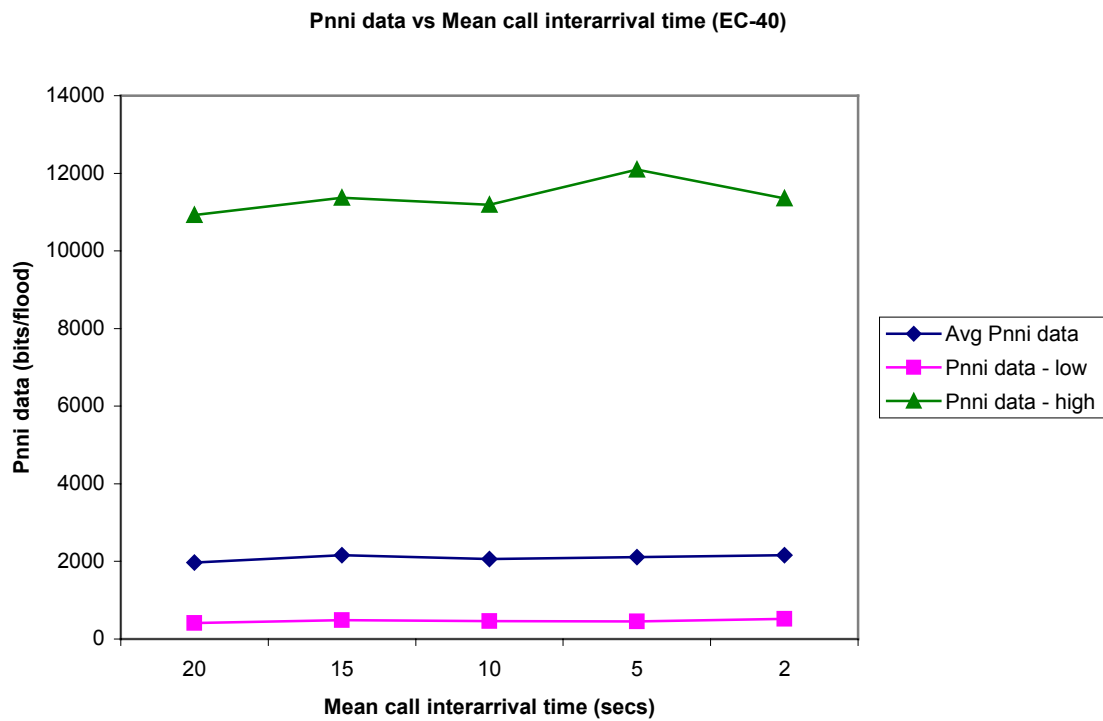


**Fig 4.4(b) PNNI data/Flood vs. Load**

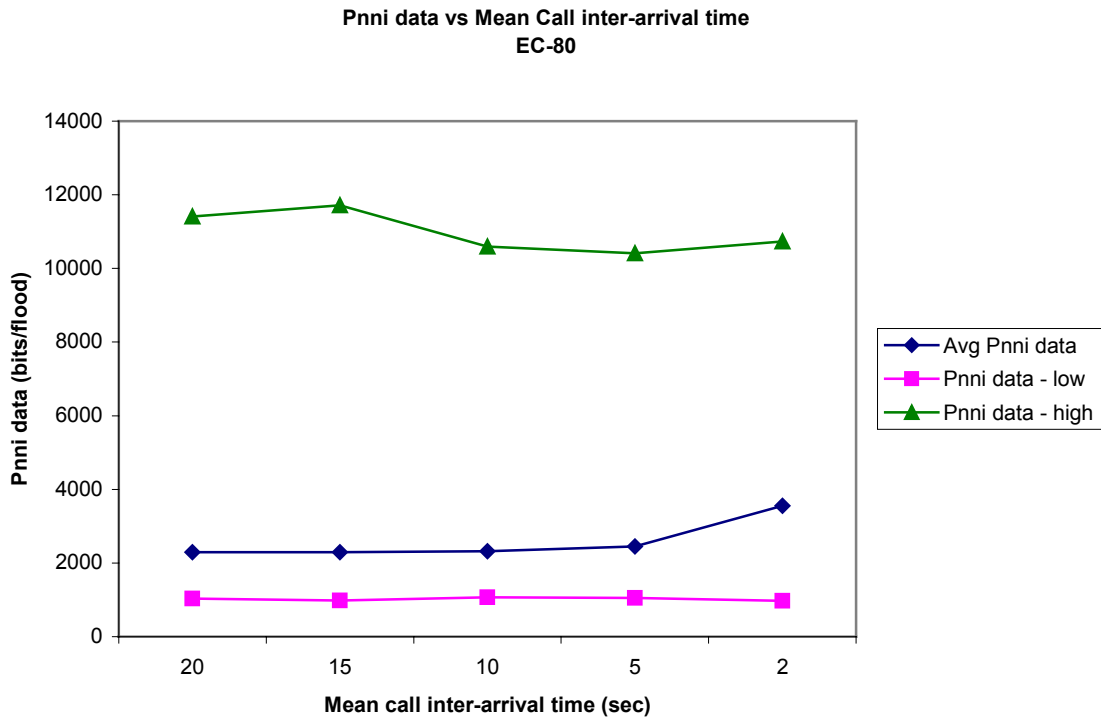


**Fig 4.4(c) PNNI data/Flood vs. Load**

The average PNNI data/flood for both EC-20 and EC-40 is almost constant for all loads, with a very small increase with increase in load. This is because the higher rate of significant changes at higher loads causes the nodes to pack a larger number of PTSEs into the PTSPs before flooding the PTSPs. The increase of average PNNI data with increasing load is very prominent in EC-80 for a mean call inter-arrival time of 2 sec

#### **4.4.5 Average number of hops**

Figure 4.5 depicts the variation of average number of hops with respect to load. The average number of hops can be expected to increase with an increase in load. This is because, as the load is increased, the *shortest path link* may not be able have sufficient bandwidth capacity to support all the calls. The call is then routed through another link, which will not be the shortest path. Thus the average number of hops can be expected to increase.



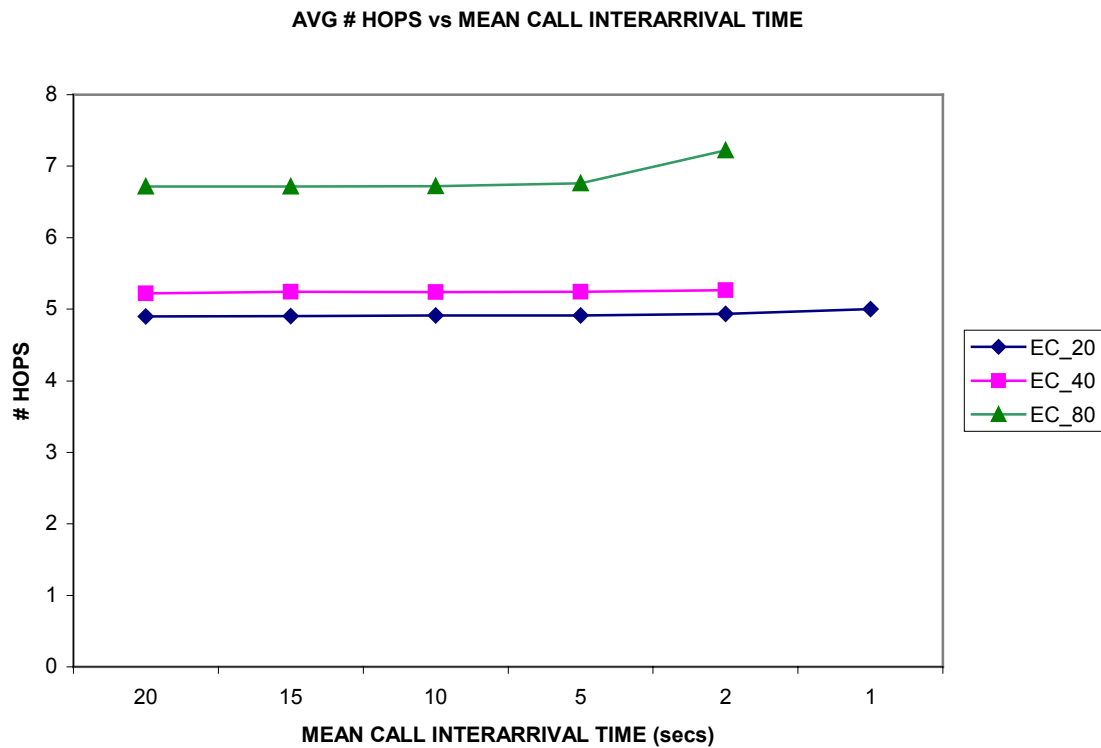


**Fig 4.5 Average hops vs. Load**

Surprisingly, the average number of hops seem to be almost unaffected by the variation in load. This is because that the topologies have been constructed such that link bandwidth is more than adequate to support all the calls. The slight variation that is seen for 80 nodes at high load is because more calls fail at higher loads in bigger topologies, which affects the value of the average number of hops.

## 4.5 Problems faced

The following were the problems faced during the course of these sets of simulations:

1. The simulator encountered out-of-memory problems and timer related problems at very high loads (call arrival rate of 1 call per second or more) for topology sizes with 40 nodes or more. Hence it was decided to strain the simulator only up to a call arrival rate of 0.5 calls per second (call inter-arrival time of 2 seconds) for all the test topologies.

## 4.6 Conclusion

It can be thus concluded that as the load in a bandwidth-rich network is increased,

- Mean Call setup time increases
- Call success percentage decreases
- Average link utilization percentage increases
- Average PNNI data / flood increases (only in large-sized networks)
- Average number of hops remains unchanged (in general, but depends on topology)

# Chapter 5

## Effect of Peergrouping test

### 5.1 Introduction

The aim of this test is to study the effect of peergrouping on the performance of the network. This test enables us to determine the topology that gives the best performance of the desired metrics, for a given fixed number of nodes.

### 5.2 Test topology

All the test topologies constructed for this set of simulations are Cluster topologies with 160 nodes and 2 levels of hierarchy. Inter-Peergroup links are all OC-12 links, Intra-Peergroup links are all OC-3 links, and the hosts are connected to the nodes through 10 Mbps links. In the figures for the topologies, a filled circle represents the leader of each peergroup. The hosts in the network generate 25 calls each.

#### 5.2.1 Cluster 4x40

This topology consists of 160 nodes, grouped into 4 clusters (Peer groups), each with 40 nodes. The 40 nodes are further grouped into 10 *mini-clusters* of 4 nodes each. In figure -5.1 the entire intra-peergroup connections are not shown; instead, the interconnections from only one mini-cluster to all other mini-clusters are shown. It can be seen that *not all* mini-clusters are connected to one another. Each mini-cluster has 7 links emanating from it. The remaining intra-peergroup connections are constructed in a similar fashion.

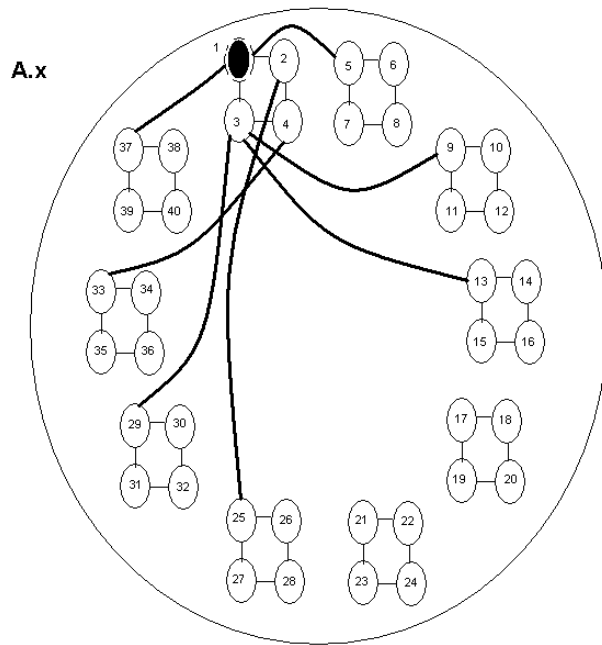


**Fig 5.1 4x40 Intra-Peergroup connections**

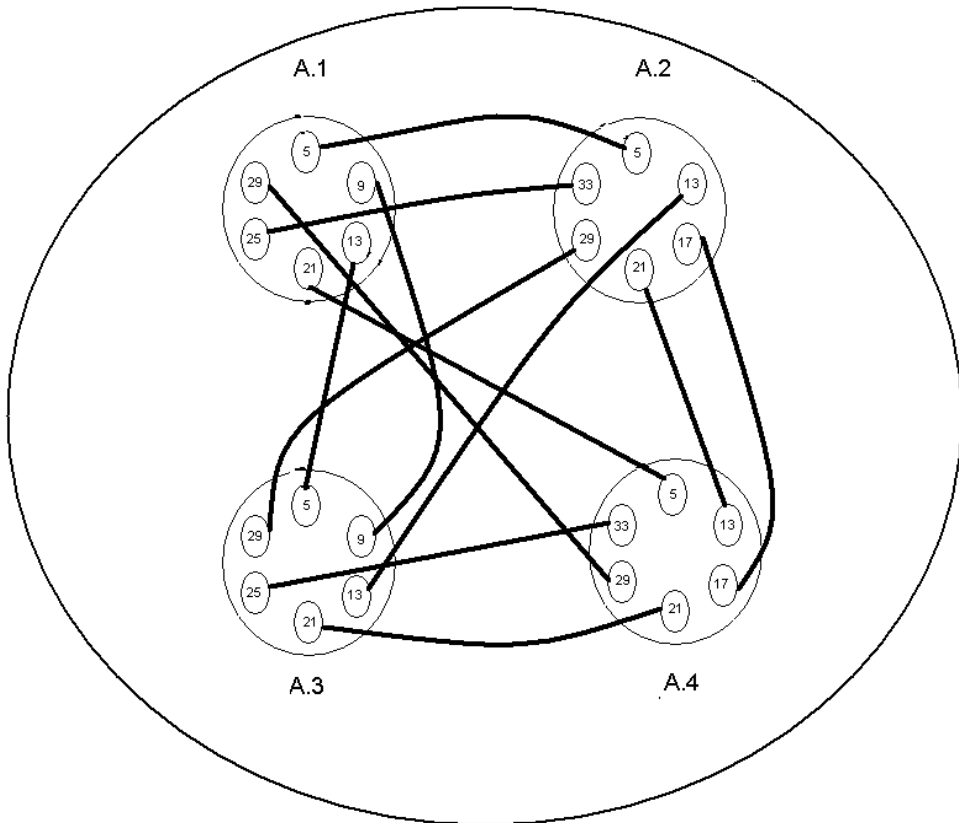


**Fig 5.2 4x40 Inter-Peergroup connections**

As shown in figure 5.2, the border nodes in each peergroup are identified as 5,9,13,21,23 and 29 (for Peergroups A.1 and A.3) and 5,13,17,21,29 and 33 (for Peergroups A.2 and A.4). Each border node has one link originating from it.

### 5.2.2 Cluster 5x32

This topology consists of 5 clusters (peergroups) each with 32 nodes in it. There are 8 mini-clusters in each peergroup. Figure 5.3 is a partial representation of the intra-peergroup connections. The entire interconnection can be constructed following the same pattern as shown in fig 5.3.

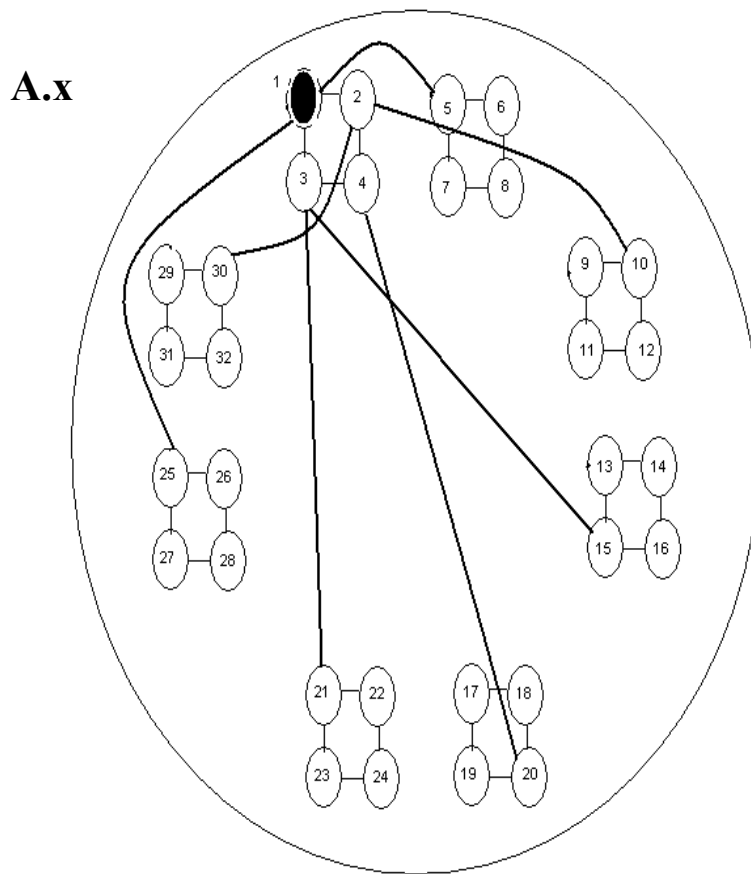


**Fig 5.3 5x32 Intra-Peergroup Connections**

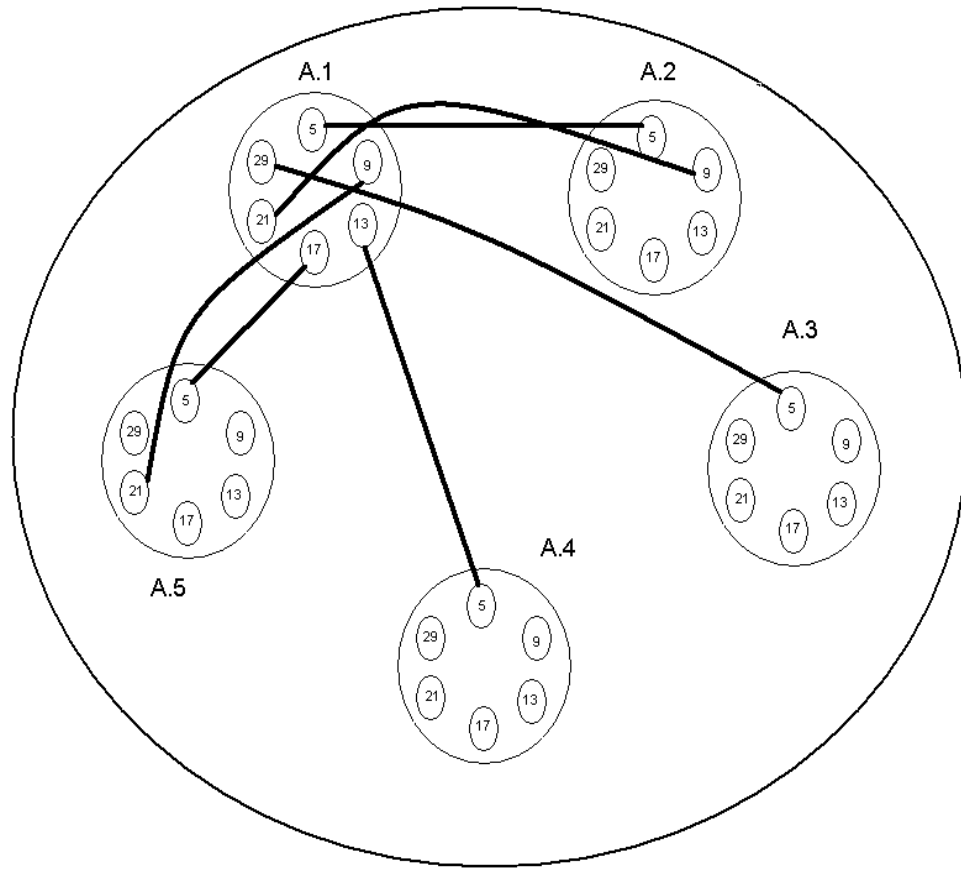


**Fig 5.4 5x32 Inter-Peergroup connections**

The border nodes are identified as 5,9,13,17,21 and 29. Fig 5.4 gives only the partial interconnections between various peergroups. The entire topology can be constructed by having 6 links originate from each peergroup and by following the same pattern as Fig-5.4.

### **5.2.3 Cluster 8x20**

This topology consists of 160 nodes grouped in 8 clusters (Peer groups), each with 20 nodes in it. The 20 nodes in each peergroup are grouped as 5 mini-clusters of 4 nodes each. Each node has one intra-peergroup link originating from it. Fig 5.5 is a complete representation of the intra-peergroup interconnections in the topology.

**A.x**

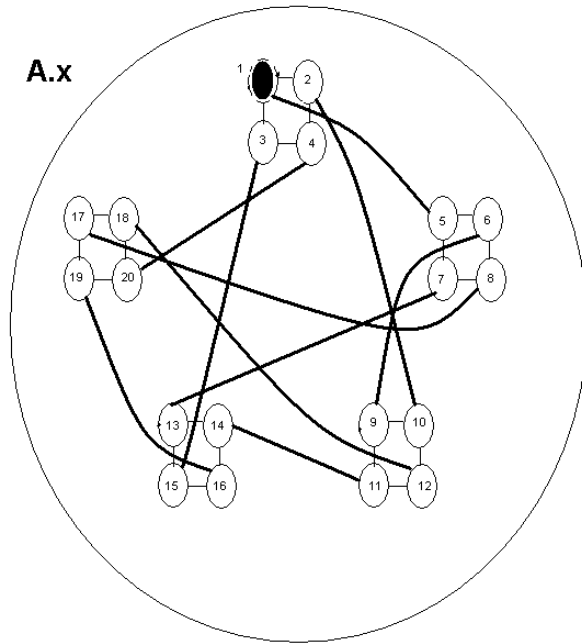


**Fig 5.5 8x20 Intra-Peergroup connections**

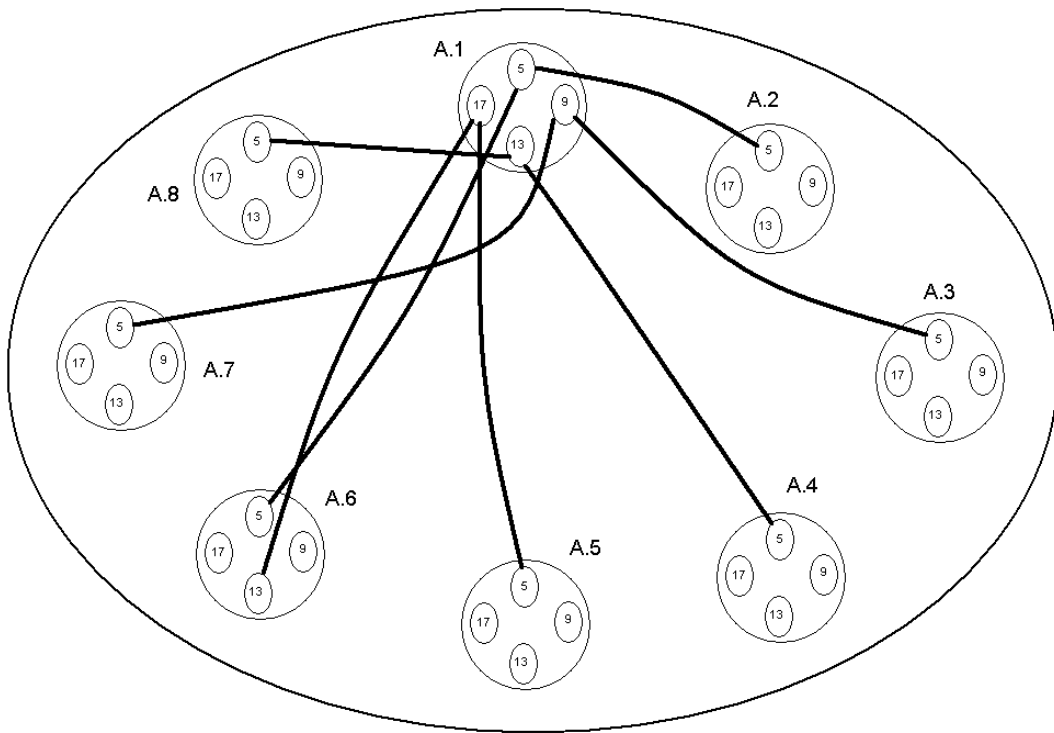


**Fig 5.6 8x20 Inter-Peergroup connections**

The border nodes are identified as 5,9,13 and 17. Fig 5.6 is an incomplete representation of the fully connected network. By configuring each border node to have two inter-peer group links originate from it, and by following the same patter as in Fig 5.6, the topology can be completely constructed.

### 5.2.4 Cluster 10x16

This topology consists of 160 nodes grouped into 10 clusters (Peer groups), each with 16 nodes in it. The 16 nodes are further grouped as 4 mini-clusters of 4 nodes each. Fig 5.7 gives complete details about the intra-peer group connections.

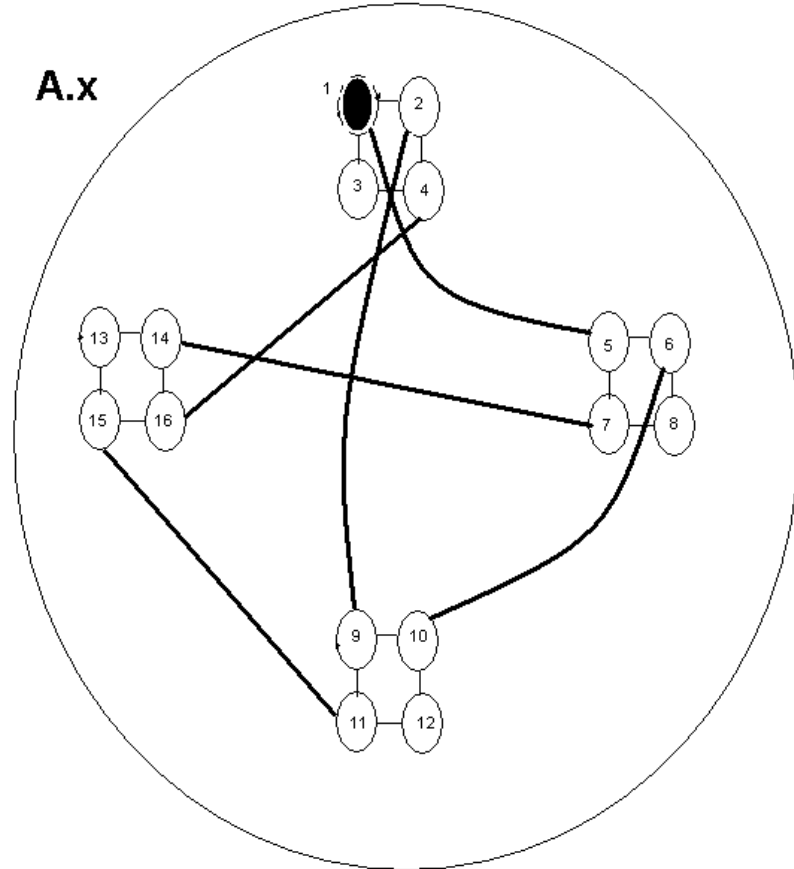


**Fig 5.7 10x16 Intra-Peer group connections**



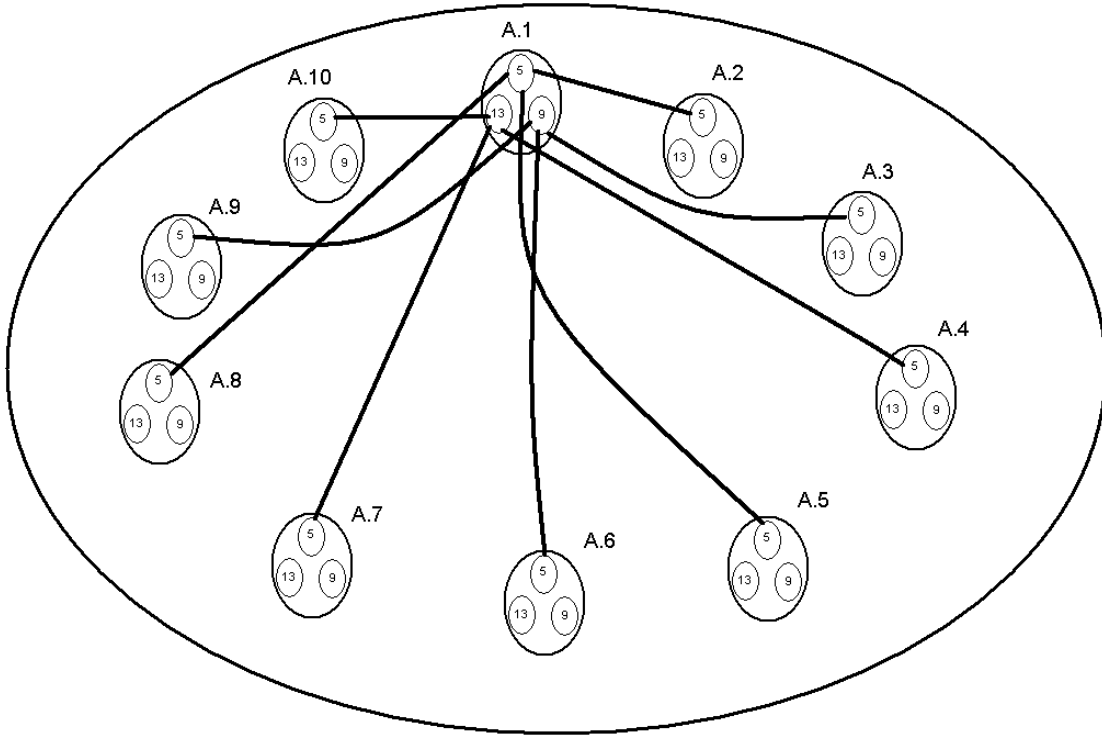


**Fig 5.8 10x16 Inter-Peergroup connections**

The border nodes are identified as 5, 9 and 13. As the number of peergroups increase, the inter-peergroup interconnections become more and more complex. Fig 5.8 is an incomplete representation of the inter-peergroup interconnections. The entire topology can be constructed by having one interconnection from one peergroup to all other peergroups.

### **5.2.5 Cluster 16x10**

This topology consists of 160 nodes grouped as 16 clusters (Peer groups), each with 10 nodes. This topology is slightly different from the other test topologies in this set of simulations in that it has the 10 nodes in each peergroup grouped into 2 mini-clusters of 5 nodes each. The mini-clusters are interconnected through 3 links. Fig 5.9 gives a complete view of the intra-peergroup interconnections.

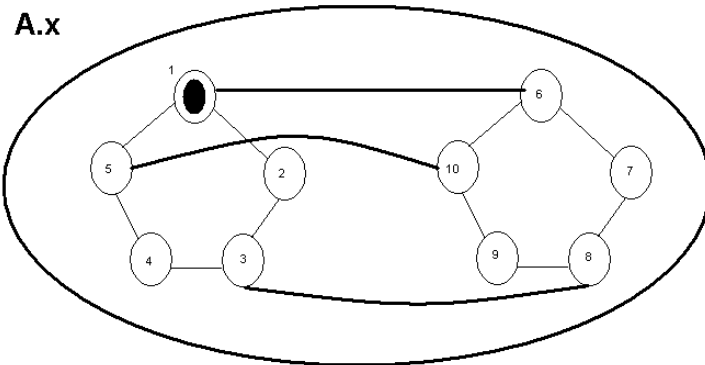


**Fig 5.9 16x10 Intra-Peergroup connections**

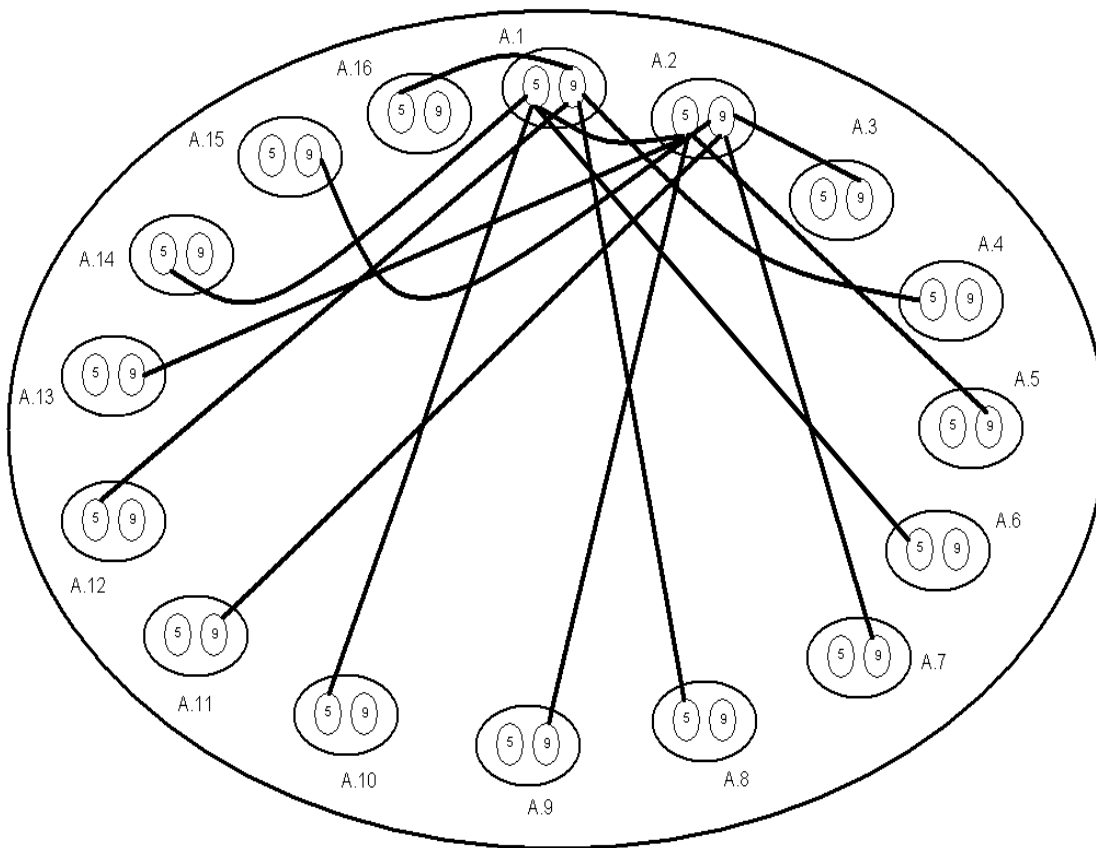


**Fig 5.10 16x10 Inter-Peergroup connections**

The border nodes are identified as 5 and 9. Fig 5.10 gives a partial representation of the actual inter-peergroup interconnections in the topology. The inter-peergroup interconnections can be completed by following the pattern exhibited by the partial interconnections.

## 5.3 Performance Metrics

The metrics of *primary* interest in this set of simulations are:

- Mean Call setup time
- Call success percentage
- Average Database size
- Convergence time

Along with these metrics, the other metrics such as Average number of hops, Average utilization percentage, total floods and PNNI data / flood are also monitored.

## 5.4 Results and Analysis

### 5.4.1 Convergence time

Figure 5.11 shows the variation of convergence time with respect to the number of peergroups. As the number of peergroups increases, we can expect the convergence time to decrease. There is a convergence number associated with each peergroup, which gives the number of nodes that each member in the peergroup has to converge with. This number is the sum of intra-peergroup links and the inter-peergroup links (links that the border nodes share with the border nodes of other peergroups); the number of links (and hence the convergence number) has a direct bearing on the convergence time. The convergence time is composed of 2 parts: intra-peergroup convergence time, and inter-peergroup convergence time. If the number of Peergroups increases (for a fixed total number of nodes in the topology), the number of intra-peergroup links decreases, while the number of inter-peergroup links increases; hence the convergence time keeps decreasing as the number of peergroups increases, until a point where the increase in inter-peergroup links more than offset the decrease in intra-peergroup links.

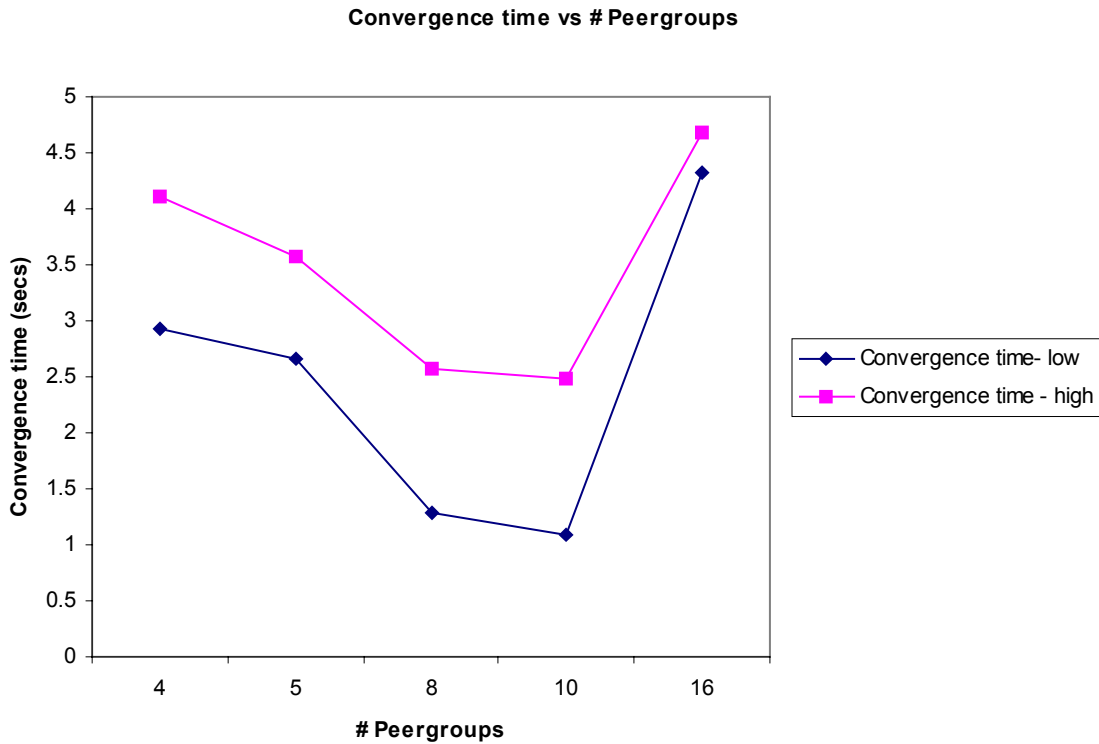


**Fig 5.11 Convergence time vs. Peergroups**

In the simulations conducted, the convergence time keeps decreasing as the number of topology moves from 4x40 to 10x16, but increases at 16x10. For example, in 10x16 each node has to converge with 16 other nodes within the same peergroup, while it needs to converge with only border nodes in 10 other peergroups. But in 16x10, the intra-peergroup convergence number is only 10, while the inter-peergroup convergence is 16. In this case, inter-peergroup convergence takes longer than intra-peergroup convergence. This validates the hypothesis just stated.

### 5.4.2 Mean Call setup time

Figure 5.12 shows the variation of mean call setup time as a function of number of peergroups. The mean call setup time decreases as the number of peergroups increases (for a fixed total number of nodes). The call setup time can again be broken down into three components: time taken for (source) intra-peergroup routing, time taken for inter-peer group routing and time taken for (destination) intra-peergroup routing (ignoring variation in the process time taken at each node, since the process time at each node is

assumed to be the same). Since the destination and source intra-peergroup routing are similar events, they shall be referred as simply intra-peergroup routing.

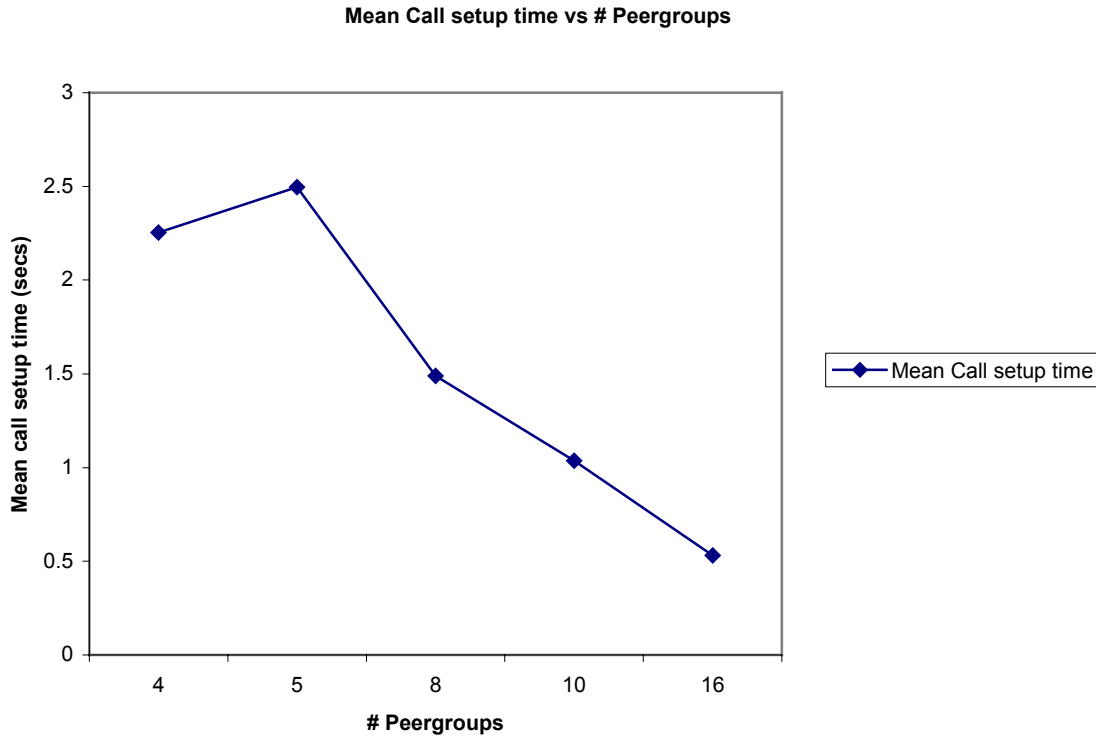


**Fig 5.12 Mean Call Setup time vs. Peergroups**

With a lesser number of peergroups, intra-peergroup routing is more complex than inter-peergroup routing. This is because with lesser number of peergroups, there are more nodes in each peergroup, thus making routing slightly more complex. The topology has been designed such that inter-peergroup routing is trivial i.e. every peergroup has at least one direct link to every other peergroup, and the inter-peergroup routing time is almost a constant. Hence the call setup time keeps decreasing as the number of peergroups increases, until it reaches a point, where the inter-peergroup routing times starts to dominate.

In the simulations conducted, the mean call setup time decreases with an increase in the number of peergroups. This validates the hypothesis just stated (the limitations of the simulator did not facilitate running a simulation with a very large number of peergroups,

to show that the inter-peergroup routing time becomes a significant factor influencing the call setup time).

There is an apparent tradeoff between cost and call setup time - by increasing the number of peergroups, the mean call setup time does decrease; but by constructing a topology such that the inter-peergroup routing is trivial, the number of high bandwidth links has been increased considerably (at least one high bandwidth link between each pair of peergroups), which adds to the cost.

### **5.4.3 Call Success percentage**

Figure 5.13 shows the variation of call success percentage as a function of number of peergroups. The call success rate is closely related to the mean call setup time; as the mean call setup time increases, the call success percent decreases - more calls are rejected since the nodes (either transit nodes or destination nodes) are busy. In these simulations, the calls do not fail because of lack of capacity in the links.

As the number of peergroups increases, the mean call setup time decreases; hence the call success percentage increases. Moreover, more the number of peergroups, lesser number of nodes are abstracted into a peergroup advertisement, which increases reachability, and hence the call success percentage increases for this reason as well.

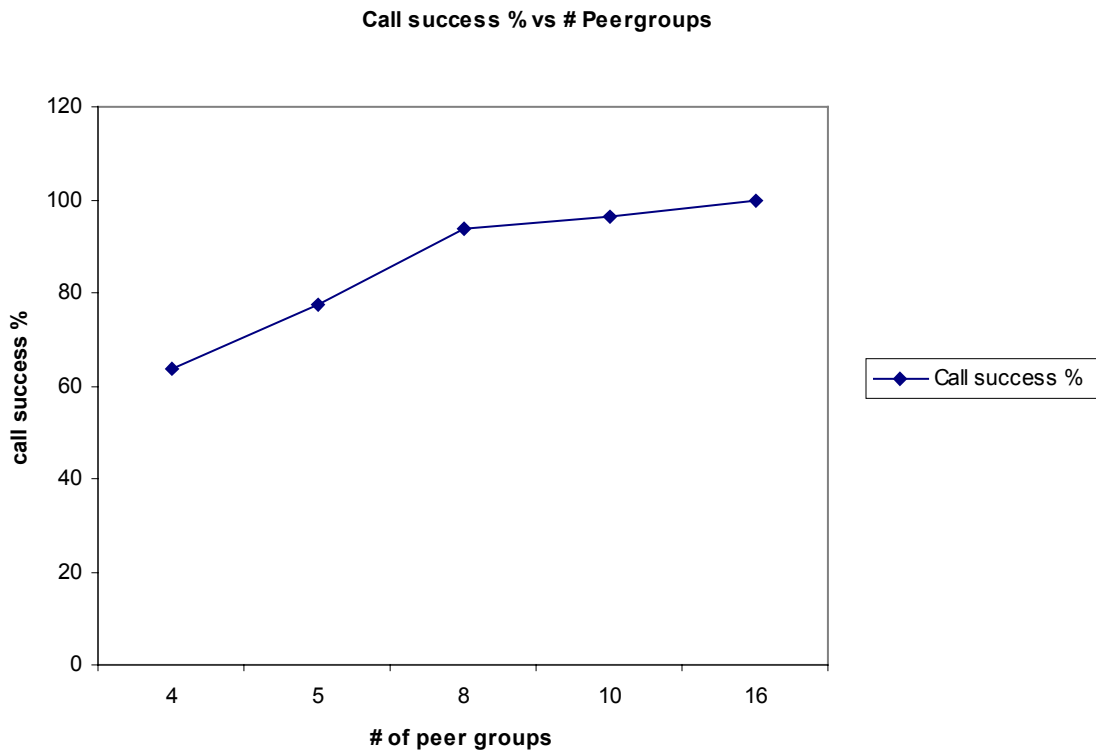


**Fig 5.13 Call success rate vs. Peergroups**

#### **5.4.4 Average Database size**

Figure 5.14 shows the variation of average database size as the number of peergroups is varied. The average database size decreases as the number of peergroups increases (up to a point). This is because as the number of peergroups increases, the database has to record (contain) only lesser information about its neighbors. This is closely related to convergence number. The information contained in the database can be broken down into two components - nodes within the same peergroup and border nodes.

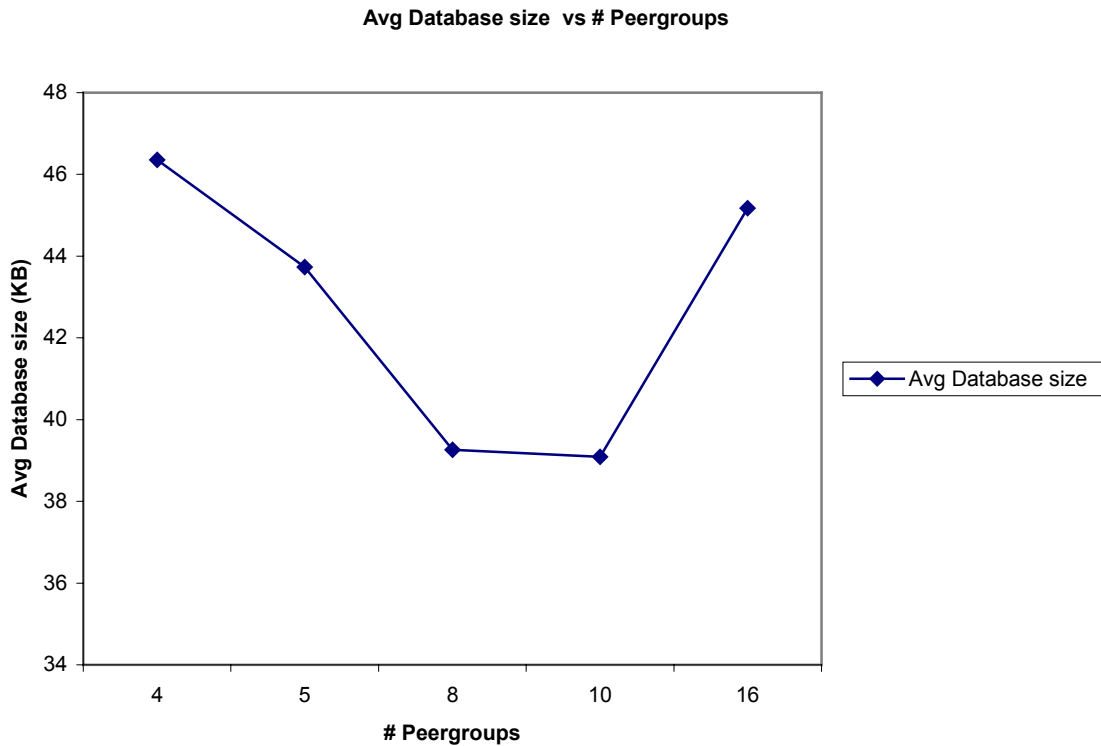


**Fig 5.14 Average Database size vs. Peergroups**

The database size keeps decreasing until a point after which the database size increases. This is because the number of border nodes becomes significant when compared to the number of nodes within the same peergroup. This trend can very well be seen from the results of the simulations

### 5.4.5 Average number of hops

Figure 5.15 shows the variation of average number of hops as a function of the number of peergroups. The average number of hops is simply a measure of how identical each topology is, which in turn is a measure of the confidence level of the results obtained.



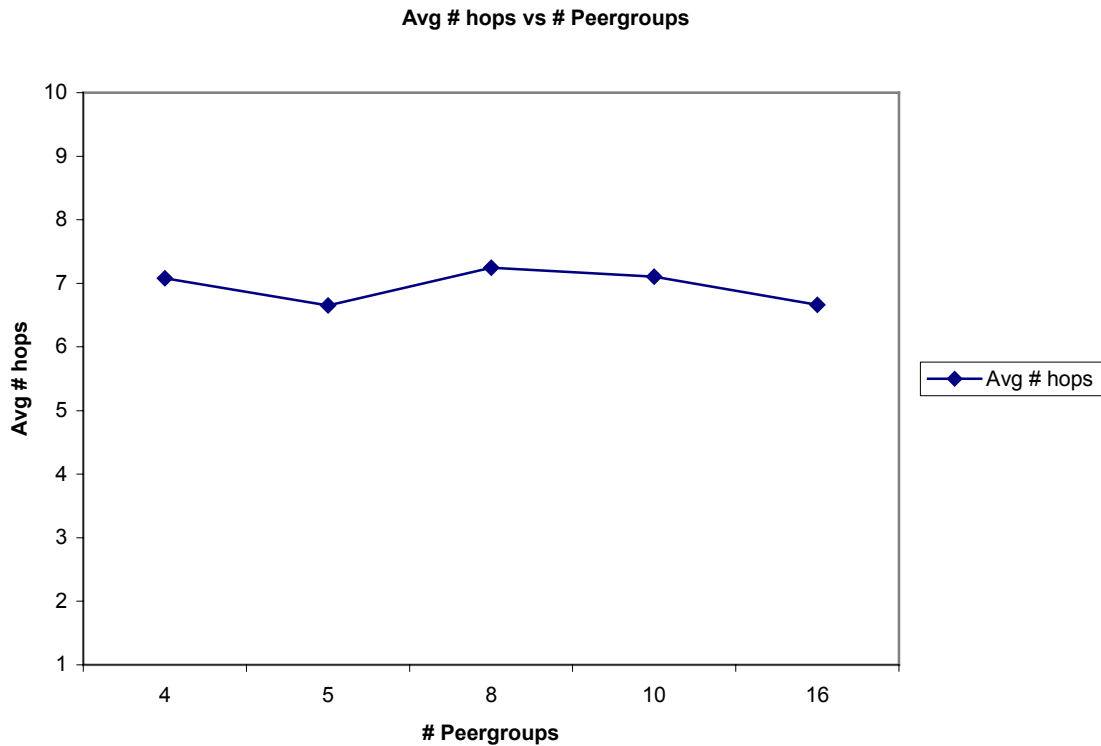


**Fig 5.15 Average hops vs. Peergroups**

In the simulation experiments conducted, the average number of hops in each case is almost the same, and thus it could be said that the topologies had no significant influence or bias on the results obtained. The slight variations in the average number of hops are due to the dissimilarities in the way inter-peergroup and intra-peergroup connections are made for each peergroup.

### 5.4.6 Floods per node

The total number of floods is composed of two components: floods when a significant change occurs in one of the node's database and the periodic flooding (hello packet, periodic PTSE refresh etc). The trend in the number of floods is dictated by the significant changes (floods, which are more frequent than the periodic floods)

Figure 5.16 shows the variation of floods per node with respect to a variation in the number of peergroups. With a lesser number of peergroups, there will be more significant changes within a peergroup; hence this will trigger intra-peergroup flooding; inter-

peergroup flooding takes place mainly for two reasons: if there is a significant change in one of the border nodes or if a peergroup loses reachability to one of the other peergroups. With a lesser number of Peergroups, the intra-peergroup floods dominate; with the increase in the number of peergroups, the inter-peergroup floods start to dominate. A point is reached whereby the increase in inter-peergroup floods will be more pronounced than the decrease in intra-peergroup floods.

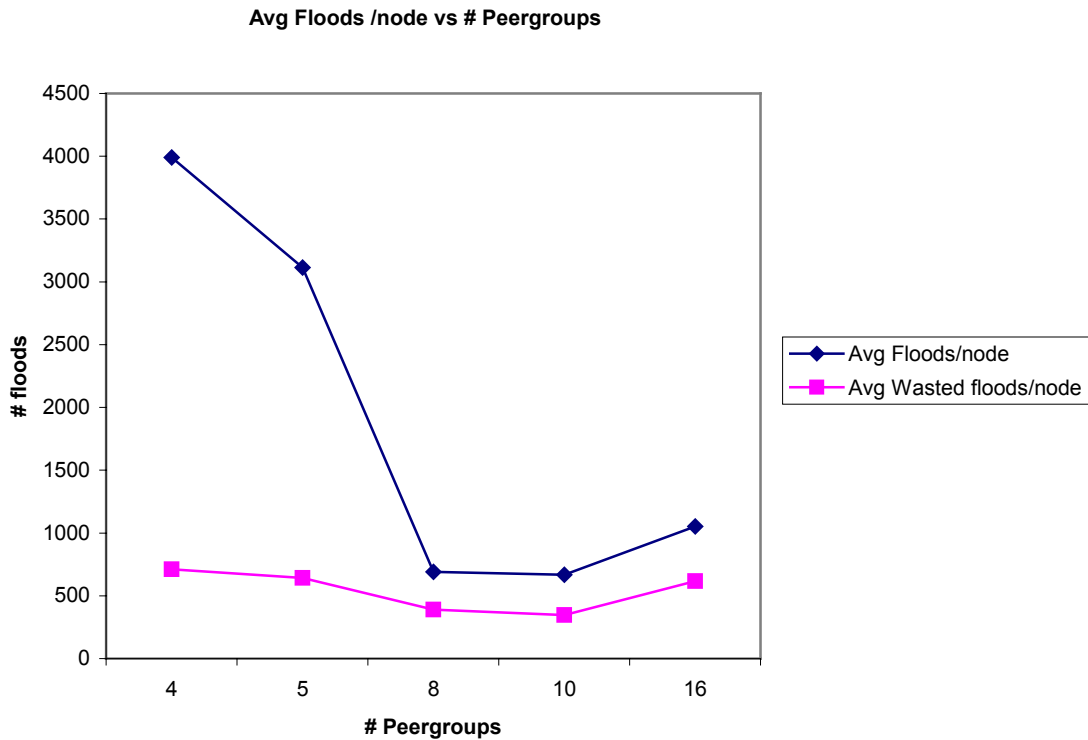


**Fig 5.16 Average Floods/node vs. Peergroups**

In this set of simulations, the number of nodes is maintained as a constant (160); hence the total floods and the floods per node both follow the same trend. The floods per node are taken as the metric of interest here. The results of the simulation behave exactly as described above. The number of floods decreases as the number of peergroups increases from 4 to 10, but again increases when the number of peergroups is 16. It can be seen that the wasted floods also follow the same trend as the total number of floods.

### 5.4.7 PNNI data per Flood

Figure 5.17 shows the variation of PNNI data per flood per node with respect to variation in the number of peergroups. The PNNI data per flood per node for similarly configured peergroups (for the same load) should remain unchanged.

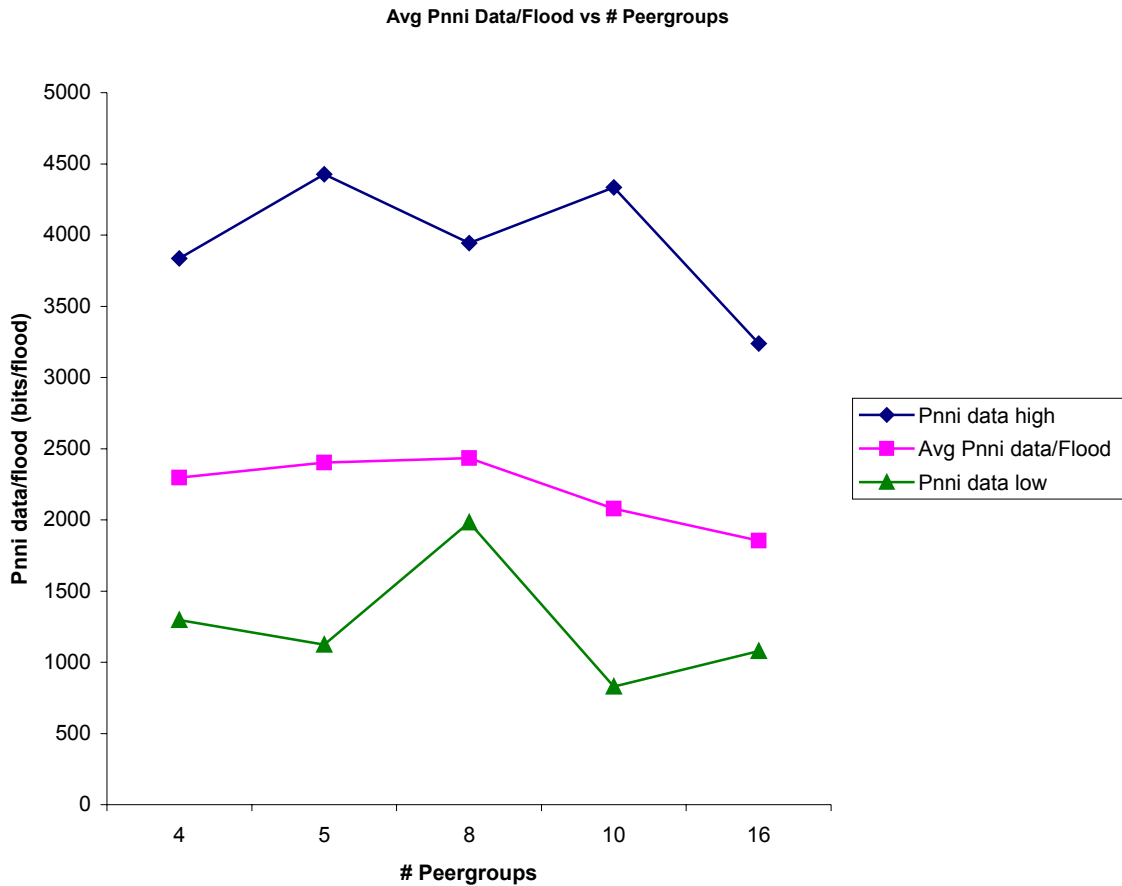


Fig 5.17 PNNI data per flood vs. Peergroups

The decrease in the average PNNI data per flood for 10x16 and 16x10 peergroups is due to the fact that, unlike the intra-peergroup connections in other peergroups, intra-peergroup links do not originate from all the nodes in the peergroup. One point to be noted here is that the ‘Average PNNI data’ metric is normalized over the *total number of floods*, while ‘PNNI data – high’ and ‘PNNI data – low’ have been normalized over *floods per node*.

## 5.6 Conclusion

It can be thus concluded that as the number of peergroups in a bandwidth-rich network is increased,

- Convergence time decreases initially, and then increases
- Mean Call setup time increases
- Call success percentage decreases
- Average Database size decreases
- Average PNNI data / flood remains unchanged
- Average number of hops remains unchanged (in general, but depends on topology)

# Chapter 6

## Effect of Hierarchy

### 6.1 Introduction

The aim of this set of simulations is to study the effect of hierarchical levels on the metrics that characterize the performance of the network.

### 6.2 Test topology

The topologies constructed for this set of simulations consist of a cluster topology with 96 nodes. The simulations are conducted on the same topology, but by varying the hierarchy from one-level (flat), two-levels, three-levels and four-levels. The topology has been constructed as follows. The 96 nodes are grouped as 6 ‘leaves’ of 16 nodes each (see figure 6.1). Each leaf has 3 mini-clusters, of which 2 mini-clusters have 5 nodes each, while the third mini-cluster has 6 nodes in it. From each leaf, two nodes from the 6-node mini-cluster have links to interconnect to other leaves. The inter-leaf interconnections are carried out through OC-3 links, while the inter-mini-cluster connections are carried out through 20 Mbps links, and the nodes within a mini-cluster are connected through 10 Mbps links. The hosts are connected to the nodes via 5 Mbps links. Darkened circles represent the leader nodes in each topology. The number of calls generated is *50 per host*.

#### 6.2.1 One-level (flat) hierarchy

This topology has been constructed such that it has just one-level hierarchy (or in effect no hierarchy at all); the topology is flat structured. All the nodes in the network fall are grouped under one single peer group. Fig 6.1 is a representation of a leaf in the flat network. Fig 6.2 is shows partially the one-level hierarchical topology, with inter-leaf interconnections.

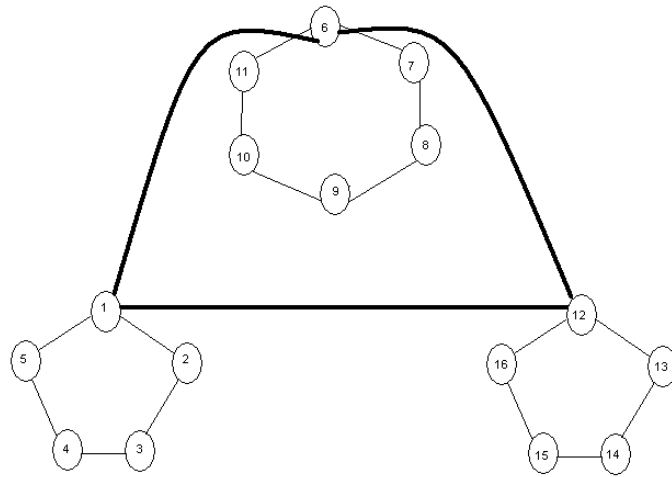


**Fig 6.1 Leaf in the One-level (flat) network**

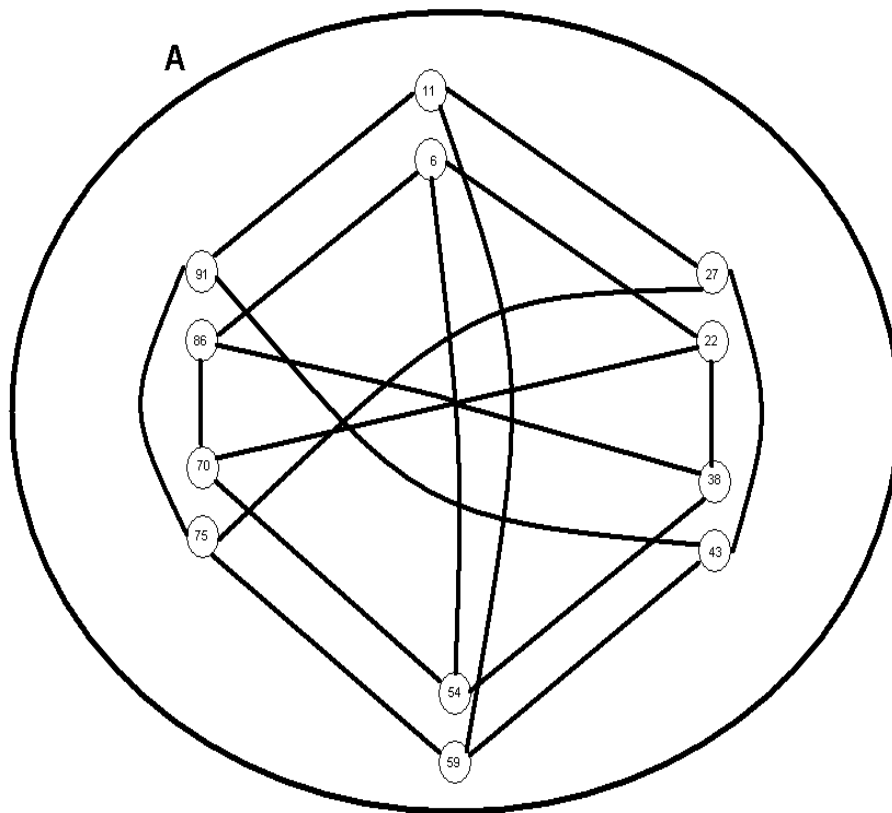


**Fig 6.2 One-level Inter-leaf interconnections**

### 6.2.2 Two-level hierarchy

This topology has been constructed such that there are two levels of hierarchy. Each leaf has been grouped under a separate peergroup as indicated in fig 6.3. Figure 6.4 gives the inter-peergroup connections, along with the logical-level of hierarchy (second-level).

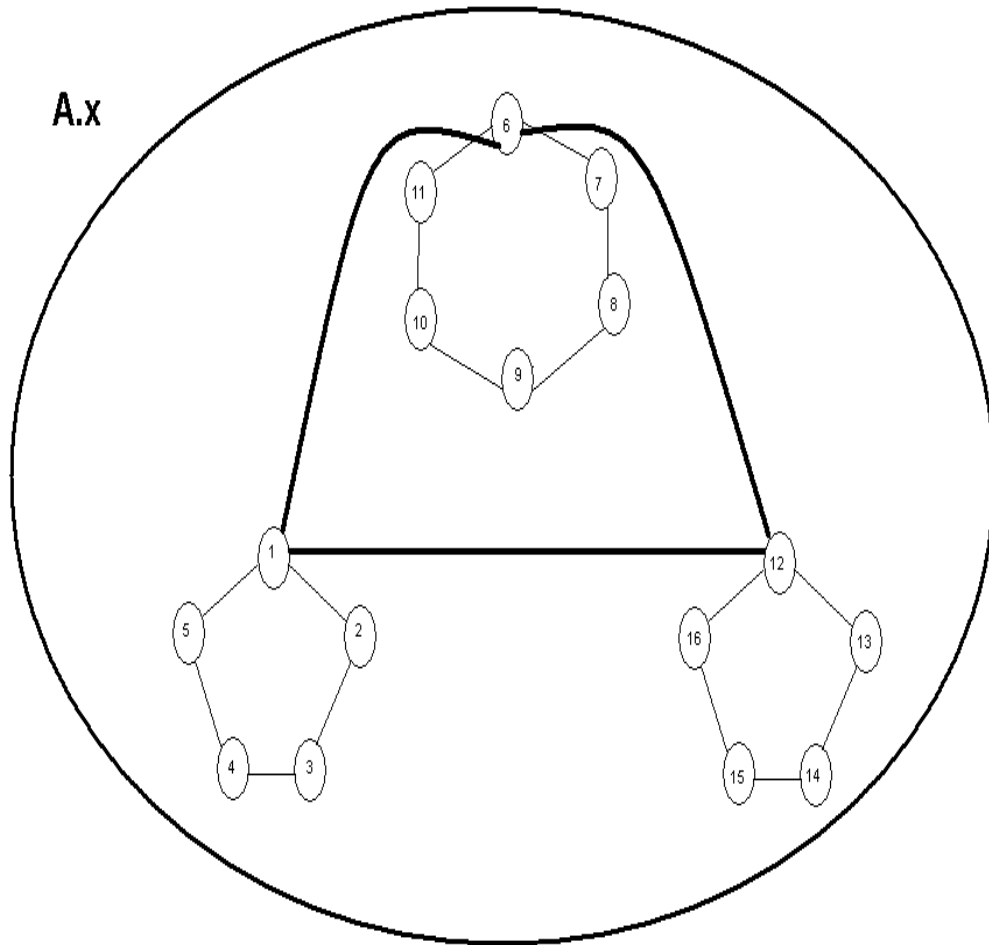
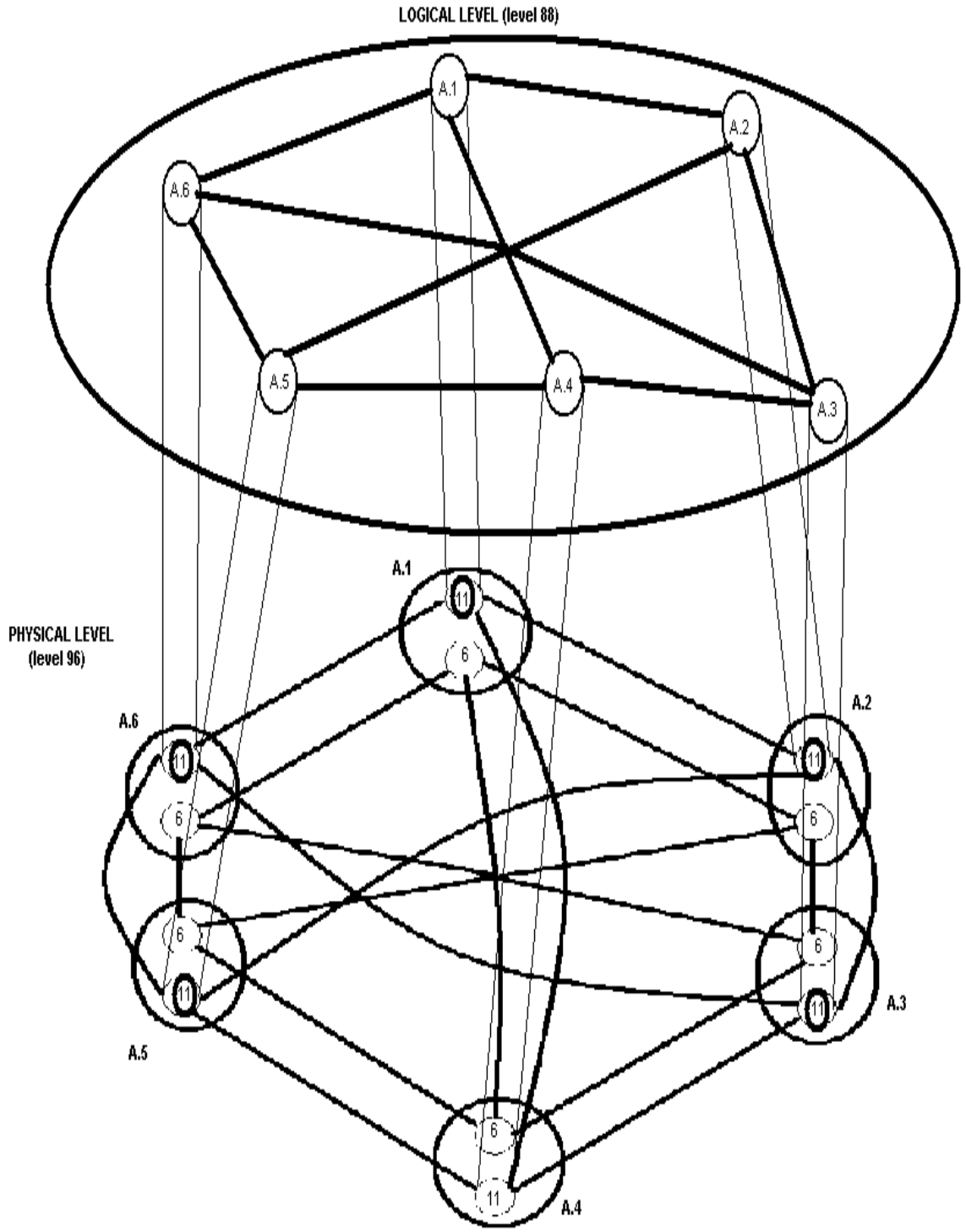


Fig 6.3 Leaf in a two-level hierarchical network



**Fig 6.4 Inter-Peergroup connections in a 2-level hierarchical network**



### 6.2.3 Three-level hierarchy

The next topology has been constructed with three-levels of hierarchy. Here, each mini-cluster is grouped into a peergroup, while the leaf serves as a logical level or a higher-level peergroup, which encompasses the mini-cluster peergroups. Fig 6.5 shows the representation of a leaf in a 3-level hierarchical network, along with its next higher-level (logical level) representation. Fig 6.6 shows the inter-peergroup interconnection at level-96 (lowest level of hierarchy), level-88 (second level of hierarchy) and level-80 (third level of hierarchy).

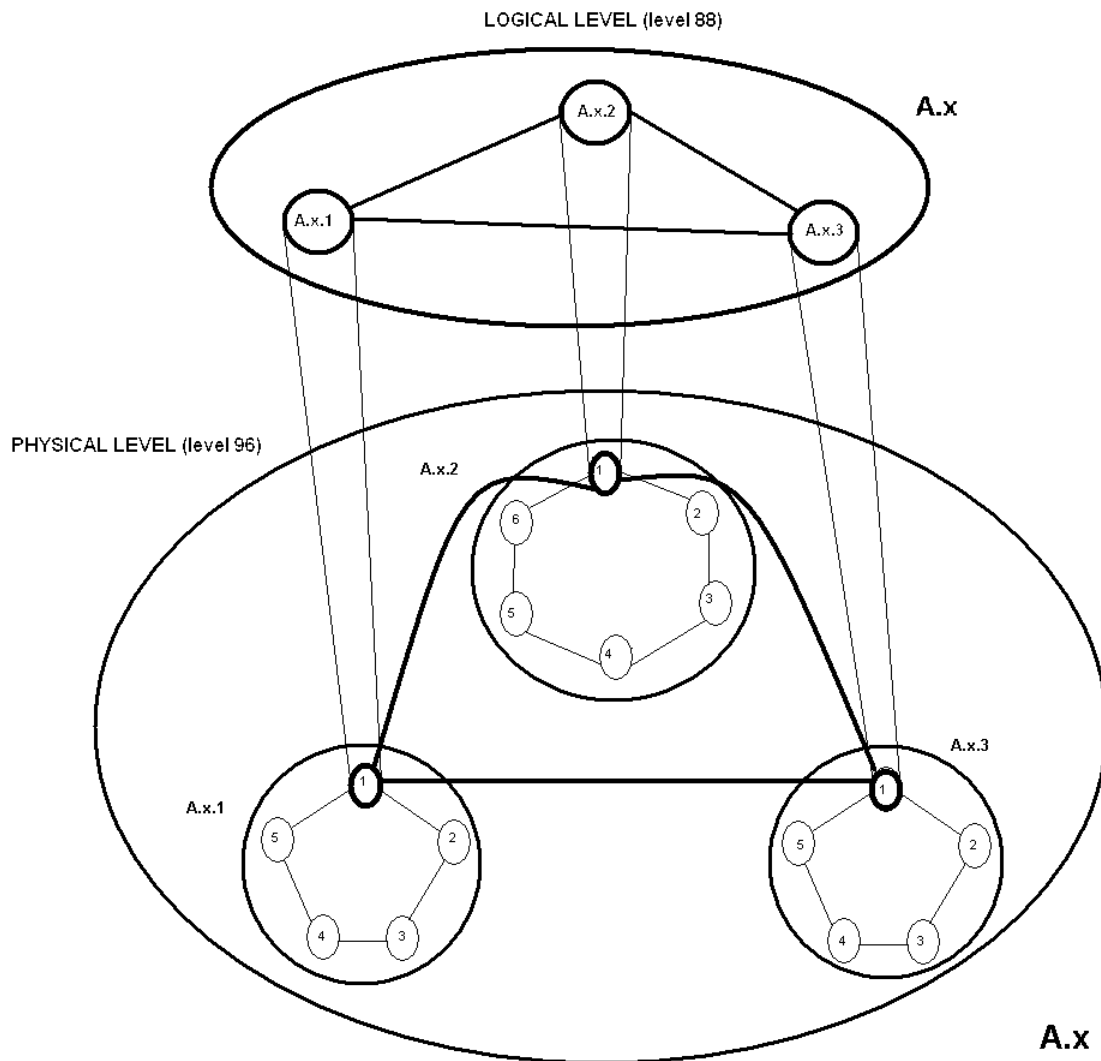


**Fig 6.5 Leaf in a 3-level hierarchical network with its logical level representation**

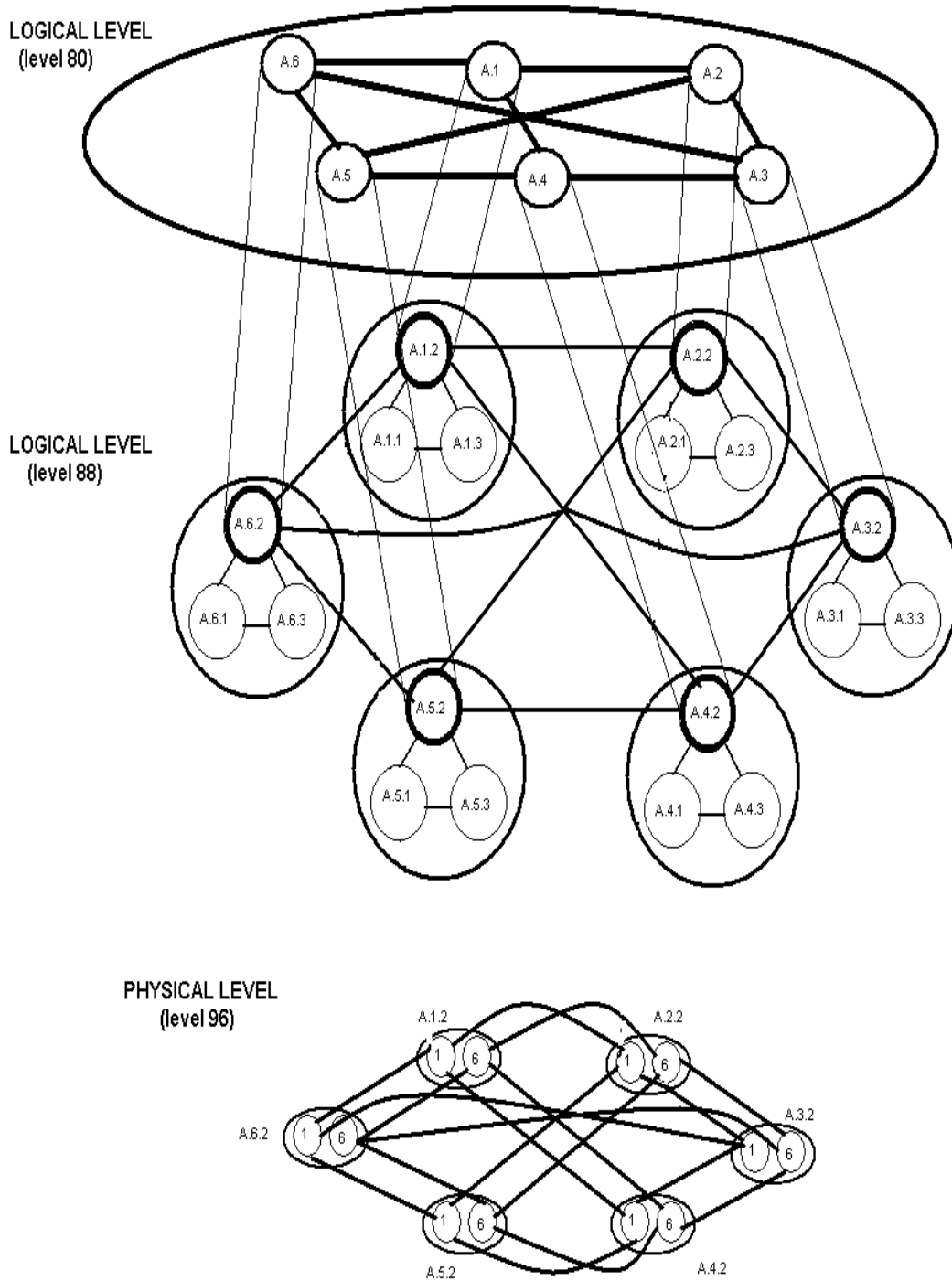


**Fig 6.6 Complete 3-level hierarchical representation of the network**

## 6.3 Performance metrics

The metrics of *primary* interest in this set of simulations are:

- Mean Call setup time
- Call success percentage
- Average Database size
- Convergence time
- Average number of hops

Along with these metrics, the other metrics such as Average utilization percentage, total floods and PNNI data / flood are also monitored.

## 6.4 Results and Analysis

### 6.4.1 Mean Call setup time

Figure 6.7 shows that the mean call setup time increases (not monotonically) with an increase in hierarchical levels. The call setup time is the sum of the queuing time at each node, the time to traverse the links and the routing time. The queuing time and the time to traverse the links can be assumed to be fairly constant. (The queuing time at each node is mainly dependent on the load in the network). With an increase in hierarchical levels, the number of decision making nodes increases and each decision-making node (the leader) does not have complete information about the entire network topology. Hence the routing decisions are not always optimal as the number of hierarchical levels increase; also, the routing decisions are made at each level, which increases the effective routing time.

### Mean Call setup time vs # hierarchical levels

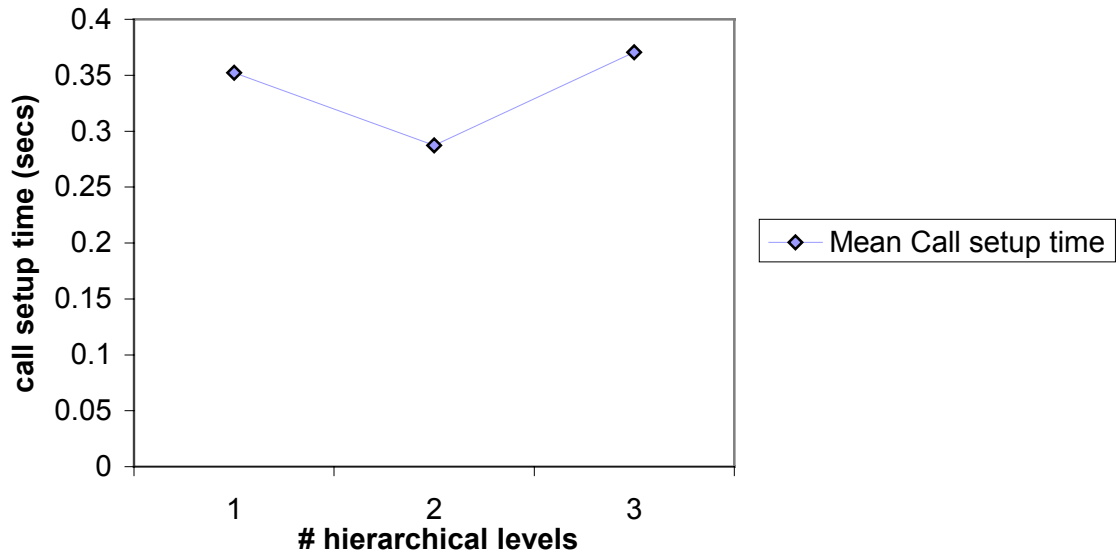


**Fig 6.7 Mean Call setup time vs. levels of hierarchy**

Thus the mean call setup time can be thought of as a function of the routing time of each call (with load and network topology remaining unchanged). The routing time can further be split as inter-peer group routing time and intra-peer group routing time. These results seem to contradict the results of “Effect of Peer grouping test”. The time for flow of control data between hierarchical levels more than offsets the decrease in routing time due to peer grouping. Hence, an increase in the number of hierarchical levels increases the routing time, thus increasing the mean call setup time.

One exception is the results of 2-level hierarchy; here the increase in routing time due to flow of control data between hierarchical levels is less than the decrease in routing time due to the effect of peer grouping. It might be interesting to note that in Gowri Dhandapani’s Master’s thesis report (page 72) [2], it was reported that the call setup time decreases with an increase in hierarchical levels; this was because the tests were

conducted only on two topologies, and the results were affected by the above stated effect.

### 6.4.2 Average Database size

Figure 6.8 shows that the average database size decreases as the number of hierarchical levels increases. This is because, with an increase in the number of hierarchical levels, the routing decisions taken to setup a call are made by more than one node, and hence each node need not have a complete and accurate picture of the network topology; all the nodes need is complete reachability information at the highest level of hierarchy. This abstraction in reachability information considerably reduces the database size at each node. Stated otherwise, the reachability information is spread over the entire topology, rather than clustered at each node.

**Average Database size vs # hierarchical levels**

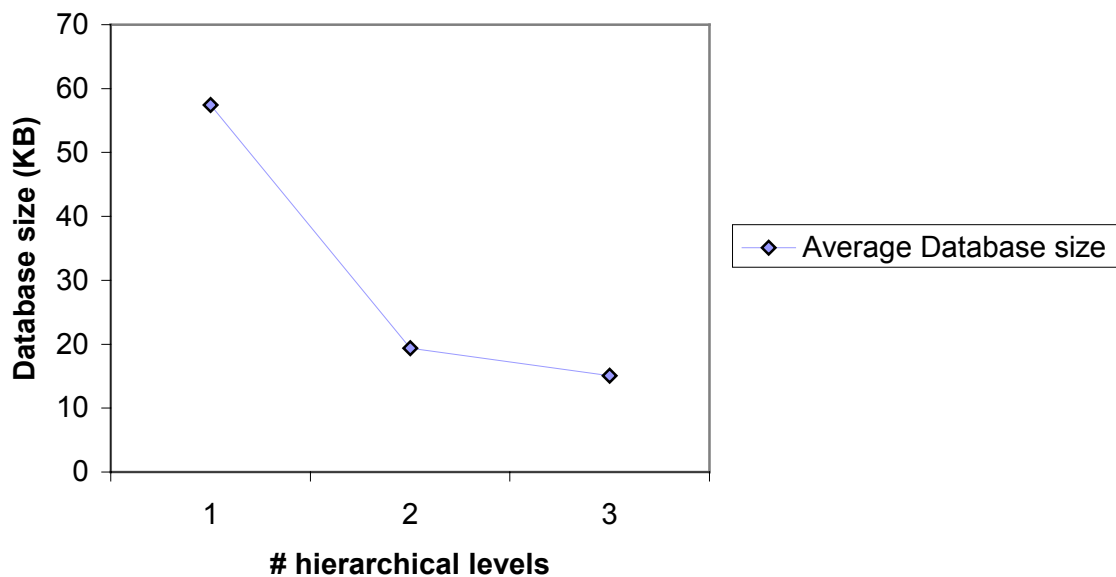


**Fig 6.8 Average Database size vs. levels of hierarchy**

The reduction in database size and the resulting inaccuracy in reachability information is actually *the* fundamental trade-off with hierarchical routing. As the topology scales in size, without hierarchical levels, each node needs to maintain state information about every other node in the topology and hence the database size increases to unmanageable proportions. With hierarchical levels, the database size is greatly reduced, but the trade-off for this reduction in size is inaccurate routing information caused as a result of abstraction of levels.

### 6.4.3 Mean Call setup success percentage

Figure 6.9 shows that the mean call setup percent decreases with an increase in the number of hierarchical levels.

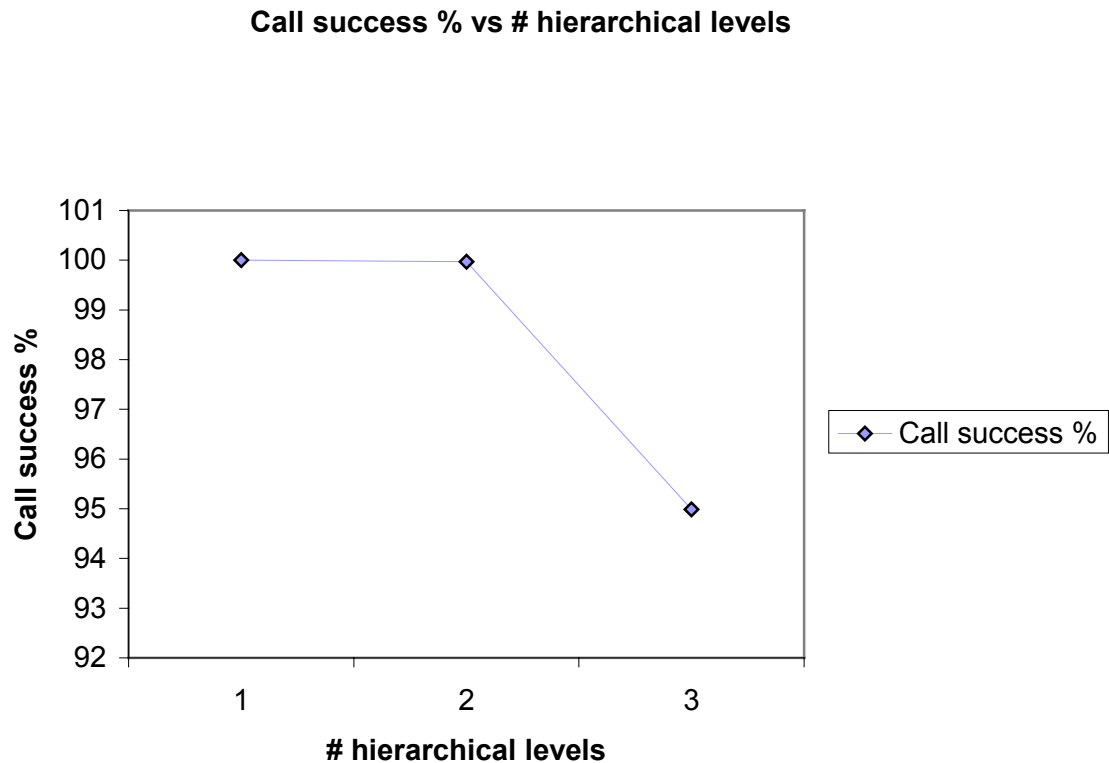


**Fig 6.9 Mean call success rate vs. Levels of hierarchy**

A call fails mainly because of routing inaccuracies and not because of unavailability of resources (computing and/or link bandwidth) when the number of hierarchical levels

increases (for a given load and network topology). Routing inaccuracies are caused because of inaccurate and incomplete information present in the nodes' database as a result of topology abstraction.

#### 6.4.4 Average number of hops

Figure 6.10 shows the variation of the average number of hops with respect to the variation in number of hierarchical levels. The average number of hops increases as the number of hierarchical levels increases. This is because, as the number of hierarchical levels increases, so do routing inaccuracies, and hence the path chosen for the call setup is not always the most optimal.

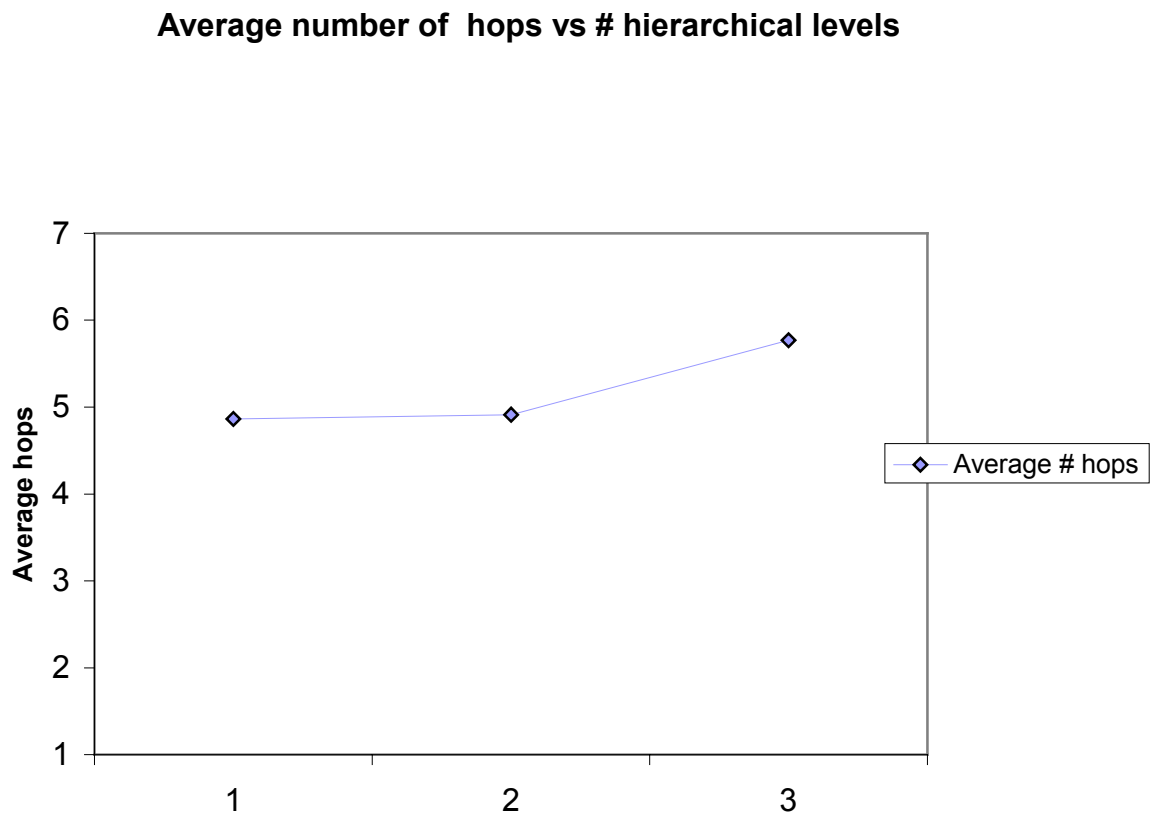


**Fig 6.10 Average hops vs. Levels of hierarchy**

The above explanation is further corroborated from a poorer call success percentage for an increased number of hierarchical levels, which is again due to inaccurate routing information in the database.

### 6.4.5 Convergence time

Figure 6.11 gives the variation of convergence time as a function of the number of hierarchical level. The convergence time decreases as the number of hierarchical levels increases.

**Convergence time vs # hierarchical levels**

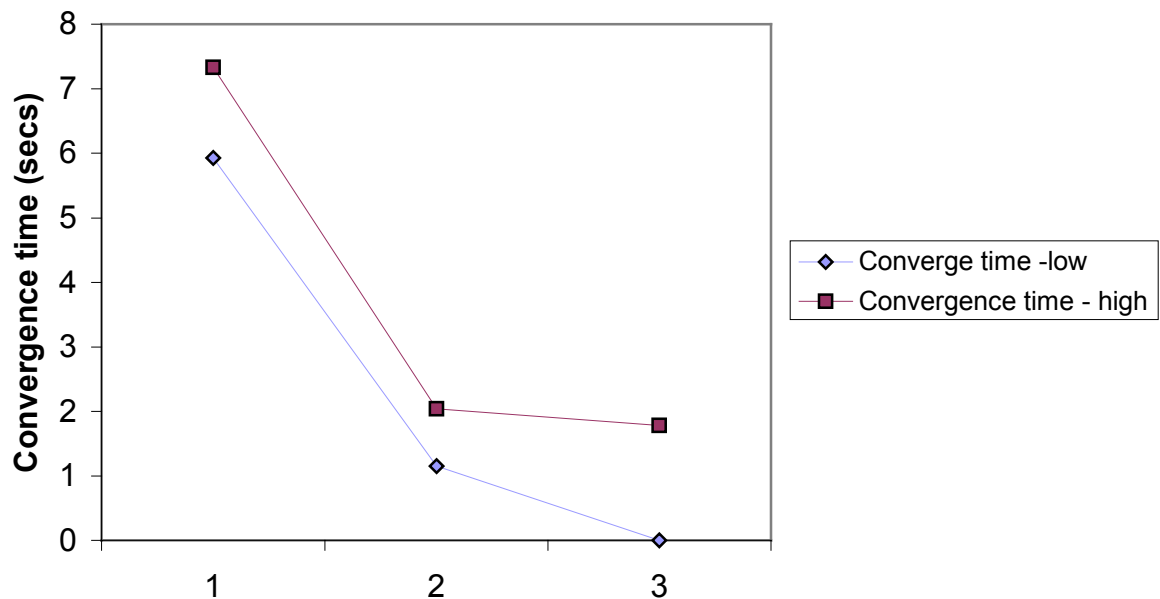


**Fig 6.11 Convergence time vs. Levels of hierarchy**

This is because the number of nodes that each node has to converge (in other words the convergence number) decreases as the number of hierarchical levels increases. This behavior was also seen in “Effect of Peergrouping” test.



### 6.4.6 Floods per node

Figure 6.12 shows that the number of floods per node increases as the hierarchical levels increases. This is because the PNNI control data is flooded to higher levels of hierarchy too; so more the number of hierarchical levels more are the number of floods.

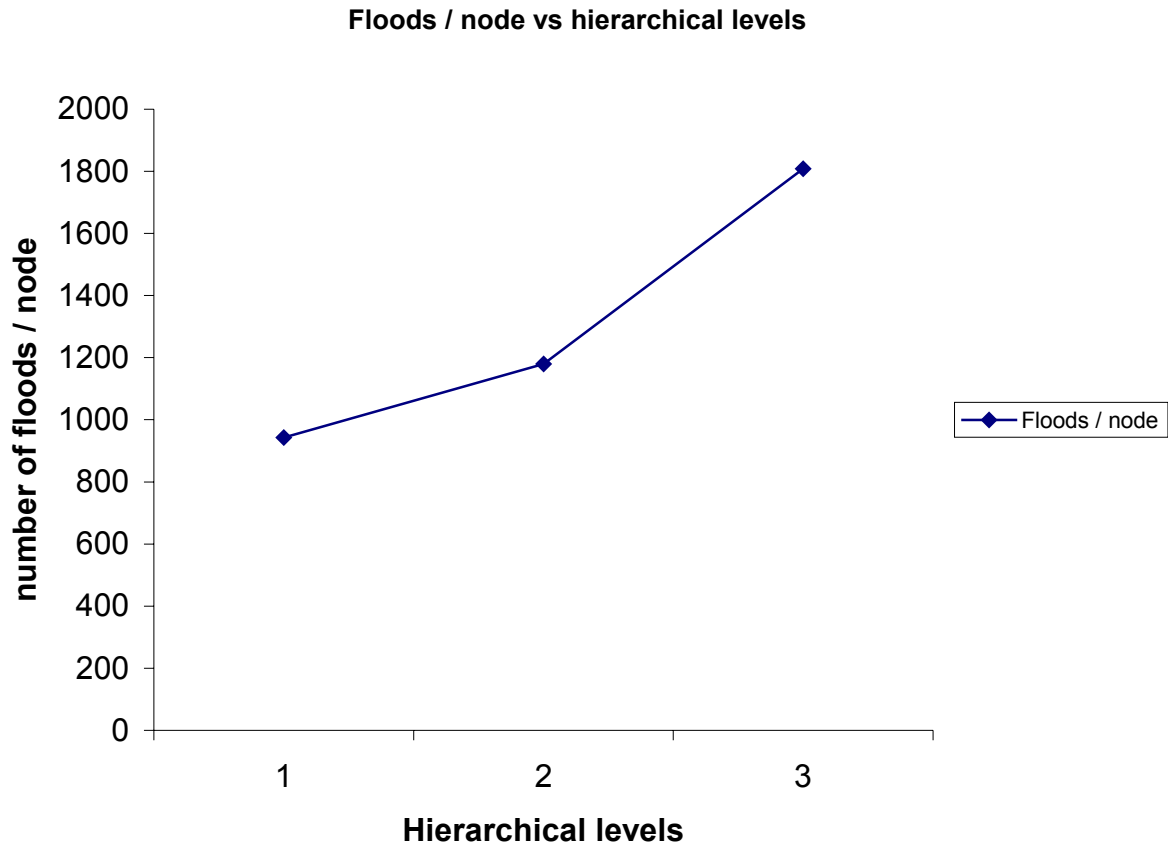
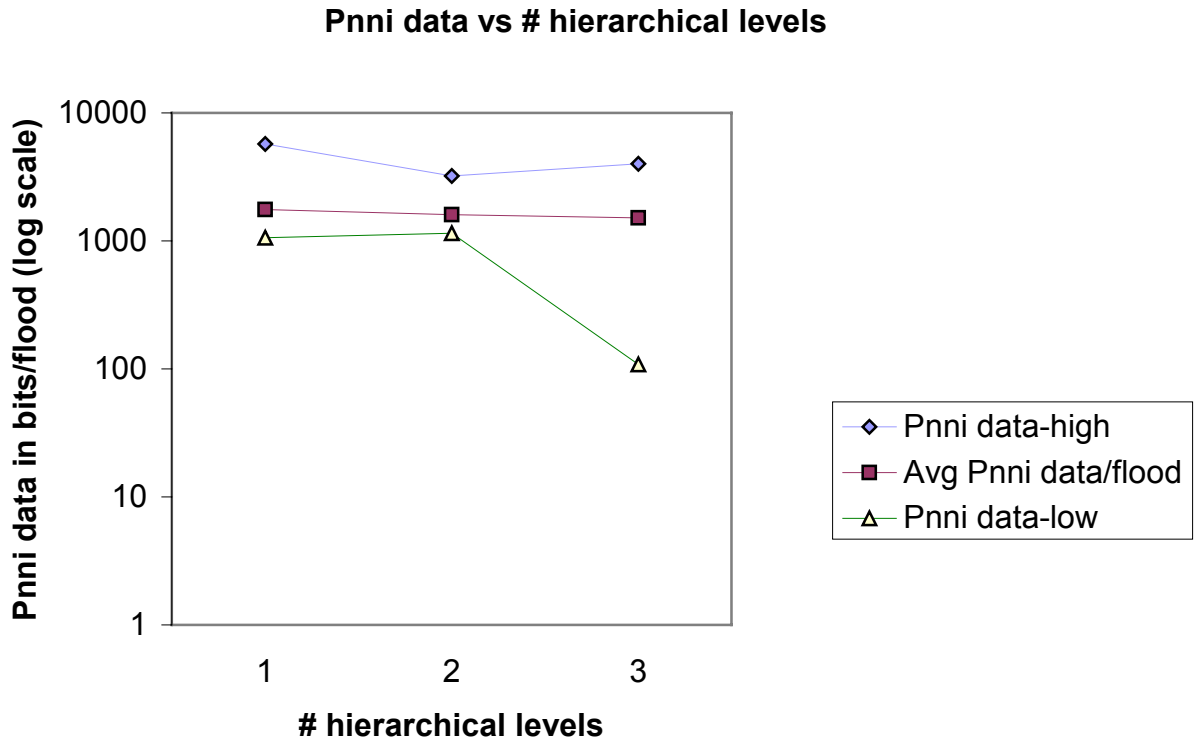


Fig 6.12 Floods per node vs. Levels of hierarchy

### 6.4.7 PNNI data per Flood

Figure 6.13 shows that the average PNNI data /flood is almost a constant. The topologies with more levels of hierarchy will have to flood PNNI data to its upper levels, too. Hence the number of floods in this case is higher but the PNNI data also increases proportionally. Hence the flat topology (without any hierarchical levels) has lesser

number of floods and lesser PNNI data, but a similar PNNI data /flood measure as that of the topologies with higher levels of hierarchy.



**Fig 6.13 PNNI data per flood vs. Levels of hierarchy**

### 6.4.8 Percentage Wasted Floods

Figure 6.15 shows the variation of percentage wasted floods with respect to variations in the number of hierarchical levels. The percentage wasted floods give a good measure of how robust the topology is to changes.

### % Wasted floods vs # hierarchical levels

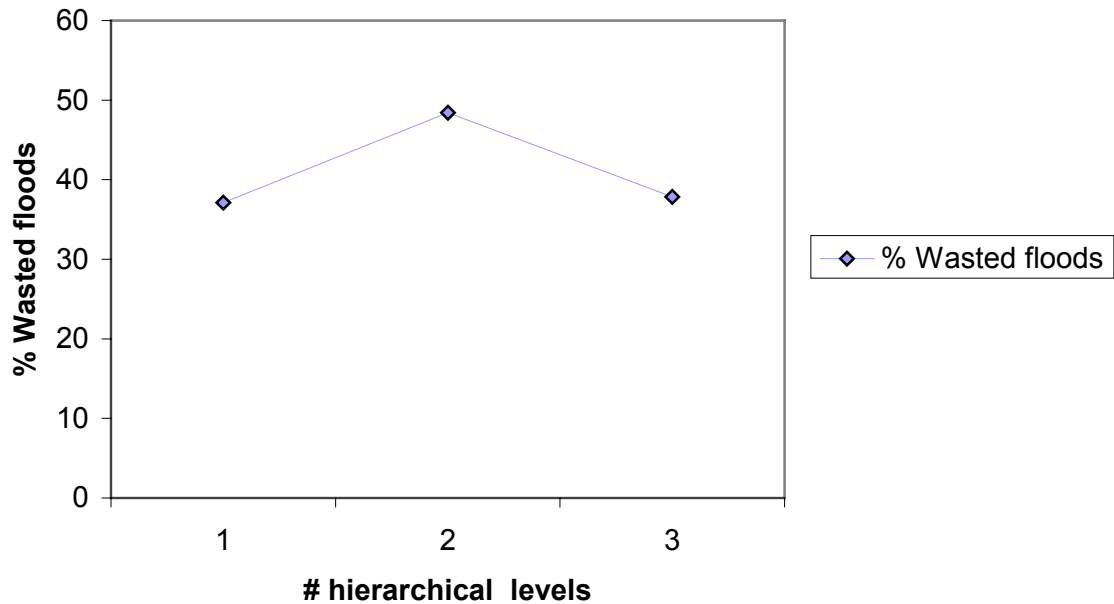


**Fig 6.14 Wasted Floods percentage vs. Levels of hierarchy**

The 2-level hierarchical topology has the maximum percentage of wasted floods. What the wasted floods indicate is that how often a significant change in one node has not affected another node's view of the entire topology. On the other hand, too much wasted floods is a waste of bandwidth. Hence, there is a trade-off between robustness (caused due to redundancy of data) and effective use of available bandwidth.

## 6.6 Conclusion

As the number of hierarchical levels increases, it can be concluded that

- Mean Call setup time increases
- Convergence time decreases
- Call success percentage decreases
- Average Database size decreases
- Average number of hops increases

# Chapter 7

## Effect of Crankback

### 7.1 Introduction

The aim of this test is to study the effect of varying the number of crankback retries on mean call setup time and call failure percentage, especially on the calls that fail due to lack of bandwidth, under fixed load and topology.

### 7.2 Test topology

The test topology is the 3-level hierarchical cluster topology with 96 nodes, as used in the “Effect of hierarchy” test. Refer to Fig 6.6 for the topology. The maximum number of crankback retries is varied as 0, 2, 5 and 8. The number of calls generated is 15 per host. Calls are generated with an exponential mean inter-arrival time of 40 seconds. A warm up ratio (similar to run in time) of 15% is used (the results of the first 15% of the calls generated by each host are ignored). The call bandwidth (Peak cell rate) of each call is changed from 64Kbps to 1250 Kbps.

### 7.3 Performance metrics

The metrics under consideration are

- Average Call failure percentage
- Mean Call setup time

### 7.4 Results and Analysis

#### 7.4.1 Average Call failure percentage

Fig 7.1 gives the variation of call failure percentage with respect to the number of crankback retries. The average call failure percentage is expected to decrease as the number of crankback retries increases. But if the topology has not much scope for

crankback i.e. if there is are not many routes to reach the destination, then crankback retries will only waste processing time, thus increasing the effective load on the system. This causes call failure percentage to increase due to processing time outs as the number of crankback retries increases.

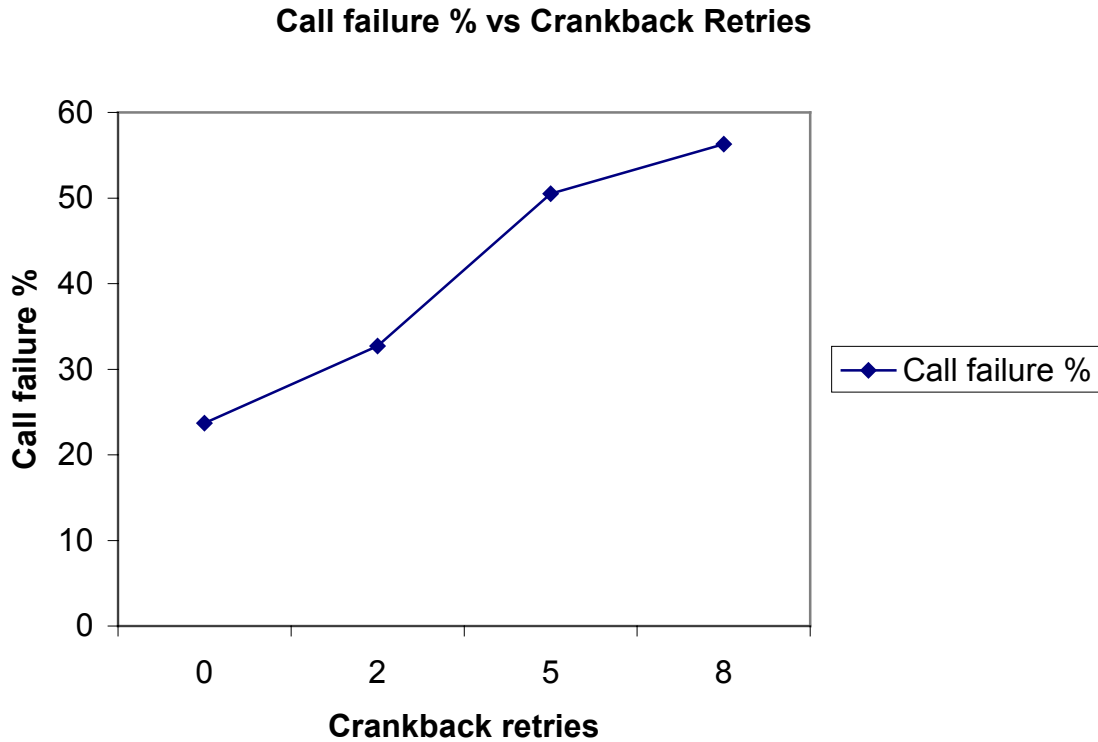


**Fig 7.1 Call failure rate vs. Crankback retries**

Figure 7.2 shows the variation of call failure rate (for calls failed due to lack of bandwidth) with a variation in the number of crankback retries. As expected, the call failure rate due to lack of bandwidth decreases initially with an increase in crankback retries, but eventually starts to increase for eight crankback retries. This behavior is seen because, with a large number of crankback retries, the effective load in the system is increased, and as a result a large number of calls are competing for bandwidth at the same time. Hence more calls fail because the effect of crankback is somewhat reduced at a higher effective load. In other words, higher crankback retries may indirectly be responsible for increase in load, and thus cause more call failures.

Call failures due to Insufficient Bandwidth vs Crankback retries

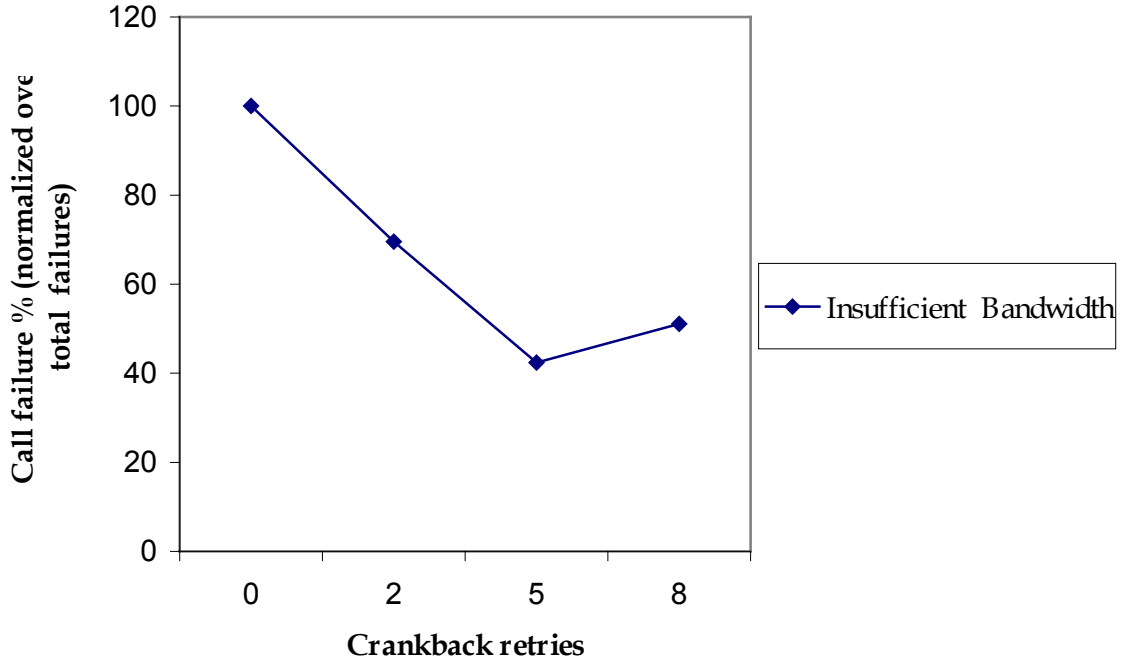


Fig 7.2 Call failures due to Insufficient Bandwidth vs. Crankback Retries

Call Failures caused by time outs due to lack of processing resource vs. Crankback retries

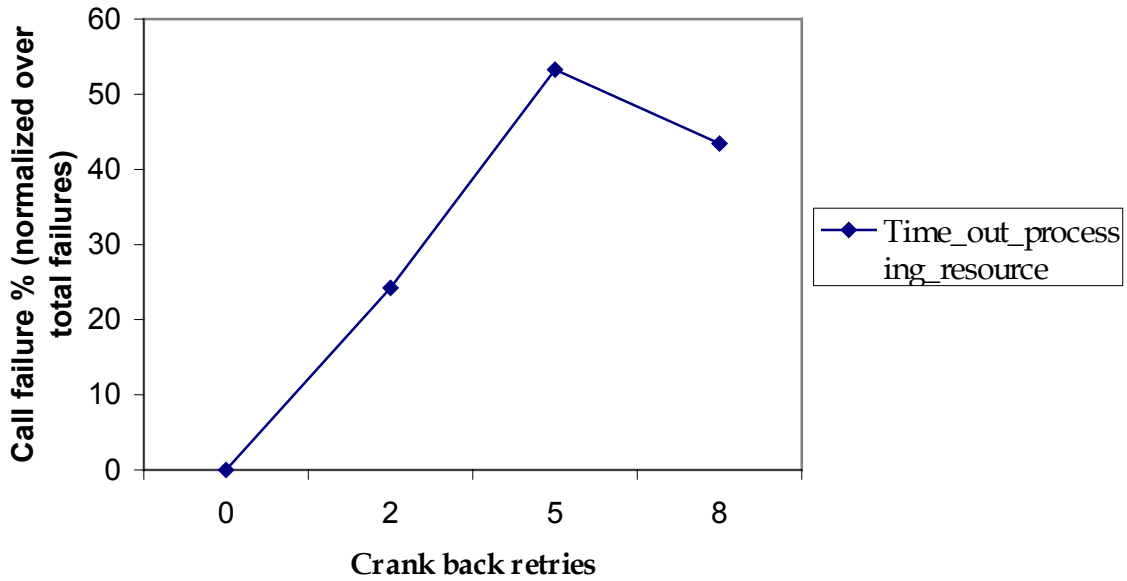


Fig 7.3 Call failures due to unavailability of processing resources vs. Crankback retries

Figure 7.3 shows the variation of call failure rate (for calls failed due to time outs caused by lack of processing resources) versus the variation in number of crankback retries. As seen above, crankback retries will increase effective load in the system. This causes an increased failure rate for calls that are timed out due to lack of availability of processing resources. Crankback will not help to alleviate the problem with lack of processing resources; in fact crankback will only serve to exacerbate the problem. For a maximum crankback retry number of 8, we see a lesser number of call failures due to time outs because more calls fail due to lack of bandwidth as well. Moreover, with 8 crankback retries, the effective load is very high, and many calls may fail at an earlier stage of the simulation itself, without progressing much into the network, and thus they reduce the number of failures due to processing time outs.

### 7.4.2 Mean Call Setup time

Figure 7.4 shows the variation of mean call setup time as a function of crankback retries. In general, more the number of crankback retries, more will be the call setup time.

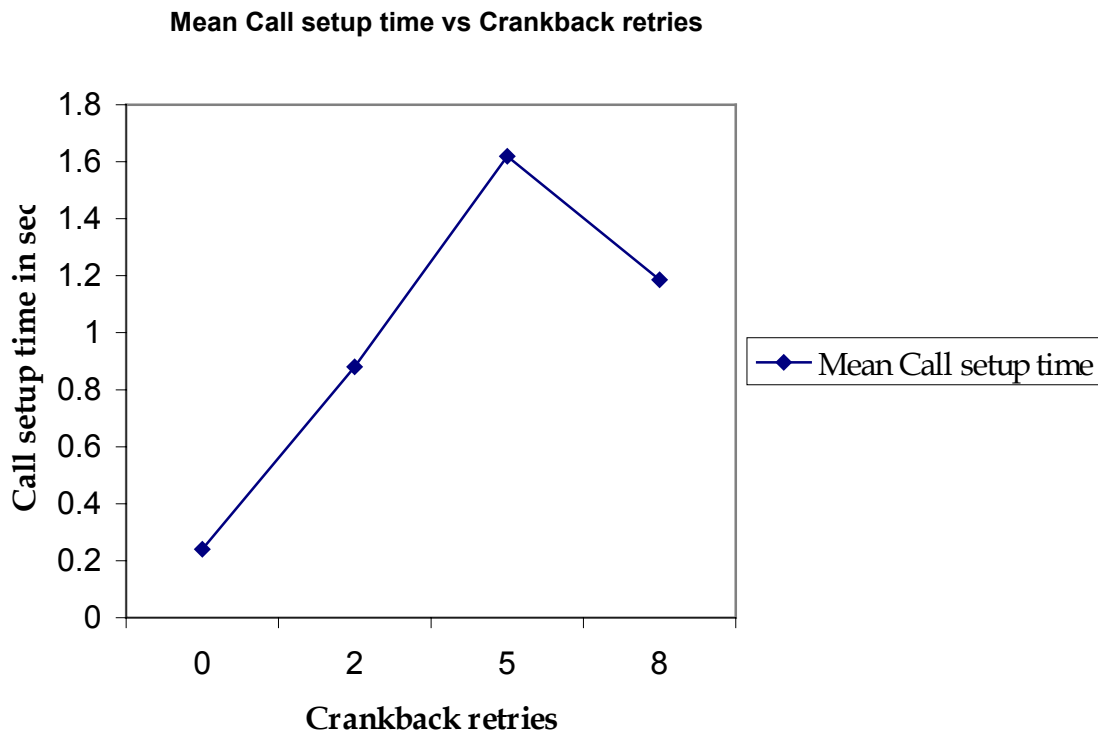


Fig 7.4 Mean Call setup time vs. Crankback retries

This is obvious because that crankback retries increase the effective load in the system, which causes an increase in the call queuing delay in the nodes. Hence, the calls experience a higher mean setup time. But, for a very high number of retries, many calls time out due to the excessive queuing delay, and the calls do not succeed. This causes a decrease in the call setup time; it also causes a decrease in the call setup percentage.

## **7.5 Conclusion**

In a bandwidth-poor network, an increase in number of crankback retries

- Increases the call success percentage, until the call failure begins to be dominated by time outs associated with lack of processing resources. Even calls failing due to lack of bandwidth, if subjected to a large number of crankback retries, may eventually time out and fail, leading to decrease in call success percentage
- Increases call setup time irrespective of the type of network, until more calls fail due to lack of processing resources.

Hence it can be concluded that crankback retries are to be used only when a large percentage of calls fail due to lack of bandwidth (or some other QoS metric). In bandwidth-rich networks, the use of crankbacks will only decrease the call success rate. In a bandwidth-medium rich network, crankbacks could be used, but the number of retries should be chosen such that the crankbacks do not cause many call failures due to time outs before they could be processed. In a low-bandwidth network, it is advisable to use crankbacks, but again, the number of retries should be chosen so as not cause more failures associated with lack of processing power (due to crankbacks), than the number of calls that succeed due to crankbacks.



# Chapter 8

## Simulator Performance

### 8.1 Introduction

The scope of this set of simulations is to study the simulator's performance with change in load and size of the network – in other words to determine the effect of load and size of the network on the duration of the simulation.

### 8.2 Test topology

The test topologies used are the same as the ones used for the scalability and load tests. The simulations were run in each of the three topologies by varying the mean call inter-arrival time as 20 seconds, 10 seconds and 5 seconds. Each host generated the same number of calls as specified in the scalability test.

### 8.3 Parameter of interest

The duration of the simulation measured in real units of time is the parameter of interest. This gives a good idea of how the simulator behaves when load and or size of the network is increased.

### 8.4 Results and Analysis

#### 8.4.1 Variation with change in size

The duration of simulation increases monotonically as the size of network is increased. This is obvious because the simulator will have to process more events generated as a result of increase in the number of calls (as a result of the number of nodes).

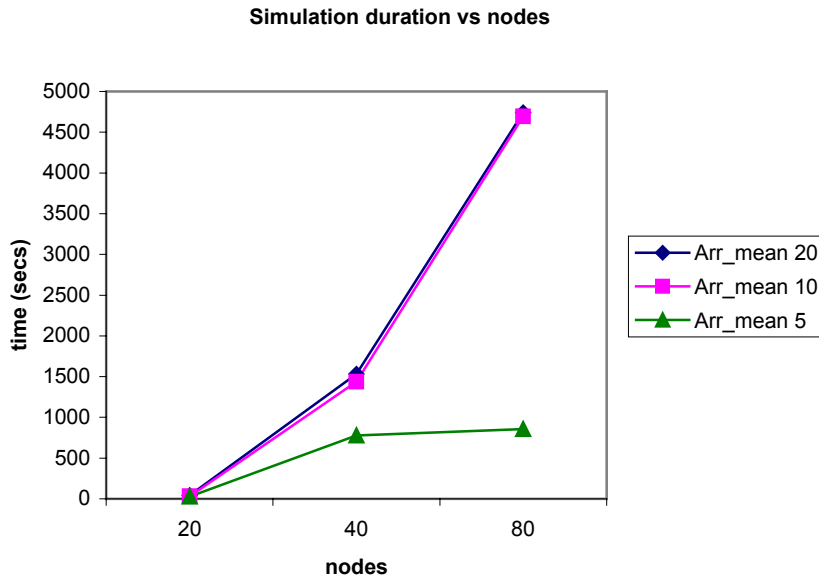


**Fig 8.1 Variation of simulation time vs. size of network**

### 8.4.2 Variation with change in load

The simulation time is expected to increase with increase in load, unless the heavy load causes calls to fail at an early stage. In such a case, the simulator runs out of events to process, and hence completes the simulation sooner.

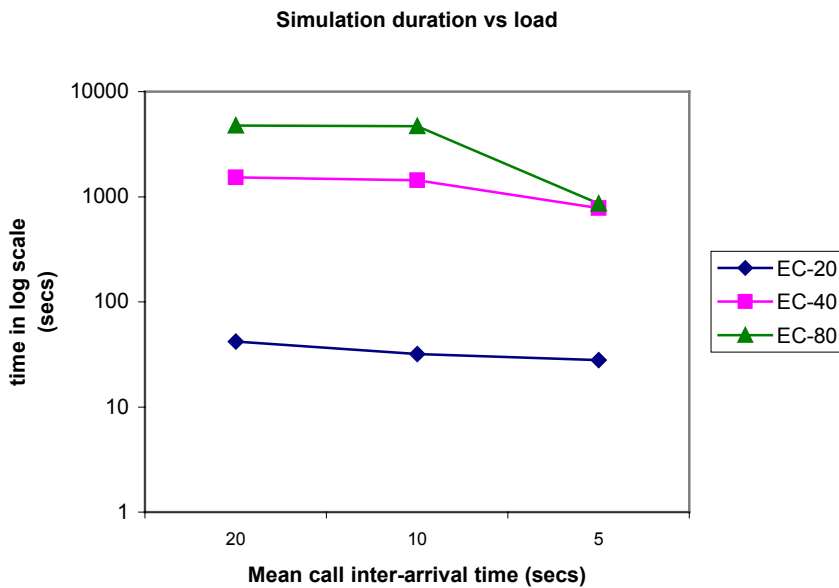


**Fig 8.2 Variation of Simulation time vs. load**

The results for variation of simulation time with changes in load (fig 8.2) are in direct contradiction with the hypothesis. For 20 nodes, changes in load hardly have any impact on simulation time. But for bigger topologies, simulation time decreases with increase in load. One possible explanation for this surprising behavior could be that the calls at high load in bigger topologies fail at an earlier stage, thus reducing the number of events the simulator has to process.

The call success rate in the case of 20 nodes is 100 percent for all loads. In case of 40 nodes, the call success rate is 100 percent for mean inter-arrival times of 20 seconds and 10 seconds, while it is 99 percent at heavy load. The duration of the simulation is almost the same at an inter-arrival mean of 20 seconds and 10 seconds, while the duration of simulation is lesser in case of a call inter-arrival mean of 5 seconds. One reason could be that, for the same call success rate, there tends to be more flooding (periodic floods, and hence more events) in case of lighter loads, since the simulated time is more.

The call success rate in the case of 80 nodes is 100 percent for mean inter-arrival times of 20 seconds and 10 seconds. But at heavy load, the call success rate is only 92 percent, which causes the duration of simulation to greatly reduce because of the reasons discussed in the preceding paragraphs.

## **8.4 Conclusion**

As the size of the network is scaled upwards appropriately, the time to complete the simulation also increases.

As the load in the network is increased, the time to complete the simulation depends on the location of the failure of the call. If calls fail at the early stages of routing, then the simulation time might decrease for heavy loads; whereas if calls fail after progressing quite deep into the network, the simulation time might increase at heavy loads.

In the test topology, at 80 nodes, under heavy loads, the calls seem to fail at the early stages of routing itself.

# Chapter 9

## Summary

### 9.1 Summary of Conclusions

It can be thus concluded that:

- **As the topology is scaled in size in a bandwidth-rich network,**
  - Mean Call setup time increases
  - Call success percentage decreases
  - Average Database size increases
  - Convergence time increases
  - Total number of floods increases
  - Average PNNI data / flood increases
  - Average number of hops increases (in general, but depends on topology)
  
- **As the load in the network is increased in a bandwidth-rich network,**
  - Mean Call setup time increases
  - Call success percentage decreases
  - Average link utilization percentage increases
  - Average PNNI data / flood increases (only in large-sized networks)
  - Average number of hops remains unchanged (in general, but depends on topology)
  
- **As the number of peer groups in the network is increased in a band-width rich network,**
  - Convergence time decreases initially, and then increases
  - Mean Call setup time increases
  - Call success percentage decreases
  - Average Database size decreases
  - Average PNNI data / flood remains unchanged

- Average number of hops remains unchanged (in general, but depends on topology)
- **As the number of hierarchical levels increases in a bandwidth-rich network,**
  - Mean Call setup time increases
  - Convergence time decreases
  - Call success percentage decreases
  - Average Database size decreases
  - Average number of hops increases

For the test topology, it can be seen that we get the best performance in the 2-level hierarchy for almost all the performance metrics. Hence, for the chosen topology, the 2-level hierarchy is the most optimal.

- **As the number of crankback retries is increased in a bandwidth-poor network,**
  - Mean Call setup time increases and then decreases
  - Call success percentage increases initially and then decreases
- **As the number of nodes in the network increases,**
  - Simulation time increases
- **As the load in the network increases**
  - Simulation time depends on topology

# Appendix - I

## Simulation Parameters

The following simulation parameters are common for all simulations (except for the “Crankback Retries” test).

### *Node Parameters*

ptse_age_offset	= uniform [-25 25]
fabric	= KU
numports	= 4
routing_policy	= max_bw
flooding_significance	= dynamic_threshold
flooding_threshold	= 2
prop_constant	= 25
default_flooding_period	= 1800 sec
default_flooding_factor	= 5
acac_policy	= call_packing
util_log_period	= 1
call_trace	= FALSE
queuesize	= 5000
crankback_retries	= 2
hello_timer	= 15
hello_inactivity_factor	= 4
summary_timer	= 20
ptsp_timer	= 20
ack_timer	= 5
request_timer	= 20
reaggregation_timer	= 0
process_time	= 2.0

### *Host Parameters*

calls	= 25/30/50/60/120
arrival_distribution	= exponential 20,15,10,5,2s
duration_distribution	= exponential 100 sec
calltype1	= cbr
pcr1	= fixed 64 kbps
share1	= 5 %
ctd1	= fixed 33 msec
cdv1	= fixed 1 msec
clr1	= fixed 8 (ie $10^{-8}$ )
calltype2	= vbr,
pcr2	= fixed 64 kbps
pcr2scr2	= fixed 2
share2	= 10 %
ctd2	= fixed 43 msec
cdv2	= fixed 11 msec
clr2	= fixed 5

calltype3	= vbr,
pcr3	= fixed 64 kbps
pcr2scr3	= fixed 1.78
share3	= 85 %
ctd3	= fixed 43 msec
cdv3	= fixed 11 msec
clr3	= fixed 5

***Scheduling info***

duration	= total # calls * mean call interarrival time
nodal_represent	= complex
mpg	= true

# References

- [1] “*KU-PNNI User’s manual version 2.1*” by Phongsak Prasithsangaree, Kamalesh S Kalarickal, Gowri Dhandapani, Bhavani Shanmugam, Santosh Golecha, Pradeepkumar Mani, David W Petr and Douglas Niehaus, May 2002
- [2] “*A Performance Evaluation Architecture for Hierarchical PNNI and Evaluation of Different Aggregation Algorithms in Large PNNI ATM Networks*” by Gowri Dhandapani, July 2000



# AUTOMATED DGD MEASUREMENTS USING POLARIZATION ANALYZER

## 1. Introduction

This report gives a detailed description of the measurement setup and the procedure used to make automated DGD measurements across a given wavelength band and over time using the Agilent lightwave polarization analyzer (PA). Jones Matrix Eigenanalysis (JME) method is used for making DGD measurements. This report assumes that the user knows how to use the Agilent PA. [If not the user is advised to go through the manual of PA first]. Also, the user should know how to compile and run Visual basic files.

## 2. Measurement Setup

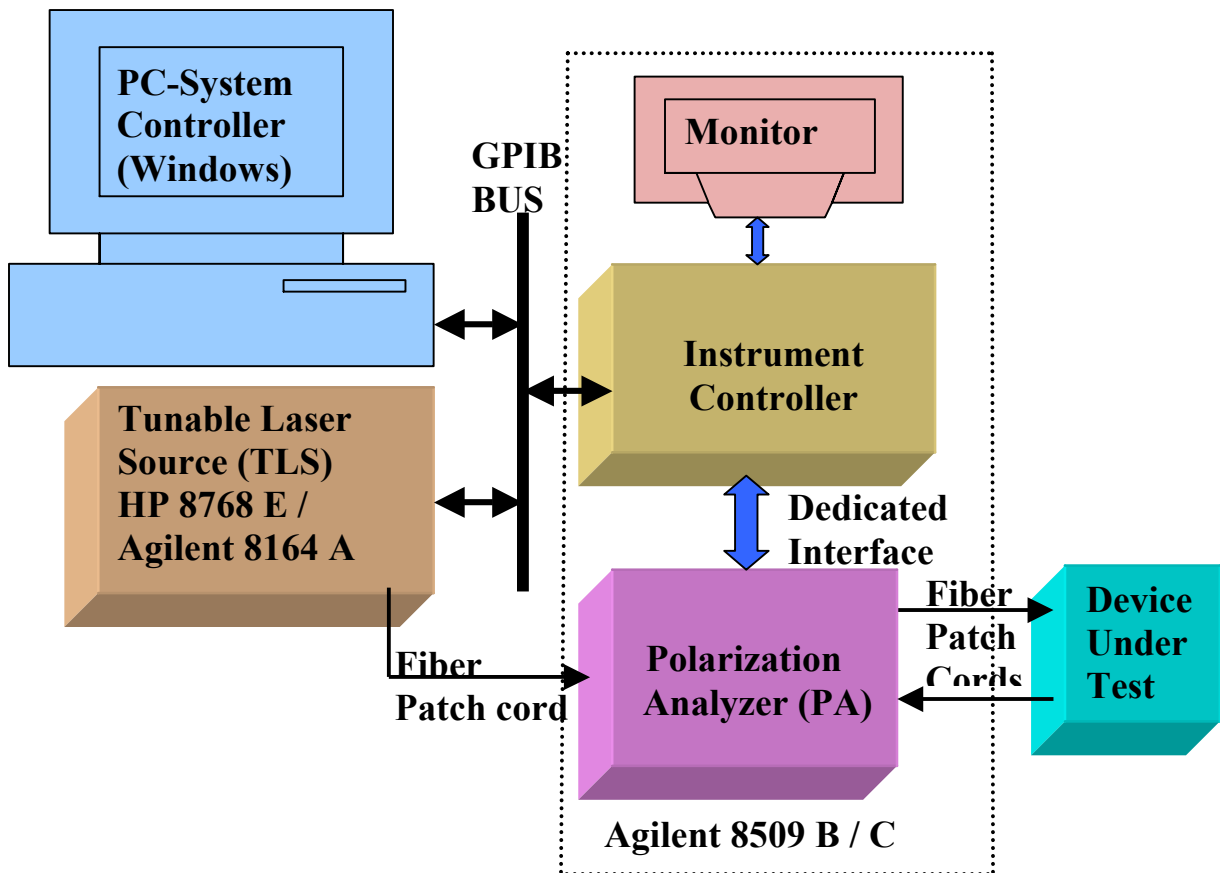


Fig 1. Measurement setup used for making automated DGD measurements.

## **2.1 Description**

The Agilent PA shown in Fig 1 comes with an instrument controller, monitor, keyboard and a mouse. The PA and the instrument controller are connected using the dedicated interface cable provided by the vendor. The monitor, keyboard and the mouse are connected to the instrument controller using their respective cables. An external Tunable Laser Source (TLS) operating in the desired wavelength band, the instrument controller and the system controller PC (a Windows machine) used for automating the measurements are connected together using a common GPIB bus. Optical output from the TLS is fed into the 'external source input' of the PA and the input and output ends of the Device Under Test (DUT) are connected to the 'optical output' and 'optical input' of the PA using fiber patch cords.

The Agilent PA provides two methods to measure the DGD, namely JME method and Wavelength Scanning (WS) method. Using JME application of Agilent PA one DGD measurement in time across the specified wavelength band can be made. To repeat the measurements in time automatically another PC is used as a system controller. A Visual Basic (VB) application running on the system controller PC communicates with the instrument controller by sending device specific commands (refer PA manual) thereby controlling the operation of the PA. Using the system controller PC, after each across-the-band measurement (one full measurement across the specified wavelength band) in time the PA sits idle for a certain period (specified by the user at the start of the measurements, usually 1 minute or so) providing the user an option to exit the application. If the user does not exit the

application within the specified time interval the PA restarts the across-the-band measurement again. This process keeps repeating until the user stops the measurements. However, the user does not have the option of stopping the measurements when an across-the-band measurement is in progress (can only be stopped forcibly). The user has to wait until that particular measurement across the specified band is completed to stop the measurements.

## **2.2 Saving data**

When the measurements are in progress, the VB application running on the system controller PC will automatically open a text file for each across-the-band measurement in the current folder of the system controller PC with a file name 'JME -'date'-'time' and records the measured data. These text files can be opened using 'Notepad' or 'WordPad' applications. Each file has three columns separated by commas, first column is the wavelength in nm, second column is the instantaneous DGD in ps and the third column is the average DGD in ps up to that point in that particular across-the-band measurement. [The data in the third column is rarely used; it is the data in the second column that is of interest to the user.]

## **3. Measurement procedure**

***Step 1:*** Connect the instruments as shown in Fig 1 and power up the instruments.

***Step 2:*** Before starting the measurements, follow the method described in the Agilent PA (8509 B/C) user's manual to perform one-time adjustment of external source polarization. This step is important as the vendor recommends it for enhanced accuracy.

**Step 3:** Open the Agilent 8509B/C and HPIB2DDE applications by double clicking on the icons on the monitor screen that comes with the PA.

**Step 4:** On the systems controller PC, open a new folder [this is recommended so that all the data files will be saved in that folder] and copy the executable file of the VB application into that folder.

**Step 5:** Start the VB application by double clicking on the executable file. This will open a window showing a few instructions that the user should follow before starting the measurements.

Clicking 'OK' will open an input dialog box showing the fields: start wavelength (nm), stop wavelength (nm), delta (step size in nm), power level (dBm) and the time interval (minutes) between the measurements (explained in Sec 2.1) and their default values. It also shows two icons namely, 'start measurement' and 'exit'.

**Step 6:** The user should provide the required values in the fields and click on the 'start measurement' icon. After that the system controller PC will start communicating with the instrument controller and the measurements will start in a few seconds.

**Step 7:** While the measurements are in progress, a plot between the instantaneous DGD (ps) and wavelength (nm) is displayed on the monitor screen that comes with the PA. This plot is refreshed after each across-the-band measurement. Both the monitors can be switched off to save power.

**Step 8:** To stop the measurements the user has to wait until the current across-the-band measurement is completed after which the VB application running the systems

controller PC will provide an option for the user to exit the application. In case the user wants to stop the measurements in the middle, it can be done using the task manager (not recommended). The data collected till that moment will be saved in the file.

**Note:** Refer to the PA manual for the details about the uncertainty in the measurements using the JME method.

#### **4. Possible errors during measurements**

The following errors are observed rarely which will stop the measurements.

- a. Error writing to the polarization analyzer – This message will appear on the system controller PC monitor. When this occurs the measurements are stopped abruptly. The user has to restart the measurements.
- b. Power under range – This message appears on the monitor that comes with the PA usually at the start of the measurements. This implies the power input to the PA from the DUT is below the sensitivity of the PA. The user has to take necessary action (such as increasing power from TLS or using an optical amplifier etc.) and restart the measurements.

It's better to check often whether the measurements are running or stopped due to some error. That way the measurements can be restarted soon in case of an error without missing much data.

#### **5. Details about using VB software**

Two zipped folders, namely, 'PMD installer.zip' and 'Sourcecode.zip' are attached to this report.

The following are required to use the above software:

- a. National instruments GPIB board installed.
- b. NI-488.2 software installed (It comes with the GPIB board).
- c. Visual basic 6.0 compiler [Only if the source code is modified].

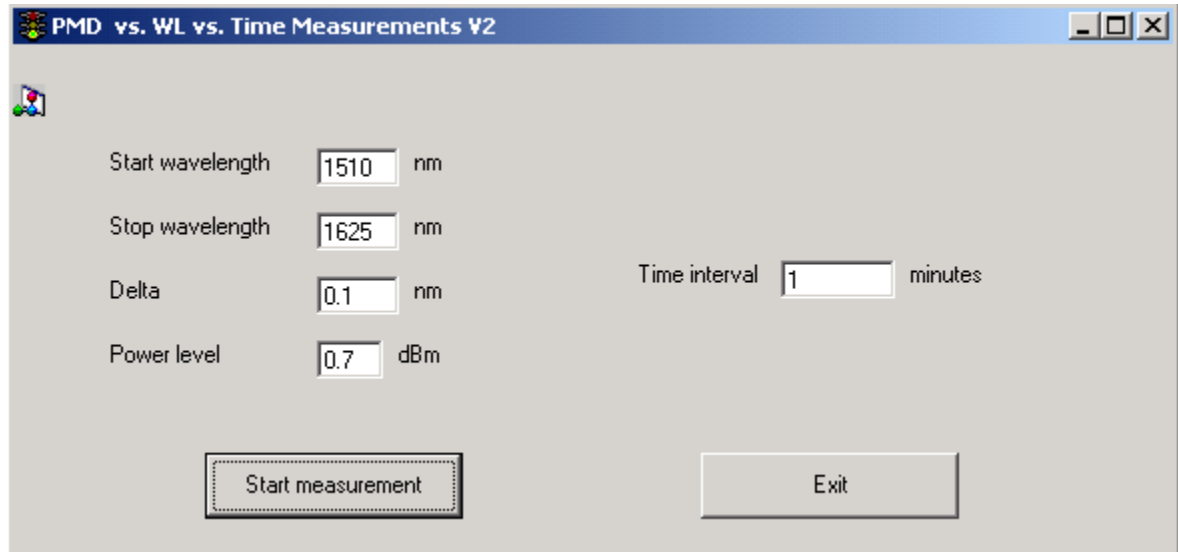
If the PMD installer folder is unzipped, it has a setup file in that. First the GPIB address of the PA has to be set to 29 and that of TLS to 24 (these are the values used in the code). Then if the setup file is run, it will install an executable file of the current version of the code. Now the user is ready to start the measurements with the specifications used in the code, namely, start wavelength is greater than 1510 nm, stop wavelength is less than or equal to 1635 nm, power level is between  $-20$  dBm and 6 dBm. If the user wants to use values within the above-mentioned ranges of wavelength and power he/she can straight away start the measurements and mention the desired values at the start of the measurements while prompted.

If the user wants to extend or change the above-mentioned ranges, modifications has to be made to the source code file (PMD-WL-Timev2.VPB, a visual basic project file which is located in the Sourcecode folder) and compile it again to get the executable file.

## 6. Sample measurement

A sample window of specifications and sample plot and data files of the measurements in lab are shown below.

### *Sample Specifications*

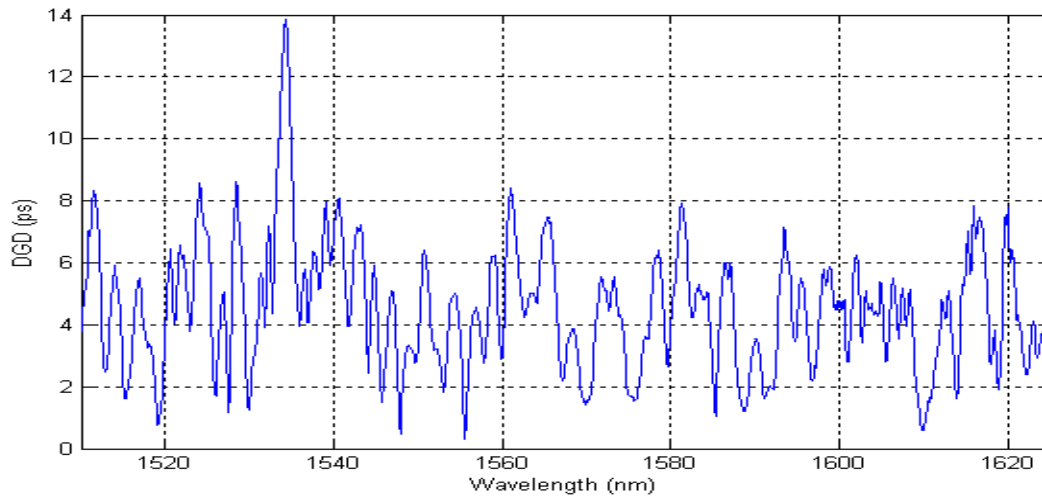


The screenshot shows a software window titled "PMD vs. WL vs. Time Measurements V2". It features a light gray background and a blue title bar. The window contains several input fields for measurement parameters:

- Start wavelength:  nm
- Stop wavelength:  nm
- Delta:  nm
- Time interval:  minutes
- Power level:  dBm

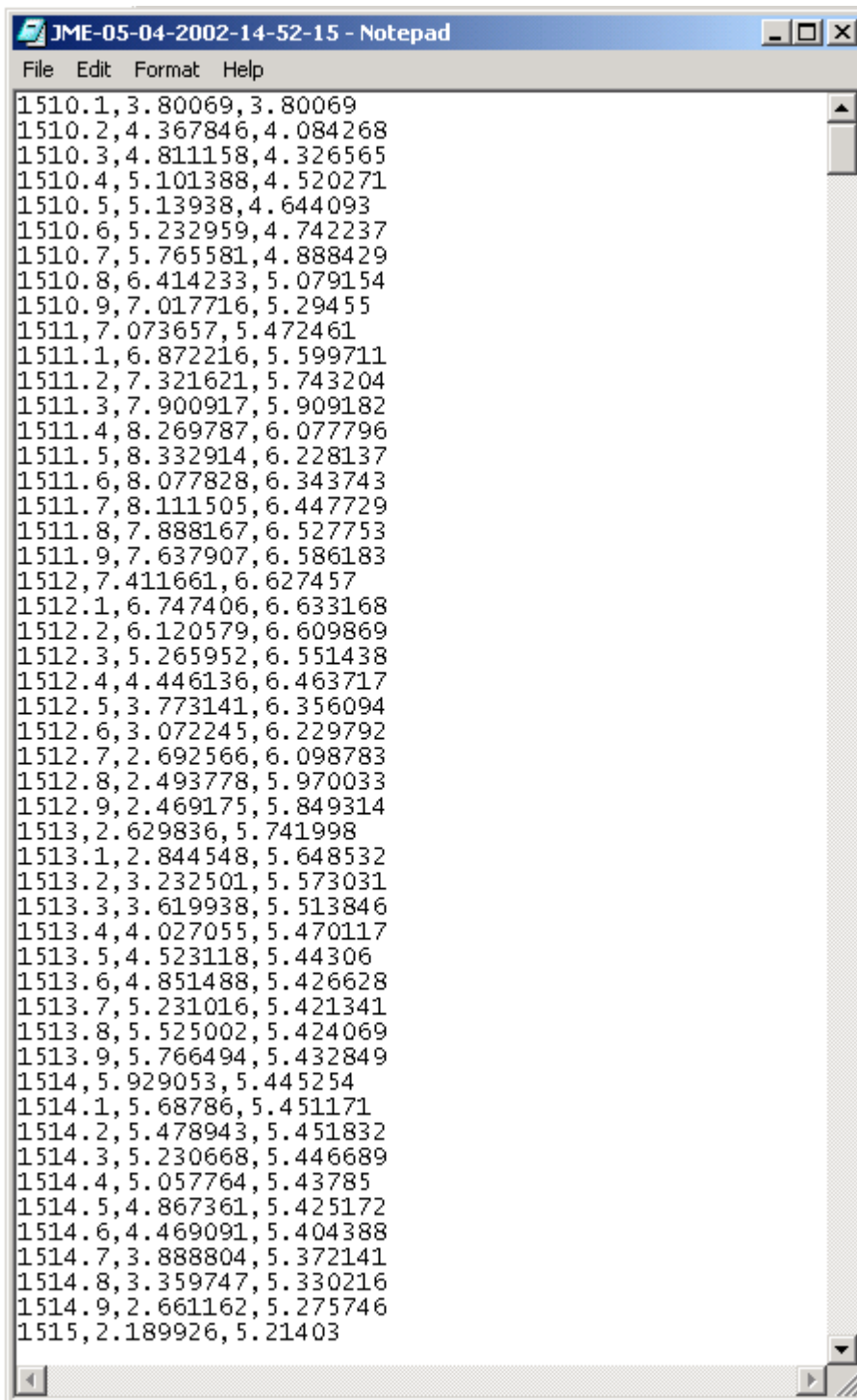
At the bottom of the window, there are two buttons: "Start measurement" (highlighted with a dashed border) and "Exit".

### *Sample plot*



The data corresponding to this plot is taken from the data file shown in the next page.

*Sample data file*



```
JME-05-04-2002-14-52-15 - Notepad
File Edit Format Help
1510.1,3.80069,3.80069
1510.2,4.367846,4.084268
1510.3,4.811158,4.326565
1510.4,5.101388,4.520271
1510.5,5.13938,4.644093
1510.6,5.232959,4.742237
1510.7,5.765581,4.888429
1510.8,6.414233,5.079154
1510.9,7.017716,5.29455
1511,7.073657,5.472461
1511.1,6.872216,5.599711
1511.2,7.321621,5.743204
1511.3,7.900917,5.909182
1511.4,8.269787,6.077796
1511.5,8.332914,6.228137
1511.6,8.077828,6.343743
1511.7,8.111505,6.447729
1511.8,7.888167,6.527753
1511.9,7.637907,6.586183
1512,7.411661,6.627457
1512.1,6.747406,6.633168
1512.2,6.120579,6.609869
1512.3,5.265952,6.551438
1512.4,4.446136,6.463717
1512.5,3.773141,6.356094
1512.6,3.072245,6.229792
1512.7,2.692566,6.098783
1512.8,2.493778,5.970033
1512.9,2.469175,5.849314
1513,2.629836,5.741998
1513.1,2.844548,5.648532
1513.2,3.232501,5.573031
1513.3,3.619938,5.513846
1513.4,4.027055,5.470117
1513.5,4.523118,5.44306
1513.6,4.851488,5.426628
1513.7,5.231016,5.421341
1513.8,5.525002,5.424069
1513.9,5.766494,5.432849
1514,5.929053,5.445254
1514.1,5.68786,5.451171
1514.2,5.478943,5.451832
1514.3,5.230668,5.446689
1514.4,5.057764,5.43785
1514.5,4.867361,5.425172
1514.6,4.469091,5.404388
1514.7,3.888804,5.372141
1514.8,3.359747,5.330216
1514.9,2.661162,5.275746
1515,2.189926,5.21403
```



# Measured temporal and spectral PMD characteristics and their implications for network-level mitigation approaches

Christopher Allen<sup>1</sup>, Pradeep Kumar Kondamuri<sup>1</sup>, Douglas L. Richards<sup>2</sup>, Douglas C. Hogue<sup>2</sup>

<sup>1</sup>Lightwave Communication Systems Laboratory, Information and Telecommunications Technology Center (ITTC)  
The University of Kansas, Lawrence, Kansas 66045  
voice 785-864-3017 fax 785-864-7789 callen@eecs.ukans.edu

<sup>2</sup>Sprint Corporation, Overland Park, Kansas

**Abstract**— Signal degradation due to polarization-mode dispersion (PMD) effects may become significant for signaling rates of 10 Gb/s, 40 Gb/s, and beyond. As expected, statistical analysis of variations in differential group delay (DGD) indicate that excursions from the mean DGD by factors of 3.7 or higher have very low probability. Temporal and spectral measurements of DGD were made on 95 km of buried standard SMF over an 86 day period to determine the distribution and rate of change of high DGD events. A drift time of about 3.4 days was found. The DGD data agree well with results of similar experiments reported in the literature. Coupling the drift time characteristic with the statistical behavior of DGD, we conclude that high-DGD episodes will be exceedingly rare and short lived. The impact of PMD on network operators is explored. Approaches are reviewed for network operators tasked with transporting high bit-rate channels over fiber links with known PMD characteristics.

## INTRODUCTION

In the phenomenon called polarization-mode dispersion (PMD), birefringence in the optical fiber provides two polarization-dependent group velocities for optical signals. In the high-coherence model of PMD (which assumes the coherence time of the light source is greater than the PMD-induced delays and no polarization-dependent loss) an input pulse will result in two orthogonally polarized pulses that preserve the shape of the original input pulse. The relative amplitudes of these two pulses is determined by the state of polarization (SOP) of the input pulse relative to the fiber's input principal states of polarization (PSPs). Thus for each pulse input, two pulses arrive at the receiver with different arrival times, called the differential group delay (DGD),  $\Delta\tau$ . This first-order model is frequency independent and is only valid over limited bandwidths. For wider bandwidths higher order effects must be considered resulting in frequency dependent polarization and dispersion [1], [2]. The bandwidth over which the PSPs can be assumed constant depend on the properties of the fiber and has been shown to vary inversely with the mean DGD,  $\langle\Delta\tau\rangle$  [3]. While the minimum bandwidth of the PSPs in single-mode fibers was found to be always over 50 GHz [3], this bandwidth for standard single-mode fiber is of the order of 100 GHz [1].

PMD may become a major impediment for network operators seeking to increase the per channel data rate on long-haul fiber-optic links. While the DGD in buried fiber had negligible impact at 2.5-Gb/s signaling rates, upgrades to

10 Gb/s, 40 Gb/s and beyond will require increasingly more attention. While there are PMD challenges facing carriers at 10 Gb/s, these challenges are not as severe as originally feared. Major carriers are successfully deploying 10 Gb/s dense-wavelength division multiplexed (DWDM) links across the core of their networks. A marked improvement in the DGD tolerance of 10 Gb/s long-reach receivers (to about 40 ps) will likely satisfy most length demands, obviating the need for PMD compensation (PMDC). Signaling rates of 40 Gb/s and beyond will most likely require some form of mitigation in long-haul applications, such as robust modulation schemes or PMDC.

To ensure signal quality on their fiber at higher bit rates, network engineers must anticipate the impact of PMD on the various fiber routes. Design of a reliable network requires a good model of the PMD characteristics on each link. An understanding of the variability of both the DGD and the PSPs is required to specify appropriate transmission parameters. Factors such as the mean DGD, PMD correlation time and bandwidth, as well as second-order effects together with performance prediction models can provide this understanding.

While PMD is a vector quantity, with a magnitude (DGD) and a direction (PSP), we are deliberately focusing exclusively on DGD as this is a readily measured parameter on installed optical networks. The statistical distribution and behavior of PSPs has been extensively studied and reported elsewhere.

## PMD STATISTICS

### Mean DGD

For long optical fibers, the PMD figure of merit typically specified is its mean DGD,  $\langle\Delta\tau\rangle$ , (having units of ps) or its PMD coefficient,  $\langle\Delta\tau\rangle/\sqrt{L}$ , (having units of ps/ $\sqrt{\text{km}}$ ) where  $L$  is the fiber length. The PMD for an installed (buried) fiber-optic cable is dominated by the inherent PMD of the bare fiber; however, the level of relaxation provided by the cabling and installation techniques also affect PMD. While the PMD in bare fiber is determined largely by the core-cladding concentricity achieved during manufacture, we have found that loose-tube cabling results in a lower PMD than other cabling methods, such as slotted core cabling. In addition, mechanical stresses introduced during cable installation (burial) also contribute to the PMD and will be affected by the installation practices used and whether the cable is in a protective conduit.

The mean DGD for a given fiber is a constant that represents both the average of DGD values at one time across a broad spectral bandwidth

$$\langle \Delta\tau \rangle = \frac{1}{N_\lambda} \sum_{i=1}^{N_\lambda} \Delta\tau(\lambda_i, t) \quad (1)$$

and the average of DGD values for a single wavelength over a long time period

$$\langle \Delta\tau \rangle = \frac{1}{N_t} \sum_{i=1}^{N_t} \Delta\tau(\lambda, t_i) \quad (2)$$

where  $\Delta\tau(\lambda, t)$  is the DGD value at wavelength  $\lambda$  and time  $t$ . Although the mean DGD for an installed fiber is constant, changing environmental factors (e.g., temperature) cause the instantaneous DGD at a given wavelength,  $\Delta\tau(\lambda, t)$ , to vary randomly about that mean.

When various fiber segments are concatenated to form a single long fiber, the mean DGD of the overall fiber is found by

$$\langle \Delta\tau_{\text{total}} \rangle = \sqrt{\sum_{i=1}^N \langle \Delta\tau_i^2 \rangle} \quad (3)$$

where  $N$  is the number of segments.

### Maxwellian distribution

The DGD for a given wavelength at any moment in time,  $\Delta\tau(\lambda, t)$ , is a random variable with a Maxwellian probability density function [4,5]

$$p(\Delta\tau) = \sqrt{\frac{2}{\pi}} \frac{\Delta\tau^2}{\sigma^3} e^{\left(\frac{-\Delta\tau^2}{2\sigma^2}\right)} \quad (4)$$

for  $0 < \Delta\tau < +\infty$ , where

$$\langle \Delta\tau \rangle = \sigma \sqrt{8/\pi} \quad (5)$$

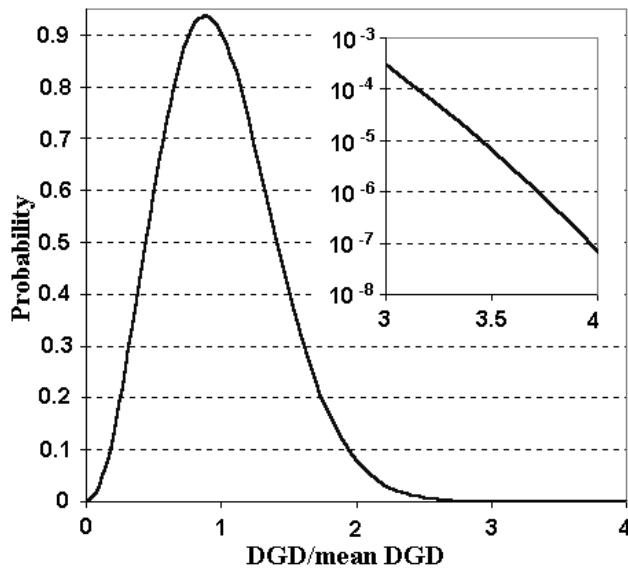


Figure 1. Maxwellian probability density function.

Therefore the single parameter  $\langle \Delta\tau \rangle$  fully specifies the distribution. Figure 1 shows the Maxwellian probability density function normalized by the mean DGD.

Using this distribution, the probability of  $\Delta\tau$  exceeding a particular value can be found using

$$P(\Delta\tau \geq X) = 1 - \int_0^X p(\Delta\tau) d\Delta\tau \quad (6)$$

For example, the probability of  $\Delta\tau/\langle \Delta\tau \rangle$  exceeding 3.7 is  $1.3 \times 10^{-7}$ . Expressed another way, if the mean DGD of a fiber link is 10 ps, 99.99999% of the time the DGD will be less than 37 ps.

### NETWORK DESIGN CONSIDERATIONS

In the design of a robust, long-haul fiber-optic network, the relationship between the maximum achievable link length and bit rate must be considered. For link designs where the maximum tolerable DGD is exceeded, techniques for coping with the effects of PMD must be explored.

#### Receiver DGD tolerance

The maximum link DGD that a receiver can tolerate before the signal degradation becomes unacceptable depends on a variety of factors, including modulation format, optical signal-to-noise ratio, and receiver design. For intensity-modulated, direct-detected (IM-DD) systems, Iannone et al. [6] found that when the transmitted signal excites both PSPs equally (a worst case condition), a 1-dB receiver sensitivity penalty results when the instantaneous DGD is about 23% of the signaling time period,  $T_{\text{bit}}$ . For a 2.5-Gb/s NRZ signal ( $T_{\text{bit}}$  is 400 ps), this corresponds to a tolerable DGD value of about 92 ps; at 10-Gb/s, about 23 ps is tolerable; and for a 40-Gb/s NRZ signal, this corresponds to about 5.7 ps. This maximum tolerable DGD level is representative of the NRZ IM-DD case; receiver DGD tolerance can be improved through careful receiver design, use of PMD-tolerant signaling formats, and the use of forward-correction codes (FEC). Khosravani and Willner [7] showed that RZ, chirped RZ, and dispersion-managed soliton signaling formats are much more tolerant of PMD effects compared to NRZ formats. Shieh et al. [8] and Xie et al. [9] have demonstrated a substantial increase in receiver tolerance of DGD when FEC is used. Modern long-haul, 10-Gb/s receivers using FEC or RZ modulation can tolerate about 40 ps of DGD with a 1-dB power penalty.

#### Probability of signal outage

For occurrences of high instantaneous DGD, signal quality may be intolerable resulting in a PMD-induced outage. Such outages may significantly affect network availability for higher bit rates (10 Gb/s, 40 Gb/s, and higher). For a network to operate with an overall availability of “five nines” (i.e., 99.999% of availability), the desired PMD-related availability factor may be “seven nines” (i.e., 99.99999%) which corresponds to a maximum tolerable DGD 3.7 times the mean DGD. For a 2.5-Gb/s IM-DD NRZ system with a DGD tolerance of 92 ps, this results in an acceptable mean DGD value of 25 ps; for a 10-Gb/s system with a DGD tolerance of 23 ps, the acceptable mean DGD is 6.2 ps; and for 40-Gb/s with a tolerable DGD of 5.7 ps, the acceptable mean DGD

level is 1.5 ps. For DGD-tolerant receivers (40 ps at 10 Gb/s) this results in an acceptable mean DGD of 10.8 ps.

### Coping with PMD

For network operators faced with the challenge of upgrading the channel data rate on a high-PMD link in the network, a handful of solutions exist that will preserve the signal quality at increased data rates.

One alternative cost solution is to selectively replace those fiber segments in the link known to be the dominant contributors to the overall link DGD, if they can be identified.

Another alternative cost solution is to regenerate the optical signal by placing a back-to-back terminals at the point in the link where the DGD affects approach an intolerable level, thus effectively reducing the optical link length.

Still another approach is to introduce error correction codes, such as FEC. In this approach the optical data payload is reduced incrementally in exchange for a marginal gain in PMD tolerance.

Yet another solution is to incorporate an adaptive PMD compensation system [8, 9, 10, 11, 12], typically located at the receiver. Typical PMD compensation systems are effective at minimizing the effects of first-order PMD, and, in some cases, second-order PMD. However both first- and second-order PMD compensation systems suffer the drawback that they reduce the effects of signal degradation over a very narrow optical bandwidth. This is a significant drawback for dense wavelength-division multiplexing (DWDM) systems. For a long-haul fiber-optic link carrying 100s of wavelengths, a separate PMD compensation system may be required for each wavelength to provide the desired seven nines availability.

For DWDM systems, another potential solution exists. Särkimukka et al. [13] proposed a method for mitigating PMD effects in a multichannel system by moving traffic off of PMD-impaired channels onto spare channels that are not experiencing PMD degradation.

One may also rely upon more traditional protection techniques (e.g. SONET ring or IP routing at layers 1 & 3, respectively). This protection can easily provide a guard against occasional PMD-induced outages of limited duration. However, for this approach to be viable, the episodes of abnormally high DGD events must be infrequent and spectrally localized. To evaluate the feasibility and limits of this solution, an understanding of the temporal and spectral nature of PMD is required.

Finally, there are also efficient optical networking solutions offering varying degrees of protection by using an optical cross-connect with a DWDM system. Operators may then construct a mesh-protected network and provide managed wavelength services that are protected against a possible PMD induced outages. Similar to the traditional protection methods, these more recent techniques will only be viable with infrequent and spectrally localized outages.

### TEMPORAL BEHAVIOR OF DGD

Given the dynamic nature of PMD and the low probability of excursions to intolerable levels, measurements of  $\Delta\tau(\lambda, t)$

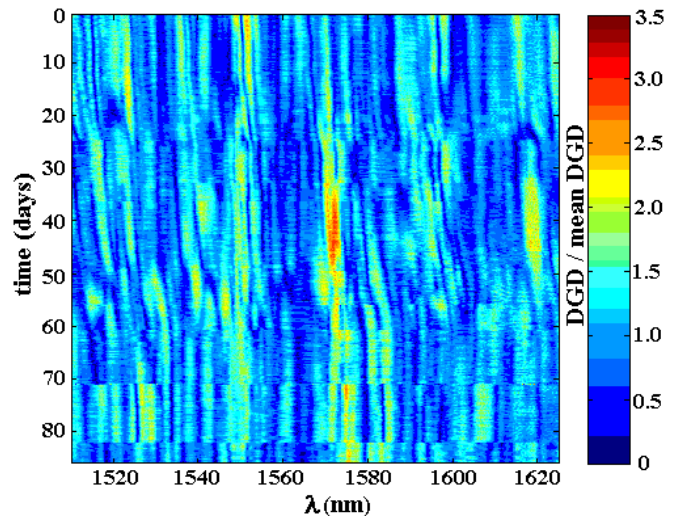


**Figure 2. Map of normalized DGD vs. wavelength and time.**

on buried fiber spans were made over long periods to enable prediction of the potential impact of PMD on network availability. Of particular interest are the frequency and duration of these rare events. The Jones Matrix Eigenanalysis (JME) technique was used to measure the DGD data on a 95-km span of slotted-core, direct buried fiber-optic cable made available by Sprint.

DGD was measured roughly every 3 hours at wavelengths from 1510 nm to 1625 nm with a spectral resolution of 0.1 nm (about 12.5 GHz). Over 86 days (from November 9, 2001 through February 2, 2002) 692 measurements were made on the 1150 discrete wavelengths. Figure 2 shows in a color-coded format this normalized DGD data (i.e.,  $\Delta\tau/\langle\Delta\tau\rangle$ ) representing 795,800 measured values. Expressed another way, if the 0.1-nm spectral samples and 3-hour time samples are statistically independent, then this data set would represent about 272 years of DGD data.

A histogram of this normalized DGD data is shown in Figure 3, and is seen to have shape consistent with a Maxwellian distribution, as expected. A curve representing a Maxwellian distribution normalized to the mean is also plotted for comparison.

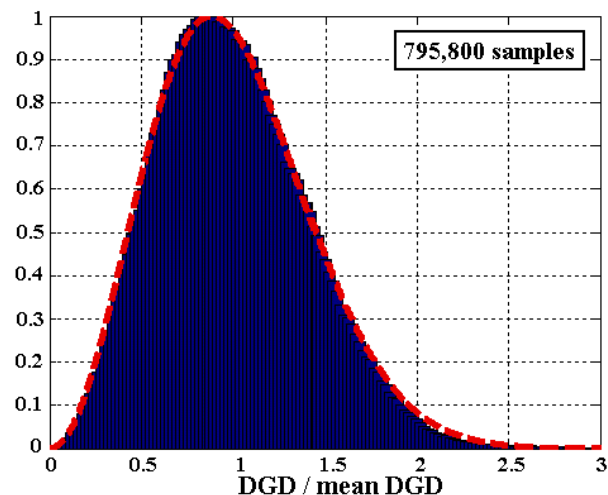


**Figure 3. Normalized histogram of measured DGD data.**

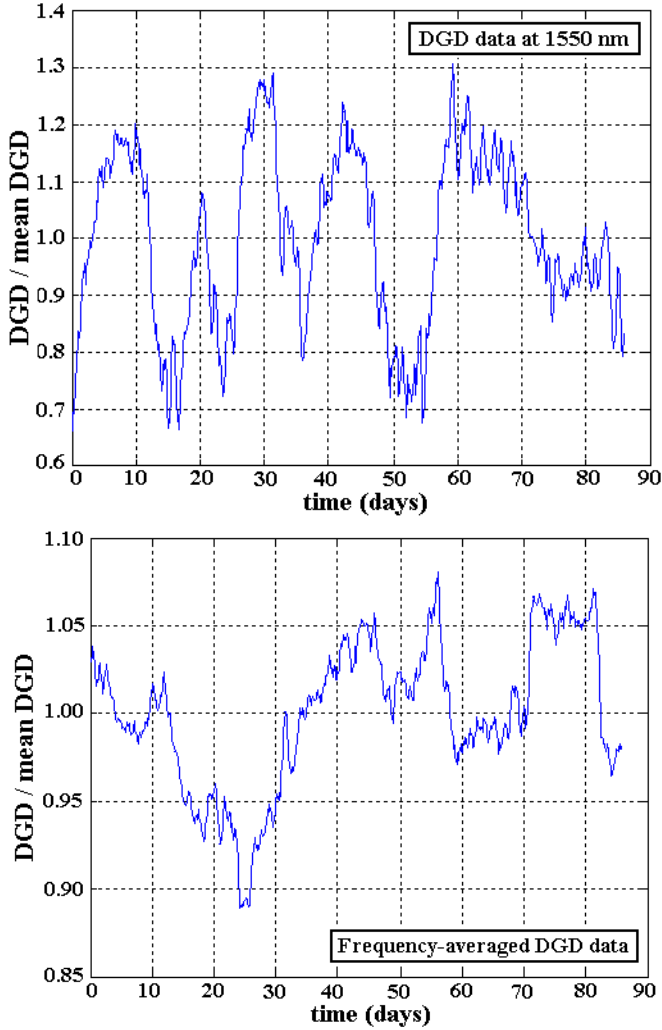


**Figure 4. Measured temporal variations in normalized DGD over 86 days (top) at 1550 nm and (bottom) averaged over all 1150 frequency measurements.**

From Figure 2 it is apparent that for buried fiber DGD values do not change rapidly. Figure 4 shows time histories of measured DGD data over the 86-day period. The top plot is DGD data at 1550 nm and the bottom plot is frequency-averaged data. While the mean value of the bottom plot is one (by definition), the mean value of the top plot is 1.088. This should not be interpreted to mean that the mean DGD is changing; rather since fewer data were used to estimate the mean, there is more uncertainty in that estimate compared to the estimate using all of the data.

To determine the DGD rate of change, an autocorrelation analysis was performed on the DGD time histories. Figure 5(top) shows the normalized temporal autocorrelation function (ACF) of the DGD data measured at 1550 nm. Figure 5(bottom) shows the ACF for the DGD time history for the frequency-averaged DGD data. Also shown in Figure 5 are curves representing the theoretical temporal autocorrelation function for DGD [14] which has the form

$$\text{AFC}(\Delta t) = \frac{1 - \exp(-|\Delta t|/t_d)}{|\Delta t|/t_d} \quad (7)$$

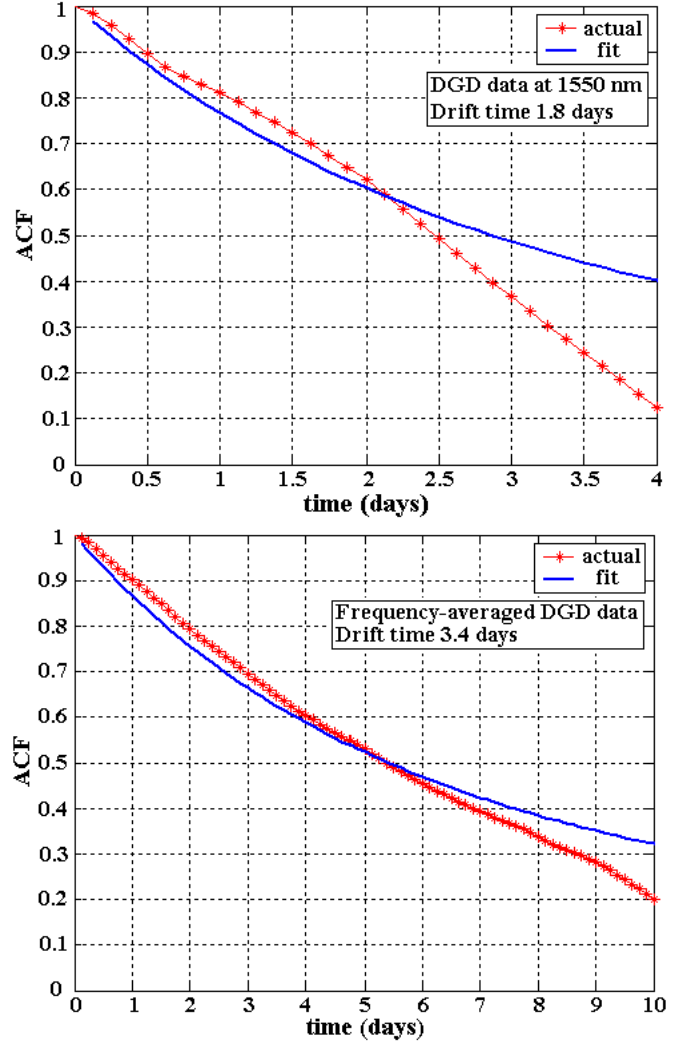


**Figure 5. Normalized temporal autocorrelation functions (ACFs) of normalized DGD data measured (top) at 1550 nm and (bottom) across 1150 frequencies. Theoretical ACF curves are fitted to the measured temporal ACFs.**

where  $t_d$  is the average drift time of DGD. The drift time indicates the timescale over which the DGD changes. Furthermore, when outages occur, the outage duration will be related to the drift time [14,15]. Based on data collected over the 86 days, the drift time for this fiber is estimated to be around 3.4 days. Expressed another way, samples should be collected about once every three days to obtain statistically independent DGD values on a specific wavelength; measurements collected more often are correlated.

For comparison, others have reported a range of DGD correlation times under various fiber conditions. For spools of fiber in a laboratory environment, correlation times of about 30 minutes on 31.6 km of fiber [16] and 3 hours on a 10-km fiber [17] have been reported. DGD variations on a 48-km aerial cable exhibited time scales ranging from 5 to 90 minutes depending the air temperature rate of change [18]. For submarine cables, a DGD correlation time of about an hour was observed on a 119-km cable [19], and [20] observed

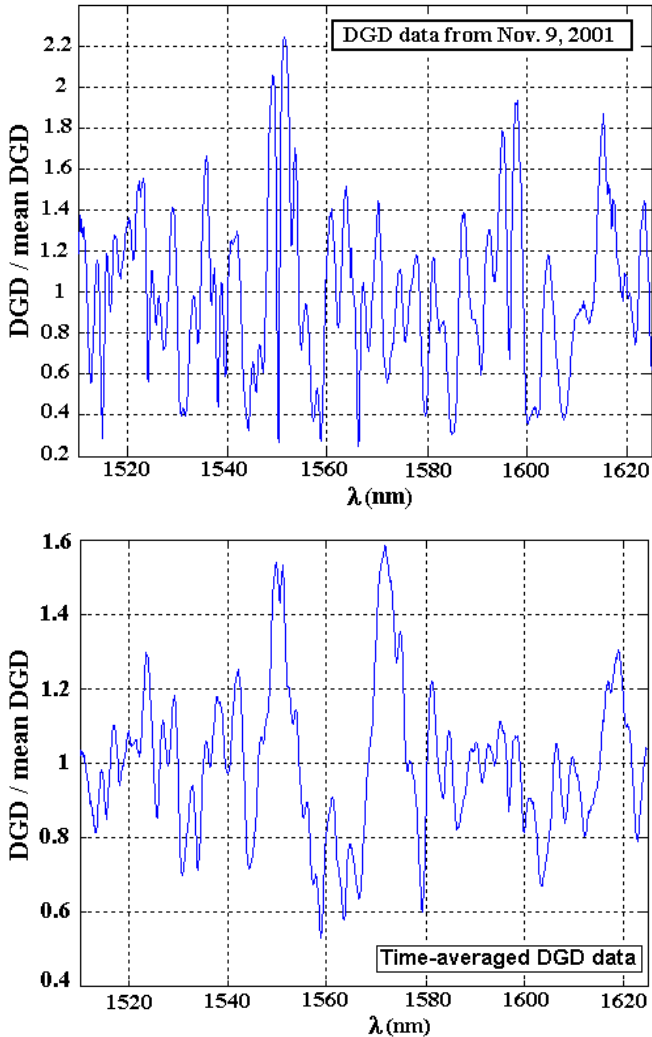


**Figure 6. Spectral variations in normalized DGD over 1150 wavelengths (top) measured on Nov. 9, 2001 and (bottom) time-averaged over all 692 time measurements.**

PMD changes with a period of about two months on a 62-km fiber-optic cable. On buried fibers, correlation times of at least 20 minutes (17 km) [21], 1-2 hours (48.8 km) [18], 3 and 5.7 days (127 km) [14], and 19 hours (114 km) [22] have been reported. Thus our observation of 3.4 days is consistent.

With knowledge gained from the ACF analysis, we can now interpret realistically our DGD data set. Over the 86 days of observation, about 25 independent samples were collected.

#### SPECTRAL BEHAVIOR OF DGD

From Figure 2 we note that the DGD varies significantly with wavelength. Figure 6(top) shows the normalized spectral variation of the first DGD data (measured on Nov. 9,2001) and the bottom plot shows the spectral variation of the time-averaged, normalized DGD data.

To determine the DGD bandwidth, spectral autocorrelation analysis was performed on the normalized DGD spectral data. Figure 7(top) shows the resulting normalized spectral ACF for one spectral measurement (data collected on

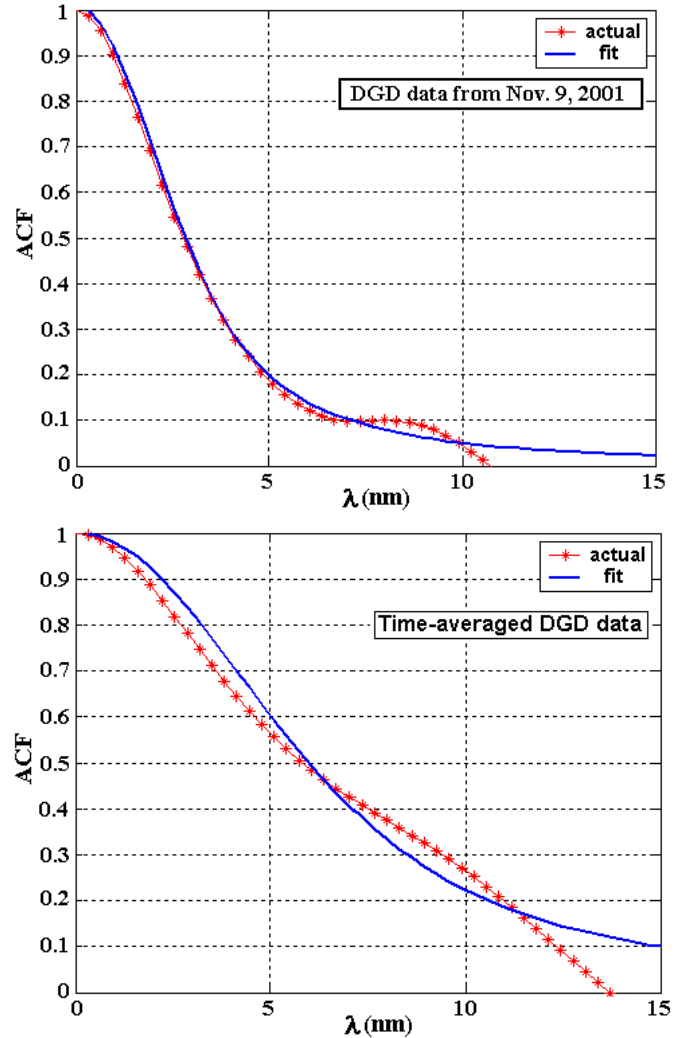


**Figure 7. Normalized spectral autocorrelation functions (ACFs) of normalized DGD data measured (top) on Nov. 9, 2001 and (bottom) time-averaged over all 692 measurements. Theoretical ACF curves are fitted to the measured spectral ACFs.**

Nov. 9,2001) and Figure 7(bottom) shows the normalized spectral ACF for the time-averaged data. Also shown in Figure 7 are curves representing theoretical spectral ACFs for DGD, with the form [23]

$$\text{ACF}(\Delta\omega) = 3 \frac{1 - \exp(-\langle\Delta\tau^2\rangle\Delta\omega^2/3)}{\Delta\omega^2} \quad (8)$$

where  $\Delta\omega$  is the radian frequency and  $\langle\Delta\tau^2\rangle$  represents the variance of the DGD.

From the measured data the bandwidth for the normalized DGD is estimated to be about 7.5 nm or 936 GHz. Therefore if the mean DGD is 1 ps and an optical channel is affected by significant DGD, nearby channels (within about 7.5 nm) may also experience this effect.

Theory and experiments [23] have demonstrated that the DGD bandwidth is inversely proportional to the mean DGD.

$$\omega_c = 4\sqrt{2}/\langle\Delta\tau\rangle \quad (9)$$

Thus fibers with a high mean DGD have a narrower DGD bandwidth than fibers with a low mean DGD. Thus for a fiber with a mean DGD of 1 ps, the predicted DGD bandwidth is 900 GHz which agrees well with bandwidth found using the spectral ACF fit in Figure 6(bottom). Note that normalized DGD bandwidth in the Figure 6(top) is about 4 nm which is significantly less than the approximately 7.5 nm bandwidth seen in Figure (bottom). This should not be interpreted to mean that the DGD bandwidth is varying; rather the bandwidth estimate obtained using all of the data will be more accurate as it is based on significantly more data points.

#### IMPLICATIONS FOR NETWORK AVAILABILITY

##### Mean time between PMD-related outages

The mean time between PMD-related outages can be estimated from the temporal characteristics of DGD variations and the Maxwellian probability density function. The DGD rate of change is characterized by the DGD drift time,  $t_d$ . This drift time may be thought of as “rolling the dice” every  $t_d$  to obtain a new, statistically independent DGD value. Therefore the mean time between high-DGD events (i.e., DGD exceeding a value X) can be estimated as

$$T_X = t_d / (k \cdot P(\Delta\tau > X)) \quad (10)$$

where k is a proportionality constant.

For example, Nagel et al. [22] observed a DGD correlation time of 19 hours, and predicts that the DGD will exceed three times its mean value once every 3.5 years. Since the probability of the DGD exceeding three times its mean is about  $4.2 \times 10^{-5}$  we can determine a value of 15 for k.

Applying (10) with a drift time of 3.4 days and a threshold of three times the mean DGD, the mean time between high-DGD events is about 14.8 years. For a PMD-induced outage probability of  $1.3 \times 10^{-7}$  (network availability of seven nines) the receiver should tolerate  $3.7 \times \langle \Delta\tau \rangle$ . With a DGD drift time,  $t_d$ , of 3.4 days, the estimated mean time between high-DGD events will be about 4,700 years, making it an extremely rare occurrence!

##### Duration of high-DGD events

Again from the DGD drift time, the Maxwellian probability density function, and the temporal ACF, the average duration of a high-DGD event can be estimated. While the correlation time represents the time delay resulting in a 63% reduction in the normalized ACF, smaller variations in the ACF require significantly shorter times. Again Nagel et al. [22] estimated a mean outage duration between 10 and 20 minutes for their link having a DGD correlation time of 19 hours. Bülow and Veith [15] found that while unusually long duration outages occur, the probability of occurrence decreases almost exponentially with outage duration. In other words, when outages occur, most will be of short duration.

Based on these findings, for the 95-km link we observed, we anticipate the typical duration of an outage to be between 1 and 2 hours with the possibility that a prolonged outage could persist for 1 to 1.5 days.

##### Impact of high-DGD events on adjacent channels

When a high-DGD episode occurs, how many DWDM channels will be affected? For a link with a mean DGD of 5 ps, the DGD bandwidth will be about 180 GHz or 1.44 nm. Therefore for a DWDM system with a 50-GHz channel spacing, during a  $3.7 \times \langle \Delta\tau \rangle$  event, the DGD in adjacent channels may also experience PMD-induced signal degradation, (i.e., only two or three channels will likely be affected by a single high-DGD episode).

##### Design rules

Based on these observations and analyses, certain rules may be developed. An important parameter in making decisions regarding PMD in a network is the ratio between the receiver’s DGD tolerance,  $\Delta\tau_{RX}$ , and the link’s mean DGD.

$$M = \frac{\Delta\tau_{RX}}{\langle \Delta\tau \rangle} \quad (11)$$

For cases where  $M > 3$ , the frequency of PMD-induced outages will be low, and their duration may be brief. In these cases the approach proposed by Särkimukka (or one utilizing new protection techniques) may be viable. The occurrences when switching this traffic may be required will likely be infrequent (spanning years), and may only be required for a few minutes or as long as a day.

For cases where  $2 < M < 3$ , PMD-induced outages may occur about once a month with typical durations measured in 10s of minutes.

For cases where  $M < 2$ , chronic PMD-induced outages will result. In these instances the option of applying PMD compensation, interrupting the link with a back-to-back terminal regenerator, or even replacing particular fiber segments may be appropriate.

##### Example scenarios

*10-Gb/s,  $\langle \Delta\tau \rangle = 10$  ps, receiver’s DGD tolerance 40 ps*

In this scenario the DGD margin, M, is 4. The probability of the DGD exceeding the receiver’s DGD tolerance level is about  $7.4 \times 10^{-9}$ , or effectively zero. In this case it is quite unlikely a PMD-induced outage will ever be observed. The DGD bandwidth will be about 90 GHz or about 0.72 nm.

*10-Gb/s,  $\langle \Delta\tau \rangle = 10$  ps, receiver’s DGD tolerance 23 ps*

In this case the margin will be 2.3 meaning that the probability of the DGD exceeding the receiver’s limit is about 0.37%. For a buried cable with a DGD drift time of about 2 days, PMD-induced outages typically will occur about once a month and last less than an hour. The DGD bandwidth will again be about 90 GHz.

*40-Gb/s,  $\langle \Delta\tau \rangle = 3.2$  ps, receiver’s DGD tolerance 5.7 ps*

The DGD margin in this case is 1.8 so the probability of the DGD exceeding the receiver’s limit is 4.4%. For a link with a drift time of 2 days, PMD-induced outages typically will occur about every third day. The typical duration will be 1 to 2 hours, however outages persisting for a day may occur. The DGD bandwidth is about 2.2 nm or 280 GHz so in a DWDM application with 50 GHz channel spacing, two or three channels may be affected during each outage.



## CONCLUSIONS

By examining the statistical behavior of DGD in an optical fiber, and using measured DGD data on a buried optical cable, predictions regarding the probability, frequency of occurrence, and spectral extent of high-DGD episodes can be made. Reports by others confirm our observation that DGD excursions of three or more times the mean DGD are infrequent and relatively short lived. This finding is significant for network operators who may consider providing a few spare channels in a DWDM environment to ensure high network availability.

For cases where the mean DGD is comparable to the receiver's maximum tolerable DGD, approaches for ensuring network availability include inclusion of PMD compensation systems, shortening the link length by strategically introducing back-to-back terminal regenerators, replacing fiber segments found to have excessively high DGD levels, or by utilizing an optical networking solution whereby traffic may efficiently share protection bandwidth.

## ACKNOWLEDGMENT

This work was funded by Sprint Corporations Company, L. P. A special tribute is paid to Francis Yarkosky, for his leadership and support.

## REFERENCES

- [1] Iannone, E., F. Matera, A. Mecozzi, and M. Settembre, *Nonlinear Optical Communication Networks*, New York: John Wiley & Sons, Inc., pp. 30-35, 1998.
- [2] Poole, C. D. and J. Nagel, Chapter 6: "Polarization effects in lightwave systems," in *Optical Fiber Telecommunications III A*, eds. I. P. Kaminow and T. L. Koch, San Diego: Academic Press, 1997.
- [3] Betti, S., F. Curti, B. Daino, G. De Marchis, E. Iannone, and F. Matera, "Evolution of the bandwidth of the principal states of polarization in single-mode fibers," *Optics Letters*, 16(7), pp. 467-469, 1991.
- [4] Curti, F., B. Daino, G. de Marchis, and F. Matera, "Statistical treatment of the evolution of the principal states of polarization in single-mode fibers," *Journal of Lightwave Technology*, 8, pp. 1162-1166, 1990.
- [5] Gisin, N., R. Passy, J. C. Bishoff, and B. Perry, "Experimental investigation of the statistical properties of polarization mode dispersion in single mode fibers," *IEEE Photonics Technology Letters*, 5(7), pp. 819-821, 1993.
- [6] Iannone, E., F. Matera, A. Galtarossa, G. Gianello, and M. Schiano, "Effect of polarization dispersion on the performance in IM-DD communication systems," *IEEE Photonics Technology Letters*, 5(10), pp. 1247-1249, 1993.
- [7] Khosravani, R. and A. E. Willner, "Comparison of different modulation formats in terrestrial systems with high polarization mode dispersion," *Proc. OFC 2000*, Baltimore, paper WL5, pp. 201-203, 2000.
- [8] Shieh, W., H. Haunstein, B. Mckay, D. Fishman, A. Golubchik, J. Diubaldi, C. Martell, V. Arya, R. Lee, and H. Choudhury, "Dynamic polarization-mode-dispersion compensation in WDM systems," *Proc. ECOC 2000*, Munich, Germany Vol. II(4.2.5), pp. 41-43, 2000.
- [9] Xie, Y., Q. Yu, L.-S. Yan, O. H. Adamczyk, Z. Pan, S. Lee, A. E. Willner, and C. R. Menyuk, "Enhanced PMD mitigation using forward-error-correction coding and a first-order compensator," *Proc. OFC'2001*, Los Angeles, CA, paper WAA2, 2001.
- [10] Rosenfeldt, H., Ch. Knothe, R. Ulrich, E. Brinkmeyer, U. Feiste, C. Schubert, J. Berger, R. Ludwig, H. G. Weber, and A. Ehrhardt, "Automatic PMD compensation at 40 Gbit/s and 80 Gbit/s using a 3-dimensional DOP evaluation for feedback," *Proc. OFC'2001*, Los Angeles, CA, Postdeadline Papers, paper PD27, 2001.
- [11] Kikuchi, N., "Analysis of signal degree of polarization degradation used as control signal for optical polarization mode dispersion compensation," *Journal of Lightwave Technology*, 19(4), pp. 480-486, 2001.
- [12] Pua, H.Y., K. Peddanarappagari, B. Zhu, C. Allen, K. Demarest, and R. Hui, "An adaptive first-order polarization-mode dispersion compensation system aided by polarization scrambling: theory and demonstration," *Journal of Lightwave Technology*, 18(6), pp. 832-841, 2000.
- [13] Särkimukka, S., A. Djupsjöbacka, A. Gavler, and G. Jacobsen, "Mitigation of polarization-mode dispersion in optical multichannel systems," *Journal of Lightwave Technology*, 18(10), pp. 1374-1380, 2000.
- [14] Karlsson, M., J. Brentel, and P. A. Andrekson, "Long-term measurement of PMD and polarization drift in installed fibers," *Journal of Lightwave Technology*, 18(7), pp. 941-951, 2000.
- [15] Bülow, H. and G. Veith, "Temporal dynamics of error-rate degradation induced by polarization mode dispersion of an installed field fiber link," *Proc. ECOC 1997*, vol. 1, Mo3C, Edinburgh, pp. 115-118, 1997.
- [16] Poole, C. D., R. W. Tkach, A. R. Chaplyvy, and D. A. Fishman, "Fading in lightwave systems due to polarization-mode dispersion," *IEEE Photonics Technology Letters*, 3(1), pp. 68-70, 1991.
- [17] Bahsoun, S., J. Nagel, and C. Poole, "Measurements of temporal variations in fiber transfer characteristics to 20 GHz due to polarization-mode dispersion," *Proc. ECOC'90*, Amsterdam, The Netherlands, Postdeadline Paper, pp. 1003-1006, 1990.
- [18] Cameron, J., L. Chen, X. Bao, and J. Stears, "Time evolution of polarization mode dispersion in optical fibers," *IEEE Photonics Technology Letters*, 10(9), pp. 1265-1267, 1998.
- [19] Takahashi, T., T. Imai, and M. Aiki, "Time evolution of polarization mode dispersion in 120 km installed optical submarine cable," *Electronics Letters*, 29(18), pp. 1605-1606, 1993.
- [20] Kawazawa, T. and Y. Namihira, "Long-term polarization-mode-dispersion measurement of installed optical submarine cable," *Proceedings of OFC'94*, pp. 228-229, 1994.

- [21] De Angelis, C., A. Galratossa, G. Gianello, F. Marera, and M. Schiano, "Time evolution of polarization mode dispersion in long terrestrial links," *Journal of Lightwave Technology*, 10(5), pp. 552-555, 1992.
- [22] Nagel, J. A., M. W. Chbat, L. D. Garrett, J. P. Soigné, N. A. Weaver, B. M. Desthieux, H. Bülow, A. R. McCormick, and R. M. Derosier, "Long-term PMD mitigation at 10 Gb/s and time dynamics over high-PMD installed fiber," *Proc. ECOC 2000*, Munich, Germany Vol. II(4.2.1), pp. 31-32, 2000.
- [23] Karlsson, M. and J. Brentel, "Autocorrelation function of the polarization-mode dispersion vector," *Optics Letters*, 24(14), pp. 939-941, 1999.



# Analysis and comparison of measured DGD data on buried single-mode fibers

Christopher Allen<sup>1</sup>, Pradeep Kumar Kondamuri<sup>1</sup>, Douglas L. Richards<sup>2</sup>, and Douglas C. Hogue<sup>2</sup>

<sup>1</sup>Lightwave Communication Systems Laboratory  
Information and Telecommunications Technology Center (ITTC)  
The University of Kansas, Lawrence, Kansas 66045

<sup>2</sup>Sprint Corporation, Overland Park, Kansas

## Abstract

Temporal and spectral measurements were made on three different 95-km fibers within a slotted-core, direct buried, standard single-mode fiber-optic cable over many days to characterize DGD variability. From this data we observed that DGD varies slowly over time but rapidly over wavelength. This data showed good agreement with a Maxwellian distribution. The frequency-averaged mean DGD varied by about 10% or less during the periods that included significant temperature swings. Outage analysis showed that for system tolerances of three times the mean DGD, outages will occur typically every 3 to 8 years with mean outage durations ranging from about one to two hours. From this analysis we conclude that high-DGD episodes are spectrally localized and will be exceedingly rare and short lived.

## Introduction

Polarization-mode dispersion (PMD) may be a major impediment for network operators seeking to increase the per channel data rate on long-haul fiber-optic links. While the differential group delay (DGD, or  $\Delta\tau$ ) in buried fiber had negligible impact at 2.5-Gb/s signaling rates, upgrades to 10 Gb/s, 40 Gb/s and beyond will require increasingly more attention. While there are PMD challenges facing carriers operating at 10 Gb/s, these challenges are not as severe as originally feared. Major carriers are successfully deploying 10-Gb/s dense-wavelength division multiplexed (DWDM) links across the core of their networks. A marked improvement in the DGD tolerance of 10 Gb/s long-reach receivers (to about 40 ps) will likely satisfy most length demands, obviating the need for PMD compensation (PMDC). Signaling rates of 40 Gb/s and beyond will most likely require some form of mitigation in long-haul applications, such as robust modulation schemes or PMDC.

To ensure signal quality on their fiber at higher bit rates, network engineers must anticipate the impact of PMD on the various fiber routes. An understanding of the variability of both the DGD and the principal states of polarization (PSPs) is required to specify appropriate transmission parameters. Factors such as the mean DGD, PMD correlation time and bandwidth, as well as

second-order effects together with performance prediction models can provide this understanding.

The availability of measured PMD data on installed, buried fibers is limited. In this paper we present measured DGD data for buried, standard single-mode fiber to improve our understanding of the variability of PMD. While PMD is a vector quantity, with a magnitude (DGD) and a direction (PSP), we are only focusing on the DGD. The statistical distribution and behavior of PSPs has been extensively studied and is shown to be correlated to DGD behavior [1,2].

## Experimental setup

Experiments were conducted to measure the instantaneous DGD on three different 95-km fibers (1, 2, and 3) within a slotted-core, direct buried, standard single-mode fiber-optic cable made available by Sprint. A polarization analyzer employing the Jones-Matrix-Eigenanalysis (JME) method was used for measurements at wavelengths from 1510 nm to 1625 nm with a spectral resolution of 0.1 nm (about 12.5 GHz). Measurements on fiber span 1 were repeated approximately every 3 hrs and they were carried on for about 86 days whereas on fiber spans 2 and 3 they were repeated approximately every 1½ hours and carried out for about 14 and 9 days, respectively. Over the 86 days (from Nov. 9, 2001 through Feb. 2, 2002) 692 measurements were made on fiber span 1 across the 1150 discrete wavelengths representing 795,800 measured values. For fiber spans 2 and 3 the corresponding number of DGD measurements is about 271,600 and 181,700.

## Plots of DGD vs. wavelength and time

Figures 1, 2, and 3 show in a color-coded format normalized DGD data (i.e., DGD/mean DGD) measured on the three fiber spans, respectively. From the plots it is clear that for buried fibers DGD changes with time but not at a rapid rate. This variation is random and differs from fiber to fiber. It is also evident that the DGD varies significantly with wavelength and relatively high-DGD events are spectrally localized.

A histogram of the normalized DGD data on fiber span 1, shown in Figure 4, is seen to have shape consistent with a Maxwellian distribution, as expected. A curve representing a Maxwellian distribution for a 1-ps mean DGD is also plotted for comparison.

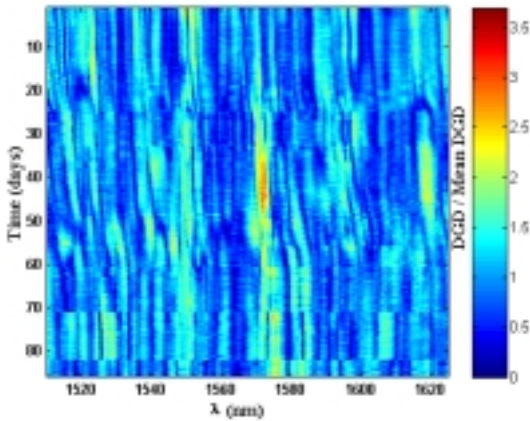


Figure 1. Measured, normalized DGD vs. wavelength and time for fiber span 1 (86 days of data).

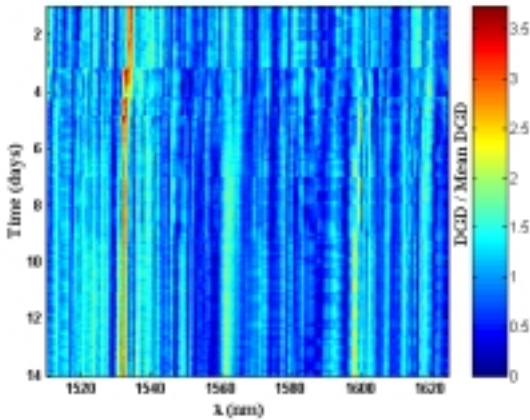
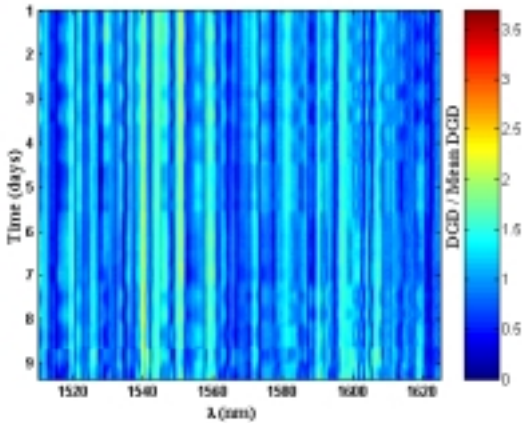


Figure 2. Measured, normalized DGD vs. wavelength and time for fiber span 2 (14 days of data).



(c)

Figure 3. Measured, normalized DGD vs. wavelength and time for fiber span 3 (9 days of data).

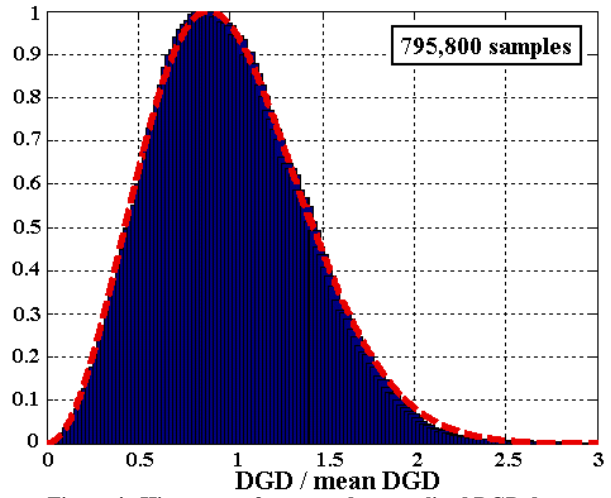


Figure 4. Histogram of measured, normalized DGD data on fiber span 1.

Similar histograms were obtained for the data on the other two fiber spans (plots not shown here) and they also showed good agreement with a Maxwellian distribution.

#### Mean DGD variation with time

To observe the time-dependent nature of DGD more closely, 1150 DGD measurements over all wavelengths were averaged together to obtain frequency-averaged DGD data, denoted as  $\langle \text{DGD} \rangle_\lambda$  normalized by the overall mean DGD (averaged over both time and frequency), denoted as  $\langle \langle \text{DGD} \rangle_\lambda \rangle_t$ . Since temperature is a known driver in changing DGD changes, hourly air temperature data for the region were collected as well. The variation of frequency-averaged DGD and temperature with time on the three fiber spans is shown in Figures 5, 6 and 7. From Figure 5 it can be observed that frequency-averaged DGD varies by only about  $\pm 10\%$  over 86 days of observations that included significant temperature swings. Since the entire length of the fiber is buried, the diurnal temperature variations do not represent the fiber temperature. Statistical analyses reveal no significant correlation between long-term temperature variations and the frequency-averaged mean DGD.

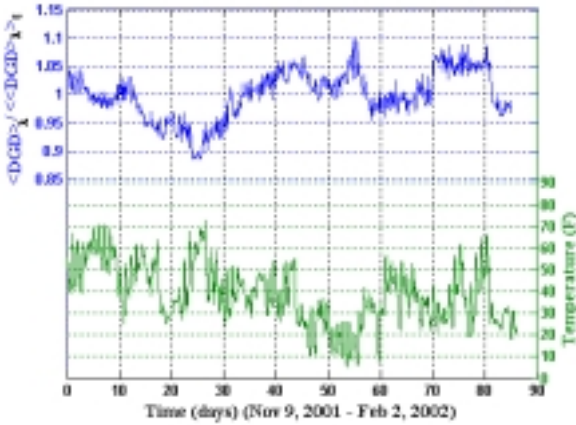


Figure 5. Frequency-averaged DGD and temperature vs. time for fiber span 1.

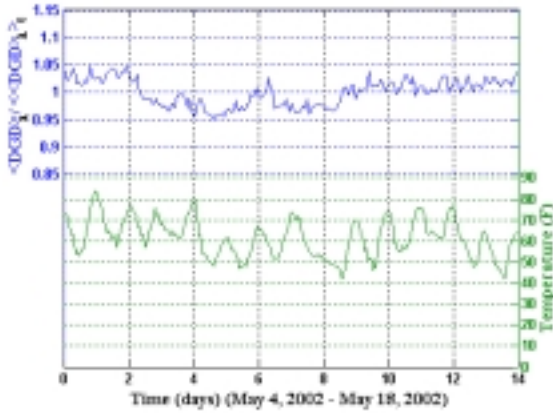


Figure 6. Frequency-averaged DGD and temperature vs. time for fiber span 2.

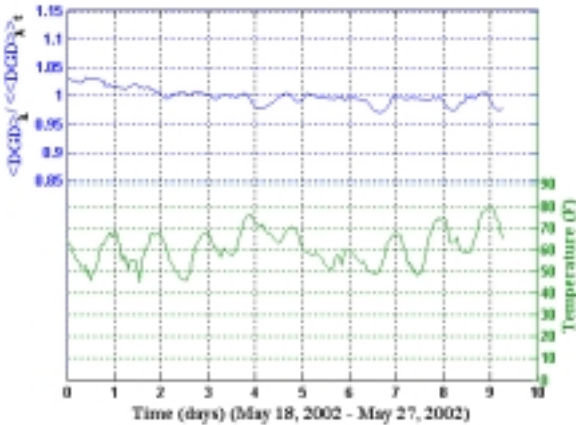


Figure 7. Frequency-averaged DGD and temperature vs. time for fiber span 3.

### System outage analysis

An outage event is one which exceeds the given threshold value of DGD,  $\Delta\tau_{th}$ . The outage probability  $P_{out}$ , expressed in minutes/year, can be calculated from

the Maxwellian probability distribution function (pdf),  $f_{\tau}(\cdot)$  as

$$P(\Delta\tau \geq \Delta\tau_{th}) = 1 - \int_0^{\Delta\tau_{th}} f_{\tau}(\Delta\tau) d\Delta\tau \quad (2)$$

and then multiplying the number of minutes in a year. As  $P_{out}$  is based on the Maxwellian pdf, it may be expressed as a function of one independent variable  $M = \Delta\tau_{th}/(\text{mean DGD})$  as  $P_{out}(M)$  and is clearly fiber independent and will be the same for all installations.

In cases where the probability of an outage is quite small,  $P_{out}$  represents the annualized outage probability based on long time records, however no insight is provided regarding the outage rates and their durations. Accurate estimation of the impact of PMD on network availability requires statistical analysis of the DGD variability. Caponi et al. [3] showed how the mean time between PMD-related outages could be estimated from the temporal characteristics of DGD variations and the Maxwellian probability density function. The mean outage rate,  $R_{out}$  (defined as the mean number of outage events per unit time with units of events/year), is found using [3]

$$R_{out} = \frac{1}{2} f_{\tau}(\text{threshold}) \int_{-\infty}^{\infty} f_{\tau}(\Delta\tau') |\Delta\tau'| d\Delta\tau' \quad (3)$$

where  $\Delta\tau'$  is the time derivative of the DGD, and  $f_{\tau}(\cdot)$  is the pdf of  $\Delta\tau'$ . Caponi et al. observed  $\Delta\tau$  and  $\Delta\tau'$  to be statistically independent and also found that  $R_{out}$  is cable and installation dependent.

Figure 8 shows the calculated outage probability,  $P_{out}$ , and the mean outage rate,  $R_{out}$ , for a given system threshold relative to the mean DGD on the three fiber spans.

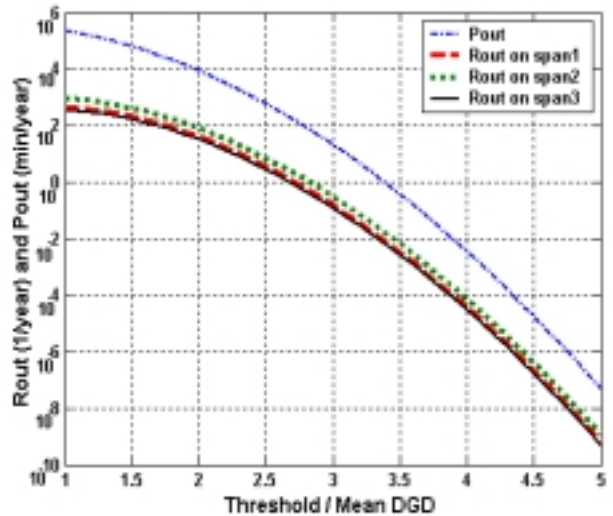


Figure 8. Calculated outage probability,  $P_{out}$ , and mean outage rate,  $R_{out}$ , versus Threshold / Mean DGD.

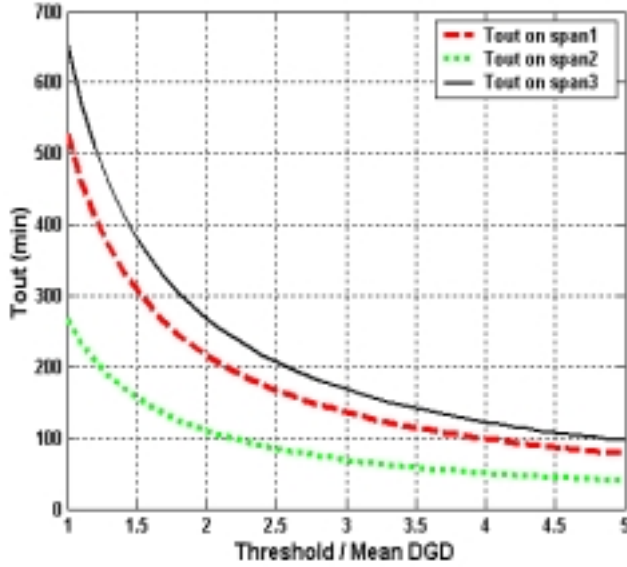


Figure 9. Calculated mean outage duration,  $T_{out}$ , as a function of Threshold/mean DGD.

Table 1. Predicted mean time between outages (MTBOs) and mean outage durations for different DGD tolerances

	$3 \cdot \langle \text{DGD} \rangle$	$3.7 \cdot \langle \text{DGD} \rangle$
Span 1		
MTBO	6.39 years	1648 years
Outage duration	136 min	108 min
Span 2		
MTBO	3.25 years	833 years
Outage duration	69 min	55 min
Span 3		
MTBO	7.91 years	2000 years
Outage duration	138 min	133 min

The mean duration of DGD-induced outages can be determined using statistical analysis as well. Caponi et al. [3] showed that the mean outage duration,  $T_{out}$ , is

$$T_{out} = P_{out} / R_{out} \quad (4)$$

which has units of minutes.

Figure 9 shows the calculated mean outage duration,  $T_{out}$ , as a function of system threshold relative to the mean DGD. Since  $T_{out}$  is found using  $R_{out}$ , which is cable and installation dependent,  $T_{out}$  will also be cable and installation dependent.

From the above analysis, we can estimate the mean outage time between outages (MTBOs) and mean outage durations for various DGD tolerances for these fiber spans. Table 1 lists these values for system thresholds of three and 3.7 times the mean DGD.

For comparison, Nagel et al. [4] predicted that for the 114-km buried link they studied, the DGD will exceed three times its mean value once every 3.5 years and estimated a mean outage duration of between 10 and 20

minutes for their link. From data measured on 37-km of buried cable, Caponi [3] predicted the DGD will exceed three times the mean DGD once every 2.5 years with a mean outage duration of 56 minutes.

### Conclusions

We have measured DGD data on three different 95-km fibers within a slotted-core, direct buried, standard single-mode fiber-optic. From these measurements we observed that DGD varies slowly over time but rapidly over wavelength or frequency. Episodes of higher-than-average DGD were observed and seen to be spectrally localized and of limited duration.

To investigate the role of changing temperature on mean DGD variations, frequency-averaged DGD data were compared to temperature histories. The frequency-averaged DGD varied by only about  $\pm 10\%$  over 86 days of observations that included significant temperature swings.

From this data predictions were made regarding the probability, and frequency of outage occurrence. While the statistics of Maxwellian processes adequately describe the annualized outage probability, further analysis of the DGD data revealed the mean time between outages and mean outage durations. For outages characterized by high DGD episodes (DGD more than three times the mean DGD), we found that the mean outage rates and durations for these three fibers to be similar. Our findings agree with reports by others that DGD excursions of three or more times the mean DGD are infrequent and relatively short lived. This finding is significant for network operators who must assess the impact of PMD on network reliability.

### Acknowledgment

This work was funded by Sprint Corporations Company, L. P. A special tribute is paid to Francis Yarkosky, for his leadership and support.

### References

- [1] Karlsson, M. and J. Brentel, "Autocorrelation function of the polarization-mode dispersion vector," *Optics Letters*, 24(14), pp. 939-941, 1999.
- [2] Karlsson, M., J. Brentel, and P. A. Andrekson, "Long-term measurement of PMD and polarization drift in installed fibers," *Journal of Lightwave Technology*, 18(7), pp. 941-951, 2000.
- [3] Caponi, R., B. Ripsati, A. Rossaro, and M. Schiano, "WDM design issues with highly correlated PMD spectra of buried optical fibers," *Proc. OFC 2002*, Anaheim, CA, Th15, pp. 453-455, 2002.
- [4] Nagel, J. A., M. W. Chbat, L. D. Garrett, J. P. Soigné, N. A. Weaver, B. M. Desthieux, H. Bülow, A. R. McCormick, and R. M. Derosier, "Long-term PMD mitigation at 10 Gb/s and time dynamics over high-PMD installed fiber," *Proc. ECOC 2000*, Munich, Germany Vol. II(4.2.1), pp. 31-32, 2000.